CELLULAR ENERGETICS IN THE CANINE MODEL OF AGING & SIRT6 AS A THERAPEUTIC TARGET FOR PARKINSON'S DISEASE:

PART 1: Innate Mitochondrial Uncoupling and Energetics Underlie Aging Diversity in Dogs

PART 2: Nicotine Promotes Neuron Survival and Partially Protects from Parkinson's Disease by Suppressing Sirt6

A Dissertation

Presented to the Faculty of the Graduate School

of Cornell University

In Partial Fulfillment of the Requirements for the Degree of

Doctor of Philosophy

by

Justin William Nicholatos

December 2018

© 2018 Justin William Nicholatos

CELLULAR ENERGETICS IN THE CANINE MODEL OF AGING & SIRT6 AS A THERAPEUTIC TARGET FOR PARKINSON'S DISEASE

Justin William Nicholatos, Ph. D.

Cornell University 2018

PART 1: Dogs display exceptional lifespan variation across their many breeds, presenting an opportunity to discover longevity-determining traits. We performed a genome-wide association study on 4,169 canines representing 110 breeds and identified novel candidate longevity-genes controlling coat phenotypes, like hair length, and mitochondrial properties, suggesting that thermoregulation and bioenergetics contribute to lifespan variation. Using primary dermal fibroblasts, we investigated mitochondrial properties of short-lived (large) and long-lived (small) breeds. We found that cells from long-lived breeds have more uncoupled mitochondria and more efficient electron transport chains. Moreover, our data suggest that long-lived breeds have higher rates of catabolism and β-oxidation, likely to meet elevated electron demand of their uncoupled mitochondria. Conversely, cells of short-lived (large) breeds accumulate amino acids and fatty acid derivatives, likely for biosynthesis and growth. The uncoupled metabolic profile of long-lived breeds likely stems from their smaller size, reduced volume to surface area ratio, and therefore a greater need for thermogenesis. Molecularly, the uncoupled energetics of long-lived breeds increases respiration, mitigates production of reactive oxygen species, and prevents stiffening of the actin-cytoskeleton, promoting cellular stress tolerance and survival. We propose that these cellular characteristics delay tissue dysfunction,

disease, and death in long-lived dog breeds, contributing to canine aging diversity.

PART 2: Parkinson's disease is characterized by progressive death of dopaminergic neurons, leading to motor and cognitive dysfunction. Epidemiological studies consistently show that the use of tobacco reduces the risk of Parkinson's. We report that nicotine reduces the abundance of SIRT6 in neurons and brain tissue by proteasome-mediated degradation. We find that reduction of SIRT6 is partly responsible for neuroprotection afforded by nicotine. Additionally, SIRT6 abundance is greater in Parkinson's patient brains, and decreased in the brains of tobacco users. We also identify SNPs that promote SIRT6 expression and simultaneously associate with an increased risk of Parkinson's. Furthermore, brain-specific SIRT6 knockout mice are protected from MPTP-induced Parkinson's, while SIRT6 overexpressing mice develop more severe pathology. Our data suggest that SIRT6 plays a pathogenic and pro-inflammatory role in Parkinson's and that nicotine can provide neuroprotection by accelerating its degradation. Inhibition of SIRT6 may be a promising strategy to ameliorate Parkinson's and neurodegeneration.

BIOGRAPHICAL SKETCH

Justin Nicholatos was born in Boston, Massachusetts in 1988 and grew up in the small-town of Uxbridge. He attended the University of Massachusetts at Amherst to study biology and Japanese. Here he studied the genetic evolution of fruit color under the tutelage of Professor Ana Caicedo. Upon graduation he worked in the laboratory of Brendan Manning at the Harvard T.H. Chan School of Public Health. Here he spent four years developing research skills while investigating the mTOR pathway. This is also where he decided to focus on aging biology as a focus for graduate studies and beyond. This is what brought him to Cornell University and to the laboratory of Sergiy Libert who shares a passion and interest in aging. He will be transitioning into a postdoctoral scientist role at Biogen in Cambridge, MA.

ACKNOWLEDGMENTS

I would like to thank the many people who have had an impact on my scientific career thus far. Ana Caicedo, who gave me my first research opportunity at UMass. Brendan Manning, who hired me out of college and started my career in biomedicine. Yinan Zhang, whom I personally worked under and learned many research skills from. Sergiy Libert, who accepted me to his lab and has given me exceptional training, support, and friendship. My committee members, Sylvia Lee, Tudorita Tumbar, and Fenghua Hu, who gave me feedback and advice on my projects. I also thank all the collaborators throughout my time at Cornell, and undergraduates who assisted me. Lastly, I thank my friends and family for a lifetime of encouragement and support.

TABLE OF CONTENTS

LIST OF FIGURES

CHAPTER 2:

CHAPTER 3:

CHAPTER 4:

LIST OF TABLES

CHAPTER 2:

CHAPTER 3:

LIST OF ABBREVIATIONS

AD - Alzheimer's Disease

BSKO - Brain Specific Knockout

BSOX - Brain Specific Overexpressed

CR – Caloric Restriction

DA - Dopaminergic

GWAS - Genome Wide Association Study

KO - Knockout

MPP+ - 1-methyl-4-phenylpyridinium

MPTP - 1-methyl-4-phenyl-1,2,3,6-tetrahydropyridine

NAD+ - Nicotinamide Adenine Dinucleotide

OX - Overexpressed

PD - Parkinson's Disease

TH - Tyrosine Hydroxylase

WT - Wild type

LIST OF SYMBOLS

$\Delta\Psi$ - Mitochondrial membrane potential

R - Pearson correlation

PREFACE

This dissertation is organized by two projects. These are the major projects I was involved with during my time at Cornell. Chapter 2 encompasses the first project and chapter 3 details the second. Chapter 1 and 4, the overall introduction and conclusions respectively, deal with both projects.

CHAPTER 1

INTRODUCTION

Why Study Aging?

Worldwide, particularly in developed countries, the population is becoming increasingly aged. More people, totally and as a percentage of the population, are developing and dying from age-associated diseases. In developed countries like the United States, the major causes of death are age-associated diseases such as cancer, cardiovascular disease, and neurodegeneration. Thus, it is increasingly important that we understand the aging process and its interconnection to disease. The primary goal of biomedicine should be to increase the functional and healthy years of living; ideally increasing lifespan too. There are two major ways to tackle this issue from a biomedical perspective. First is by studying basic mechanisms of aging to better understand what aging is and how it is regulated. Second is by studying specific age-associated diseases and how to treat or prevent them. I have carried out both strategies during my tenure at Cornell within the Libert lab.

Basic Mechanisms of Aging and the Canine Model

Why does one individual age more slowly compared to another? why does one species live longer than another? We do not know what the major drivers of these differences are. We do know that as we get older our bodies become frailer and more susceptible to disease (with an exponential increase in mortality). Quite simply are bodies lose the

ability to carry out homeostasis, but whether this is due to a controlled process, stochastic events, or combination is still debated. A more robust understanding of the cellular and molecular mechanisms that underpin the aging process and its accompanying decline in tissue and organ function is needed. A better understanding of the mechanisms of aging that lead to greater disease susceptibly will also help us mitigate said diseases of aging.

Cellular properties contribute to the functional decline of tissues during the aging process. Examining cellular properties in long-lived versus short-lived groups can help us understand and identify novel processes that regulate aging and longevity. The canine model is an excellent avenue to elucidate such principals. There is tremendous phenotypic diversity between dog breeds, which is exemplified in differences of lifespan and size. Lifespan negatively correlates with size, where smaller breeds live longer than larger breeds. Along with diversity in longevity and size, breeds have different propensities for numerous diseases (Fleming *et al.* 2011; Hayward *et al.* 2016). For example, the Golden Retriever has a cancer rate of 10%, while the Saint Bernard is significantly lower at 0.09% (VetCancer Registry). Dogs thus represent a unique model to elucidate mechanisms of aging and its associated diseases.

Aging biology is complex and its surrounding theories are often controversial. This is true for the canine-model, where small breeds have an increased metabolic rate relative to larger breeds, contradicting the “rate of living” theory, which posits that faster metabolism decreases lifespan (Pearl 1928). Elevated metabolism is also theorized to shorten lifespan by increasing production of reactive oxygen species

(ROS) and oxidative-damage (Harman 1956), which is an unexplored mechanism in the canine-model. Uncoupled proton movement in mitochondria, which generates heat, is similarly theorized to increase lifespan through dampened ROS (Brand 2000). Examining differences in cellular and tissue properties between short and long-lived breeds will help uncover processes responsible for organismal aging. In the Libert lab, we acquired primary cells from many different dog breeds spanning short to long-lived. With this cell collection, we performed a comprehensive analysis correlating metabolism, biophysical properties, and stress response to breed longevities.

Age-Associated Neurodegeneration, Parkinson's Disease, and SIRT6

Parkinson's disease (PD) is one of the most common neurodegenerative disorders, and is characterized by the loss of dopaminergic neurons in the *substantia nigra* (Tanner 1992). Current treatments focus on symptom management but do not slow the underlying neuronal loss. The incidence and burden of PD is set to drastically increase as effective therapies are yet to be developed and as the U.S. population grows continuously older. In fact, the cost to the healthcare system and overall economic burden to the U.S. is staggering at an estimated $25 billion for 2016 alone (Parkinson's Disease Foundation 2016). Due to an increasingly aged population the number of those diagnosed with PD is expected to double by 2040, with the costs substantially growing in those years (Kowal *et al.* 2013). Halting or slowing the progression of PD is critically important to improve the lives of those suffering and to reduce the economic burden. A therapy that even partially ameliorated this disease would provide massive benefits (Johnson *et al.* 2013).

Sirtuin 6 (SIRT6) is a member of the sirtuin family, which are NAD^+-dependent enzymes known to mediate numerous aspects of metabolism and stress responses (Westerheide *et al.* 2009; Libert & Guarente 2013). SIRT6 has promise as a target for various diseases of aging (Beauharnois *et al.* 2013), and is emerging as a potential therapeutic target for neurodegeneration (Jung *et al.* 2016; Shao *et al.* 2016). However, SIRT6 has never been studied in the context of PD.

Preventing neuronal death is central to an effective neurodegenerative intervention. In PD the dopaminergic neurons of the *substantia nigra* are most vulnerable to death; their loss is the disease's hallmark and is responsible for the most debilitating symptoms. No currently available medical interventions prevent the loss of these neurons. One of our critical discoveries in the Libert lab is that neurons with loss or suppression of SIRT6 resist stress-induced apoptosis. This finding holds true for primary neurons and other cell types. We sought to understand how SIRT6 regulates neuronal survival and demonstrate the utility of its suppression as a bona fide therapy. Additionally, the reduced prevalence of Parkinson's disease in tobacco users is a fascinating phenomenon with no mechanistic explanation. We also explored the connection between the tobacco component nicotine and SIRT6, seeking to understand if nicotine promotes cellular and neuronal survival through regulation of SIRT6. Our main methods included analysis of human brain tissue, transgenic mouse models, and primary neuronal cultures

CHAPTER 2

INNATE MITOCHONDRIAL UNCOUPLING AND ENERGETICS UNDERLIE AGING DIVERSITY IN DOGS

Author list for final publication: Justin W. Nicholatos[1], Timothy M. Robinette[1], Saurabh V.P. Tata[1], Jennifer D. Yordy[1], Adam B. Francisco[1], Michael Platov[1], Tiffany K. Yeh[1], Olga R. Ilkayeva[5], Frank K. Huynh[5], Maxim Dokukin[3], Dmytro Volkov[3], Michael A. Weinstein[4], Adam R. Boyko[1], Richard A. Miller[2], Igor Sokolov[3,4], Matthew D. Hirschey[5], Sergiy Libert[1]

1. Department of Biomedical Sciences, Cornell University, Ithaca, NY, 14850, USA
2. Department of Pathology, University of Michigan, Ann Arbor, MI, 48109, USA,
3. Department of Mechanical Engineering, Tufts University, Medford, MA, 02155, USA
4. Department of Biomedical Engineering, Tufts University, Medford, MA, 02155, USA
5. Duke Molecular Physiology Institute and Sarah W. Stedman Nutrition and Metabolism Center, Duke University Medical Center, Durham, NC, 27701

Author Contributions: Conceptualization, J.W.N. and S.L.; Formal Analysis, J.W.N.; Investigation, J.W.N., M.P., T.M.R., S.V.T., A.B.F., J.D.Y., T.K.Y., D.V., M.W., F.K.H., and O.R.I.; Writing – Original Draft, J.W.N.; Writing – Review & Editing, J.W.N., T.M.R., J.D.Y., T.K.Y., I.S., M.D.H., and S.L.; Supervision, S.L.; Funding Acquisition, J.W.N. and S.L.

SUMMARY:

The first domesticated companion animal, the dog, is currently represented by over 190 unique breeds. Across these numerous breeds, dogs have exceptional variation in lifespan (inversely correlated with body size), presenting an opportunity to discover longevity-determining traits. We performed a genome-wide association study on 4,169 canines representing 110 breeds and identified novel candidate regulators of longevity. Interestingly, known functions of some of the identified genes included control of coat phenotypes such as hair length, as well as mitochondrial properties, suggesting that thermoregulation and mitochondrial bioenergetics play a role in lifespan variation. Using primary dermal fibroblasts, we investigated mitochondrial properties of short-lived (large) and long-lived (small) dog breeds. We found that cells from long-lived breeds have more uncoupled mitochondria and more efficient electron transport chains. Moreover, our data suggest that long-lived breeds have higher rates of catabolism and β-oxidation, likely to meet elevated electron demand of their uncoupled mitochondria. Conversely, cells of short-lived (large) breeds accumulate amino acids and fatty acid derivatives, which are likely used for biosynthesis and growth. The uncoupled metabolic profile of long-lived breeds likely stems from their smaller size, reduced volume to surface area ratio, and therefore a greater need for thermogenesis. Molecularly, the uncoupled energetics of long-lived breeds increases respiration, mitigates production of reactive oxygen species, and prevents stiffening of the actin-cytoskeleton, promoting cellular stress tolerance and survival. We propose that these cellular characteristics delay tissue dysfunction, disease, and death in long-

lived dog breeds, contributing to canine aging diversity.

INTRODUCTION:

The domestic dog, *Canis lupus familiaris*, is an emerging model for aging biology and age-related disorders. Genomic studies suggest that canine domestication began between 20,000-40,000 years ago (Botigue *et al.* 2017). Throughout this period and up to the present, humans and dogs have shared an intimate proximity with common environmental exposures (air, water, food, and pathogens). With age, dogs undergo a similar functional decline as humans (Hoffman *et al.* 2018); they develop many of the same age-associated diseases, including cancers, metabolic syndromes, and neurodegeneration (Kaeberlein *et al.* 2016). Moreover, genetic analysis has demonstrated strong parallel co-evolution between our species, particularly in metabolic and neurological processes (Wang *et al.* 2013). Together these factors make scientific findings in dogs informative to human biology and aging.

Dogs have immense genetic and phenotypic diversity across individual breeds. Extensive human-led breeding efforts have created significant variation in size, disease prevalence, and longevity, among many other parameters. For example, there is a 30-fold difference in weight and 2.5-fold difference in lifespan between the Chihuahua (~5 pounds, ~16 years) and Great Dane (~150 pounds, ~7 years). Interestingly, body size is a strong predictor of lifespan in dogs, with smaller breeds generally living longer than larger breeds (Greer *et al.* 2007). This holds true with the hundreds of breeds registered with the American Kennel Club (AKC) which fall along this size-lifespan continuum (**Fig. 1A**). Importantly, mortality-data modeling shows

that the dominant reason small dogs live longer is by aging more slowly, where the rate of mortality increases with age slower than their larger counterparts (Kraus *et al.* 2013). Furthermore, although larger breeds tend to have higher levels of inbreeding, variation in longevity cannot be explained by variation in the strength of inbreeding (Yordy *et al.*).

Dog breed size has been associated with SNPs in the pro-growth hormone insulin-like growth factor-1 (IGF-1) (Sutter *et al.* 2007; Hayward *et al.* 2016). Suppressed IGF-1 signaling can increase longevity, and small dogs are known to have reduced circulating IGF-1 (Greer *et al.* 2011). Growth signaling from IGF-1 certainly plays a significant role in controlling breed size, but it is not clear if (or to what degree or mechanism) it might regulate lifespan in dogs. Variation in IGF-1 and the rate of aging would suggest that differences in cellular and tissue physiology underlie canine longevity. The only known cellular property that correlates with breed longevity is telomere length, where long-lived breeds display longer telomeres (Fick *et al.* 2012). However, the involvement of telomeres in the aging process is not fully understood and even disputed. To elucidate what governs the variation in aging rate between dog breeds, additional unbiased studies are needed. Dogs provide an excellent model to identify novel longevity pathways, which will not only help us understand the true nature of aging but can also be exploited for human and canine health.

Using genome-wide association (GWAS), we identify novel longevity-associated genes that are known to regulate thermogenic and bioenergetic processes. We investigate these processes in detail with a comparative metabolic and biophysical

analysis of primary dermal fibroblasts derived from short- and long-lived dog breeds. Previous studies have indicated that primary dermal fibroblasts can recapitulate organismal metabolism and have demonstrated their utility in uncovering physiological differences between short- and long-lived animals (Murakami *et al.* 2003; Wang & Miller 2012). We analyzed fibroblasts for bioenergetic-metabolite (organic acids, amino acids, and acylcarnitines) profiles, mitochondrial and electron transport chain (ETC) properties, stress tolerance, and cytoskeletal dynamics. We report that, even after isolation and culturing, canine fibroblasts retain breed-specific *in vivo* metabolism that correlates with donor breed longevity. We show that cells from long-lived breeds have more mitochondrial uncoupling, more efficient ETC properties (greater respiration with less ROS formation), and a more flexible cytoskeleton. Our data suggests that long-lived breeds utilize greater amino and fatty acid catabolism, which is required to sustain their uncoupled-energetic demand. We also demonstrate greater stress tolerance in cells from long-lived breeds and propose that these breeds age more slowly due to superior tissue homeostasis conferred by these properties.

RESULTS:

The functionality and properties of cells are known to contribute to the robustness and longevity of whole organisms. To narrow the range of cellular processes to analyze, all of which could potentially contribute to aging variation in dogs, we performed a GWAS for breed-average lifespan. The analysis included 150,000 loci in 4,169 individuals representing 110 breeds. We used a linear mixed model as described

previously (Hayward *et al.* 2016), and after multiple testing correction identified top candidate genes that associate with canine longevity (**Fig. 1B & C, Table 1, Supplementary Information**). Fascinatingly, our GWAS identified FGF5 and RSPO2 to associate with breed longevity (**Table 1**), which are two out of the three known genes that control canine coat phenotypes such as hair length (Housley & Venta 2006; Cadieu *et al.* 2009). We next checked whether coat length in dogs correlated with the size and longevity of breeds. We found that on average, coat length was inversely related to breed size, where larger breeds tend to have shorter hair and smaller breeds are likelier to have longer hair (**Fig. 1D**). The principal purpose of hair is thermoregulation, and it is logical that smaller breeds would have longer hair to retain heat, and for larger dogs to have shorter hair to keep cool. This not only indicates that canines possess thermoregulatory strategies but that similar mechanisms may influence breed longevity.

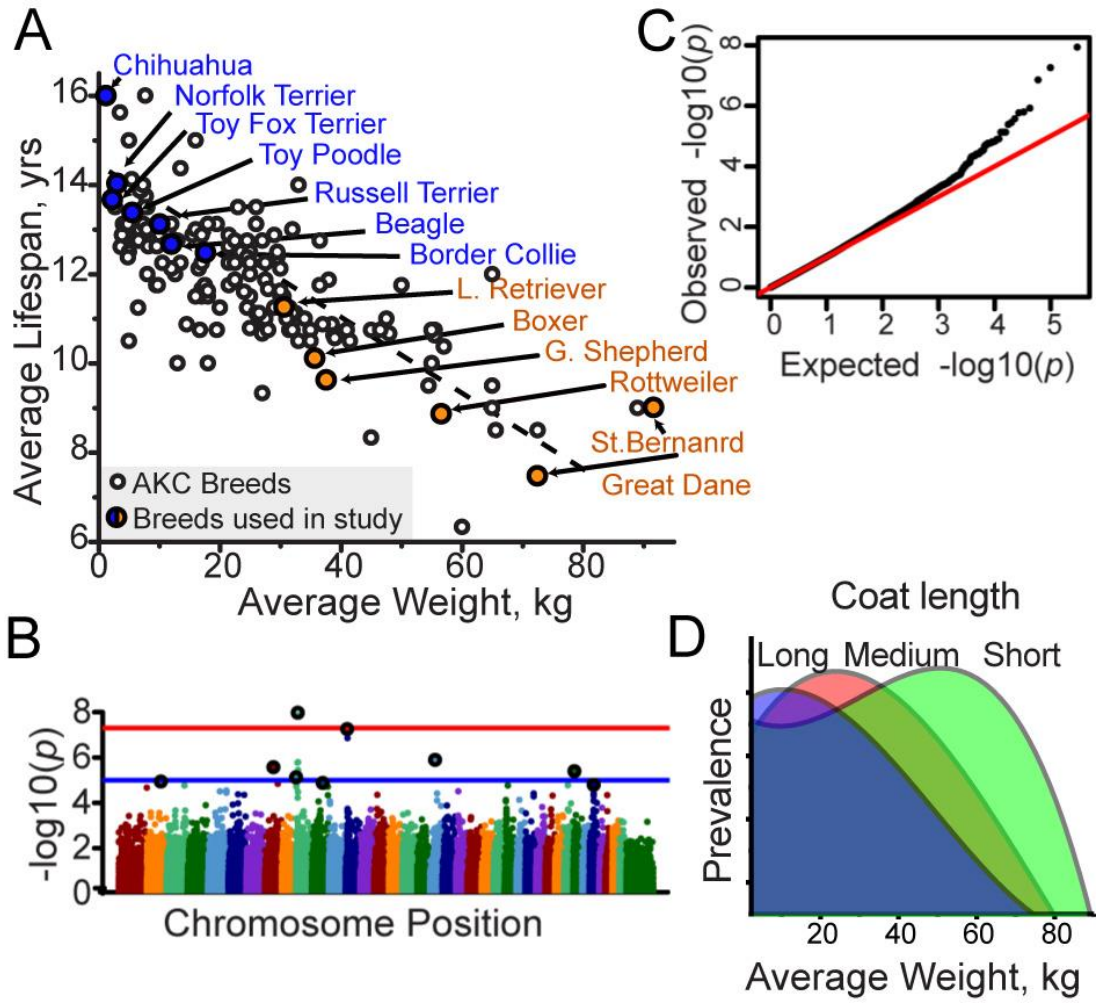

Figure 1. Thermoregulatory and mitochondrial genes associate with canine breed longevity. (A) Scatter plot of breeds registered with the American Kennel Club plotted average lifespan by average weight. Cells from breeds used in this study are highlighted in blue (long-lived) or orange (short-lived). (B) Manhattan and quantile-quantile (C) plots from GWAS of breed average life expectancy (n=4,169 individuals, 110 breeds, See **Table 1**). (D) FGF5 and RSPO2 govern variation in coat length and phenotype, this plot shows the relative distribution of coat length over the average weight of breeds (see methods). Note that the smaller the breed the more likely it is to have longer hair.

Other top GWAS hits were loci within or near mitochondrial and bioenergetic regulators including IGFBP2, MSRB3, ATP23, and TRMT5 (**Table 1**). IGFBP2 inhibits IGF signaling and its overexpression increases lifespan in mice (Hoeflich *et al.* 2016). Other identified genes - MSRB3, ATP23, and TRMT5 are known to regulate various mitochondrial properties, such as ROS production, respiration, and ATP synthesis (**Supplementary Information**). Importantly, and in addition to the aforementioned properties, mitochondria also have a prominent role in thermogenesis via proton uncoupling. Overall, the candidate genes identified by GWAS suggested mitochondrial-bioenergetic and thermoregulatory mechanisms as major factors driving canine aging diversity.

Table 1.

Across-breed life expectancy GWAS results with *p*-values below or near 1E-05.		
Top marker(s) in region (chr: position)	***P*-value**	**Candidate gene(s)**
10: 8183593	1.15×10^{8}	MSRB3, HMGA2
13: 8654384	5.46×10^{8}	RSPO2, ANGPT1
19: 19107981	1.19×10^{6}	PRDM5
8: 36016977	2.67×10^{6}	SLC38A6, TRMT5
32: 4503644	4.12×10^{6}	FGF5
10: 2185035	7.44×10^{6}	ATP23

10: 2201298 10: 2224239		
2: 59036686	1.24×10^5	
11: 47400651	1.28×10^5	
34: 18341784	1.54×10^5	IGF2BP2

To investigate differences in mitochondrial-bioenergetics in cells derived from different dog breeds we moved to *ex vivo* primary cell culture. We used a targeted mass spectrometry approach to profile major bioenergetic-metabolites. These included organic acids, amino acids, and acylcarnitine species (fatty acid derivatives primed for β-oxidation) in cells from a subset of breeds; Boxers (short-lived), Chihuahuas (long-lived), and Labradors (in between Boxer and Chihuahua) (**Supplementary Information**). Three independently prepared samples from each of five to seven donors per breed were used. Unsupervised hierarchical-clustering of measured metabolites clearly segregated by donor breed (**Fig. 2A**), suggesting that each breed has its own unique metabolite signature. Principal component analysis (PCA) of the separate metabolite classes revealed that acylcarnitines distinguished the breeds with the best resolution (**Fig. 2B**). Moreover, acylcarnitine clustering and PCA positioned Labradors as an intermediate between Boxers and Chihuahuas (**Fig. 2B**, **Fig. S1**), which mirrors the average lifespan of these breeds. These data indicate that bioenergetic metabolites (acylcarnitines in particular) derived from primary canine fibroblasts can predict the donor's breed, and importantly for our study, that there are

breed-distinct cellular metabolic profiles that are retained *in vitro*.

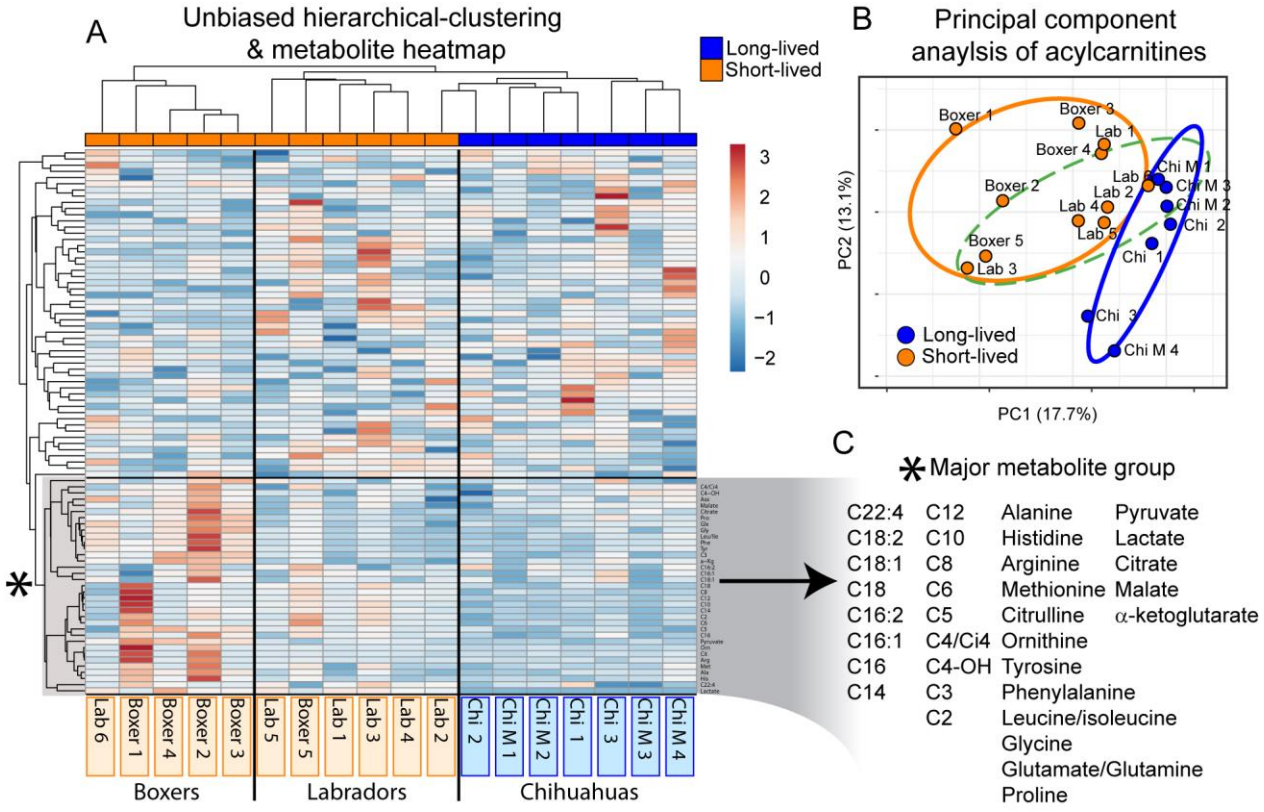

Figure 2. **Primary canine fibroblasts retain breed-specific bioenergetic-metabolite profiles *in vitro***. Multiple donors were utilized from: Chihuahuas, Chihuahuas-mixed (Chi-M), Labrador Retrievers, and Boxers for targeted mass spectrometry of organic-acids, amino acids, and acylcarnitines. Raw metabolite values were normalized to protein concentrations and averaged across three replicates for every donor cell line. (A) Unbiased hierarchical-clustering of donor metabolite profiles, note the clustering of donors by breed. (B) Principal component analysis of acylcarnintine metabolites. Circles denote 90% confidence interval (orange-short lived breeds, blue-long lived, dashed green-Labradors). (C) Magnification of major

metabolite branch driving distinctions between breeds. See **Supplementary Information** for raw data, fibroblast donor information, and analysis.

Next, we utilized the Seahorse Analyzer to measure rates of oxygen consumption and extracellular acidification, which represent oxidative phosphorylation/respiration and anaerobic glycolysis. We assessed metabolic rates before and after treating cells with oligomycin (which stimulates glycolysis) and FCCP (which maximizes respiration). In doing so, we could measure the baseline and maximum metabolic rates of cells. From these rates, we calculated the "metabolic potential," which is the degree of change in respiration or glycolysis from baseline to maximum possible levels. We observed no trends in respiration or glycolysis at baseline levels. However, the respiration potential clustered strongly by breed longevity, where long-lived breeds had on average 65% greater potential to upregulate their respiration ($p^{**} = 0.008$), when stimulated (**Fig. 3A, B**). Furthermore, the respiration potential significantly correlated with breed longevity ($R = 0.74$, $p^{*} = 0.024$). Greater respiration potential in long-lived breed cells could arise from two possible mechanisms: more abundant mitochondria or more efficient ETC complexes within mitochondria (less electron escape). To examine these possibilities, we utilized mitochondria-specific dyes. MitoTracker Green staining showed that the abundance of mitochondria was not significantly different between breeds (**Fig. 3C, E**). This suggests that the greater respiration potential of long-lived breeds derives from innate properties of the mitochondria and ETC.

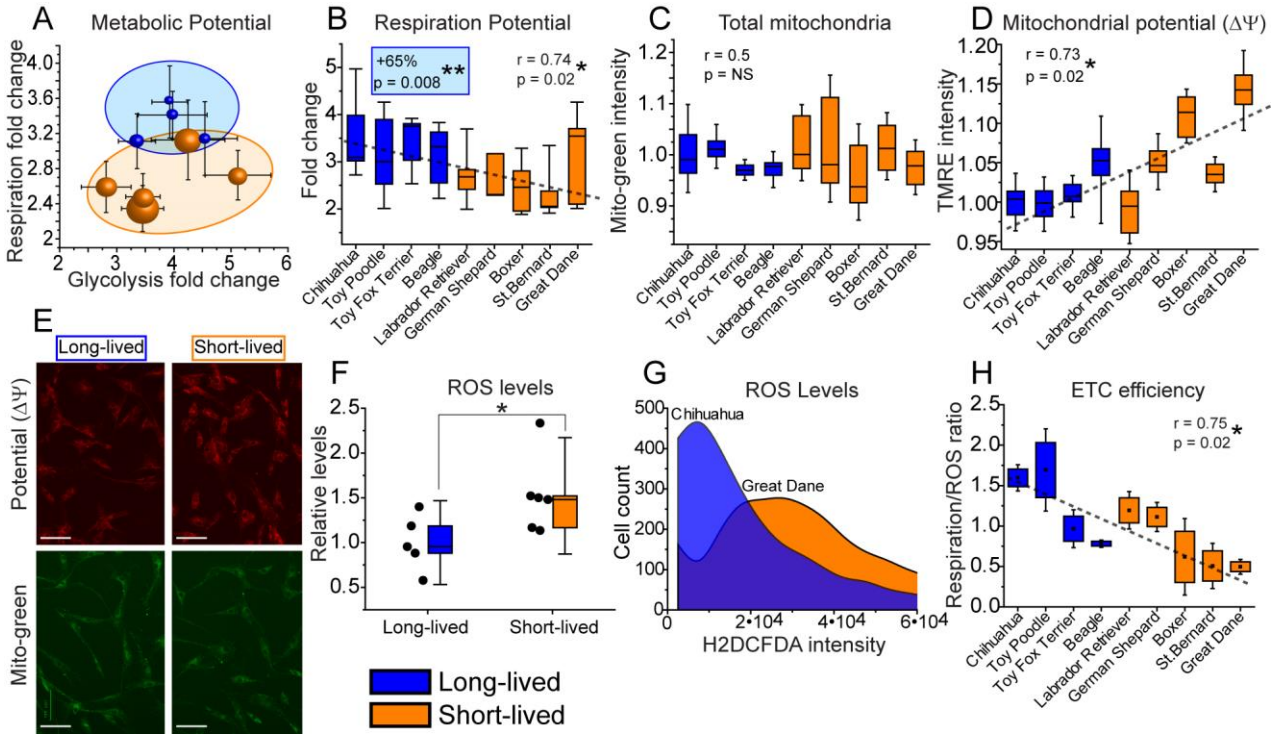

Figure 3. Fibroblasts from long-lived breeds have greater respiration potential, lower mitochondrial potential, and more efficient electron transport chains than short-lived breeds. Seahorse assay results are from 3-5 (dependent on breed) independent experiments. (A) Plot depicting seahorse assay results for metabolic potential with fold change of respiration (y axis) and glycolysis (x axis), standard error shown. Each point corresponds to an individual breed and the size of the point approximately correlates to the average size of the breed. Note the clustering of breeds by longevity on the respiration y-axis. (B) Box plot representations of the fold change in respiration depicted in A. Note the trend of decreasing respiration fold change with decreasing breed longevity. (C) Box plots of relative MitoTracker Green intensity (mitochondrial mass) in primary canine fibroblasts. (D) Box plots of relative TMRE (mitochondrial membrane potential-ΔΨ

intensity). (E) Representative fluorescent microscopy images of fibroblasts stained with MitoTracker Green and TMRE as quantified in C & D. Results are pooled from three independent experiments with standard deviations shown. Note the equivalent mitochondrial abundance between breeds but increasing potential with decreasing breed longevity. (F) Box plots depicting the average and relative levels of ROS in fibroblasts from long and short-lived breeds, measured by H2DCFDA staining. (G) Example of H2DCFDA staining in fibroblasts from the Chihuahua and Great Dane. (H) Electron transport chain efficiency calculated from the ratio of oxygen consumption under maximum ETC flux (measured by Seahorse) to ROS H2DCFDA intensity. Note short-lived breeds have and produce more ROS relative to oxygen consumed.

Next, to examine ETC properties we stained the fibroblasts with tetramethylrhodamine ethyl ester (TMRE), which measures the mitochondrial membrane potential ($\Delta\Psi$). The $\Delta\Psi$ represents the proton electrochemical gradient that is responsible for ATP production via oxidative phosphorylation. The movement of protons across the electrochemical gradient can be disconnected or "uncoupled" from ATP synthesis (notably for thermogenesis). Furthermore, the degree of uncoupling inversely correlates with the $\Delta\Psi$, where increased uncoupling results in lower $\Delta\Psi$ and lower uncoupling results in a higher $\Delta\Psi$. We found that the $\Delta\Psi$ correlated with breed longevity ($R = 0.73$, $p^* = 0.027$), where long-lived breeds had lower $\Delta\Psi$, with the difference being as high as 15% between breeds (**Fig. 3D, E**). The lower $\Delta\Psi$ in long-lived breeds indicates more proton uncoupling and further suggests innate variation in

mitochondrial and ETC properties between long and short-lived breeds.

Differences in mitochondrial membrane potential ($\Delta\Psi$) and the degree of uncoupling influence ROS production. More specifically, the higher the $\Delta\Psi$, the higher the rate of mitochondrial ROS production (Mookerjee *et al.* 2010). The main source of ROS is electrons that escape from the ETC, which generate superoxides (precursors to harsher ROS) instead of oxygen reduction by respiration. Because we observed differences in the $\Delta\Psi$ between long and short-lived breeds, we next measured cellular ROS using H2DCFDA dye. We found that cells from long-lived breeds had reduced levels of ROS compared to short-lived (**Fig. 3F, G**). This suggests that long-lived breed fibroblasts do have more efficient ETCs, as their baseline respiration is equivalent to short-lived breeds but ROS levels are lower, meaning they have less electrons escaping. ETC efficiency can also be gauged from the ratio of oxygen consumed to ROS produced. A higher ratio indicates greater ETC efficiency, as more oxygen is converted to water versus ROS. We found that the respiration/ROS ratio correlated with breed longevity ($R = 0.75$, $p^* = 0.02$), particularly under maximum ETC flux and respiration, with long-lived breeds having superior efficiency (**Fig. 3H**). These data suggest that longer-lived breeds have a greater respiration potential due to more efficient ETCs. Overall, the data show that mitochondria of longer-lived breeds are more uncoupled, have lower $\Delta\Psi$, and have more efficient ETCs that produce less ROS. Furthermore, these data suggest that long-lived breed cells would more readily handle bioenergetic stress.

The stress tolerance of cells has been shown to correlate with organismal and species

longevity (Murakami *et al.* 2003; Harper *et al.* 2011), including variation in metabolic response to oxidative and nutrient stress (Wang & Miller 2012). Furthermore, mild mitochondrial uncoupling is known to promote cellular survival, particularly under stress (Baffy *et al.* 2011). We hypothesized that long-lived breed fibroblasts would tolerate oxidative and nutrient stress more effectively due to being more uncoupled and having more efficient ETCs that produce less ROS. To test this, we stressed cells with nutrient deprivation or rotenone exposure. Survival of cells was measured by staining with the apoptosis markers Annexin-V and propidium iodide followed by flow cytometry, as described previously (Domanskyi *et al.* 2017). Fibroblasts from long-lived breeds survived on average 8% more after rotenone challenge ($p^* = 0.01$) (**Fig. 4B**). Moreover, there was a significant correlation between breed longevity and survival after nutrient deprivation ($R = 0.58$, $p^* = 0.03$), where long-lived breed fibroblasts had up to 25% greater survival (**Fig. 4A, C**). These data demonstrate that long-lived breed cells possess greater stress tolerance than those from short-lived breeds, especially in low nutrient conditions.

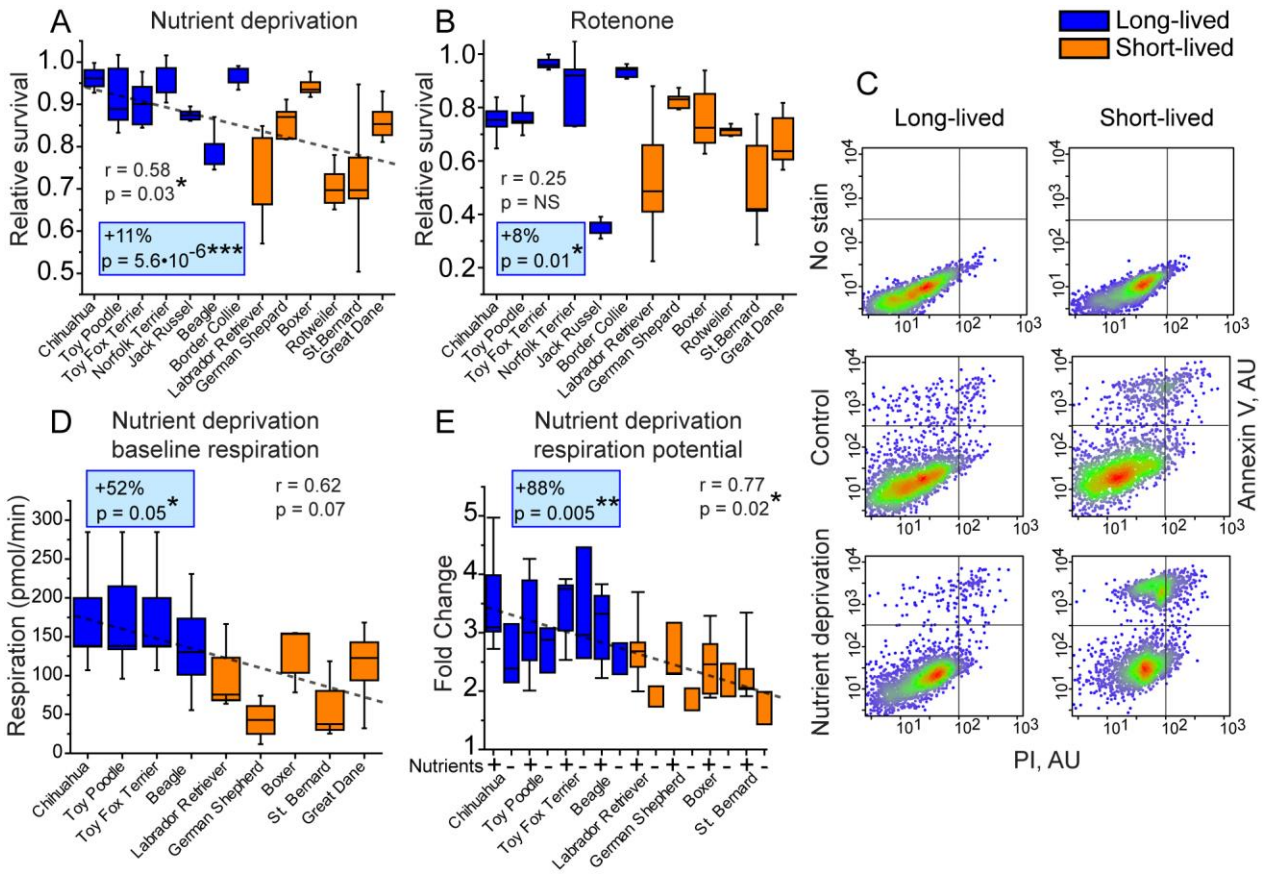

Figure 4. Fibroblasts from long-lived breeds have greater stress tolerance and consume more oxygen in low nutrient conditions. Box plots showing relative survival of fibroblasts after (A) nutrient deprivation and (B) rotenone exposure. (C) Example of flow cytometry plots (Annexin V by PI staining) used to quantify survival of fibroblasts as depicted in A & B. Relative survival is defined as the fraction of cells unstained by Annexin or PI. (D) Baseline respiration rates measured by Seahorse under low nutrient conditions. (E) Respiration potential measured by Seahorse under low nutrient conditions, also shown is potential under nutrient replete conditions. Cells from long-lived donors have elevated baseline and potential respiration under low nutrient conditions.

Next, we performed Seahorse analysis on the fibroblasts with low nutrients to asses if mitochondrial response also varied between breeds in this condition. Fascinatingly, we found a stronger correlation of baseline respiration and breed longevity with low nutrients, where respiration was 52% ($p^* = 0.05$) higher on average in long-lived breeds (**Fig. 4D**). The respiration potential was also significantly higher for long-lived breeds and correlated with breed longevity (**Fig. 4E**). An argument can be made that these low *in vitro* nutrient conditions more accurately reflect a physiologically-relevant state. Cells in tissues (especially in skin) are not saturated with glucose and growth factors, as they are *in vitro*. Overall, these data suggest that long-lived breed fibroblasts are more uncoupled, produce less ROS, and have a greater respiratory capacity (due to more efficient ETCs). These differences are apparent under normal physiological stress and contribute to the cells' greater stress tolerance and survival.

To maintain greater proton uncoupling and respiration, cells from long-lived breeds need greater substrate oxidation to fuel their ETCs and the pumping of protons to the mitochondrial intermembrane. Detailed analysis of our mass spectrometry data revealed a significant enrichment of acylcarnitines in short-lived breeds (**Fig. 5B**). Long-chain acylcarnitines (C14 and above) normally undergo β-oxidation and generate energy to fuel the ETC. The accumulation of these long-chain acylcarnitines suggests that this process is partially blocked in short-lived breeds. Such a blockade could result in diminished respiration, elevated glycolysis, and promotion of "Warburg effect"-like conditions. Indeed, we observed lower respiration in short-lived breeds, including the Labrador and Boxer (**Fig. 3B, Fig. 4D**)**.** Additionally, cells from short-

lived breeds had higher concentrations of pyruvate and lactate, suggesting increased reliance on glycolysis (**Fig. 5A**). Under such conditions, cells will also preferentially shuttle metabolites for biosynthesis. The short-lived breeds had higher concentrations of many amino acids (particularly the Boxers, the shortest-lived breed in this analysis), supporting enrichment in biosynthesis (**Fig. 5A**). Interestingly, serine was the only amino acid enriched in the long-lived Chihuahuas and is required for a major detoxification pathway involved in longevity (Kabil *et al.* 2011). Overall, these data suggest that longer-lived breeds are utilizing amino acid catabolism and fatty acid oxidation to fuel their uncoupled-energetic demands, whereas short-lived breeds preferentially shuttle metabolites into biosynthetic pathways.

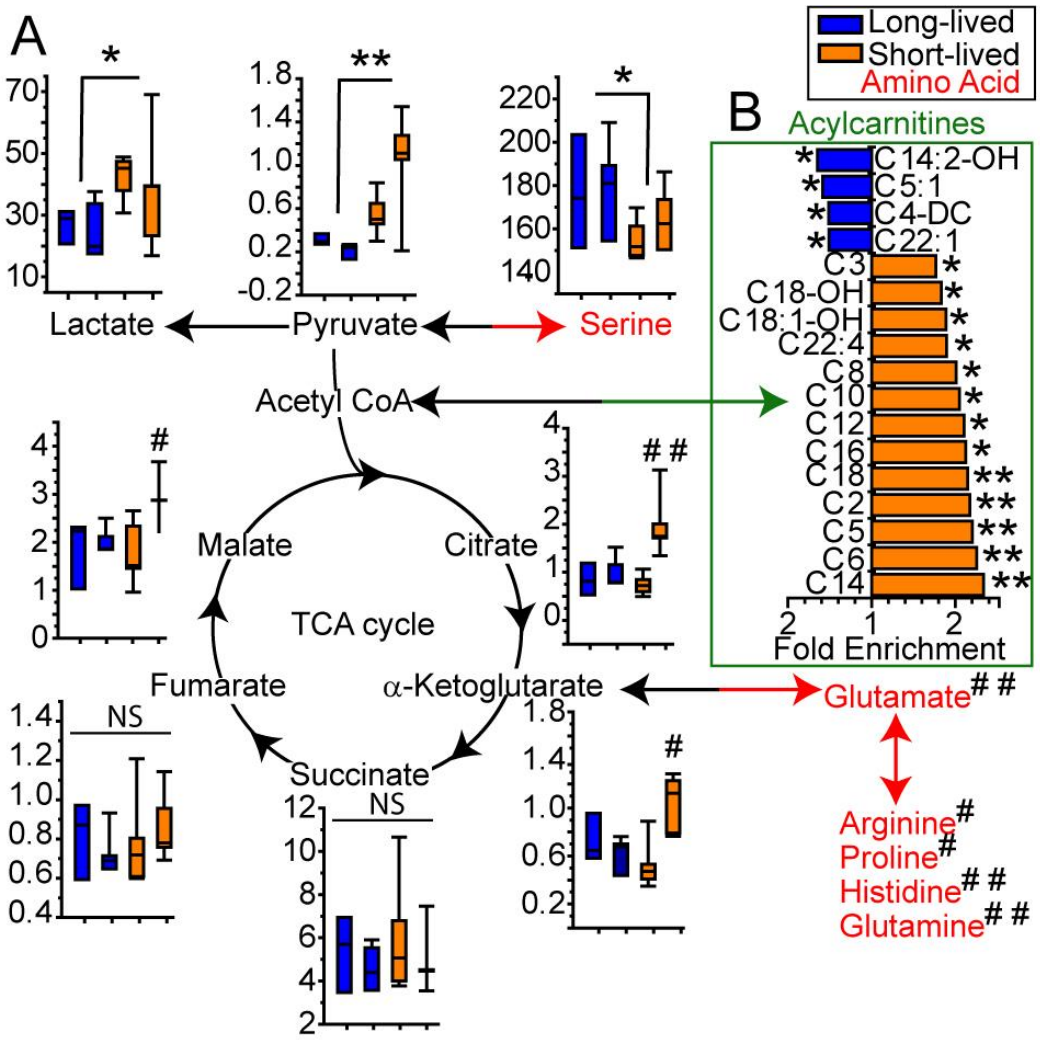

Figure 5. Short-lived breeds are enriched in acylcarnitines, amino acids, and glycolytic metabolites. Raw metabolite values were normalized to protein concentrations and averaged across three replicates for every donor cell line. * Indicates significant difference, in the respective metabolite, between the short and long-lived breeds. # indicates significant difference between the Boxers and all other breeds. (A) Glycolysis and citric acid cycle metabolite pathway schematic. (B) Fold enrichment of significantly different acylcarnitines between short and long-lived breeds. See **Supplementary Table 3** for raw data, fibroblast donor information, and

analysis.

In addition to metabolic and survival dynamics, the functionality of tissues also depends on physical properties of cells. Here, we applied atomic force microscopy (AFM) combined with a brush computational model to measure the elastic modulus (rigidity) on a subset of canine fibroblasts. There was a correlation of rigidity with breed longevity, despite only four breeds being represented (Beagle, Labrador, St. Bernard, and Great Dane). The short-lived Great Dane had significantly stiffer cells at both early and late passages, while the Beagle (longest-lived breed used for AFM) had the most flexible overall (**Fig. S2**). These data suggest that shorter lived-breed fibroblasts are stiffer than their longer-lived counterparts, due to an altered cytoskeleton. More flexible cells may be better able to mitigate ROS and other damage because they are more deformable in response to everyday mechanical stresses. This would help maintain cellular function and homeostasis through age.

DISCUSSION:

In this study we demonstrate innate variation in mitochondrial-bioenergetics between cells of short- and long-lived dog breeds. We show that primary canine fibroblasts have equivalent mitochondrial mass but that long-lived (smaller) breeds have a lower $\Delta\Psi$ (**Fig. 3C, D**), indicating more uncoupling. When the fibroblasts are not saturated with nutrients, which is more representative of the *in vivo* tissue microenvironment, we observe higher baseline respiration in long-lived breeds (**Fig. 4C**), supporting a

higher metabolic rate and uncoupling. Mild mitochondrial uncoupling lowers $\Delta\Psi$ and ROS levels and increases ETC flux and respiration (Brand *et al.* 2004). In fact, mild uncoupling in primary human dermal fibroblasts suppresses ROS (Cho *et al.* 2014). We find that fibroblasts from long-lived breeds have greater respiration potential (consume more oxygen with maximized ETC flux) and produce less ROS (**Fig. 3B, F**). This suggests that longer-lived breeds move electrons through the ETC more efficiently with less escaping to form ROS. Regardless of nutrient conditions, long-lived breed fibroblasts have greater respiration potential (**Fig. 3B, Fig. 4E**), which further supports superior efficiency in their ETCs.

The innate variation in uncoupling and ETC properties has functional consequences on stress tolerance. Specifically, short-lived breeds display lower respiration, more ROS, and greater cell death under nutrient and oxidative stress (**Fig. 4**). These properties are also regulated by the distribution and motility of mitochondria in a cell, which is dependent on the cytoskeleton. The fibroblasts from the shortest-lived breed in our study had the stiffest actin-cytoskeleton, while the longest-lived had the most flexible (**Fig. S2**), which potentially contributes to variation in mitochondrial function and stress tolerance. Furthermore, mitochondrial stress and ROS hasten telomere attrition and its associated dysfunctions (Sanderson & Simon 2017). Inferior mitochondrial stress response and ROS management in short-lived breeds may explain their reduced telomere length in comparison to long-lived breeds (Fick *et al.* 2012).

Mass spectrometry revealed unique bioenergetic-metabolite signatures that persist in primary culture and distinguish breeds (**Fig. 2, Fig. S1**). Fibroblasts of short-lived

breeds have higher amino acid concentrations (**Fig. 5**); agreeing with the results from a study which examined *in vivo* plasma metabolites in dogs (Middleton *et al.* 2017). Acylcarnitines were also significantly enriched in short-lived breeds (**Fig. 5B**) and showed strong clustering and predictive capacity for breed longevity (**Fig. 2B**). A study on plasma lipids in dogs also showed strong clustering by breed, with differences in long-chain fatty acids being a significant factor (Lloyd *et al.* 2017). The accumulation of amino and fatty acids in large short-lived breeds suggests preferential shuttling of these molecules for biosynthesis, whereas long-lived (small) breeds likely oxidize these products to sustain uncoupling. Indeed, mitochondrial uncoupling is associated with increased β-oxidation (Sukumar *et al.* 2016).

In addition to dampened ROS, an alternative or parallel mechanism that could promote cellular function downstream of uncoupling would be caloric restriction (CR) like metabolism. A CR-like metabolic state induces quality control processes, suppresses ROS and oxidative damage, and promotes β-oxidation. Long-lived breeds likely have lower concentrations of acylcarnitines due to higher fatty acid breakdown (**Fig. 5B**). This would explain how long-lived breeds maintain their uncoupled energetics, which requires greater substrate oxidation to supply electrons to the ETC (**Fig. 6**). Further supporting a CR-like metabolic state is the reduced levels of cellular pyruvate and lactate in the long-lived breeds (**Fig. 5A**), because CR suppresses glycolysis. These data suggest that larger short-lived dogs have a more glycolytic cellular profile, which has been observed (Jimenez *et al.* 2018). Greater reliance on glycolysis in larger dogs may predispose them to cancer and other diseases. Furthermore, decreased uncoupling

combined with lower β-oxidation and accumulation of acylcarnitines promotes inflammation, oxidative stress, cell death, and disease (McCoin *et al.* 2015). Together these metabolic properties reduce cellular stress tolerance and may contribute to the suppressed longevity of large dogs.

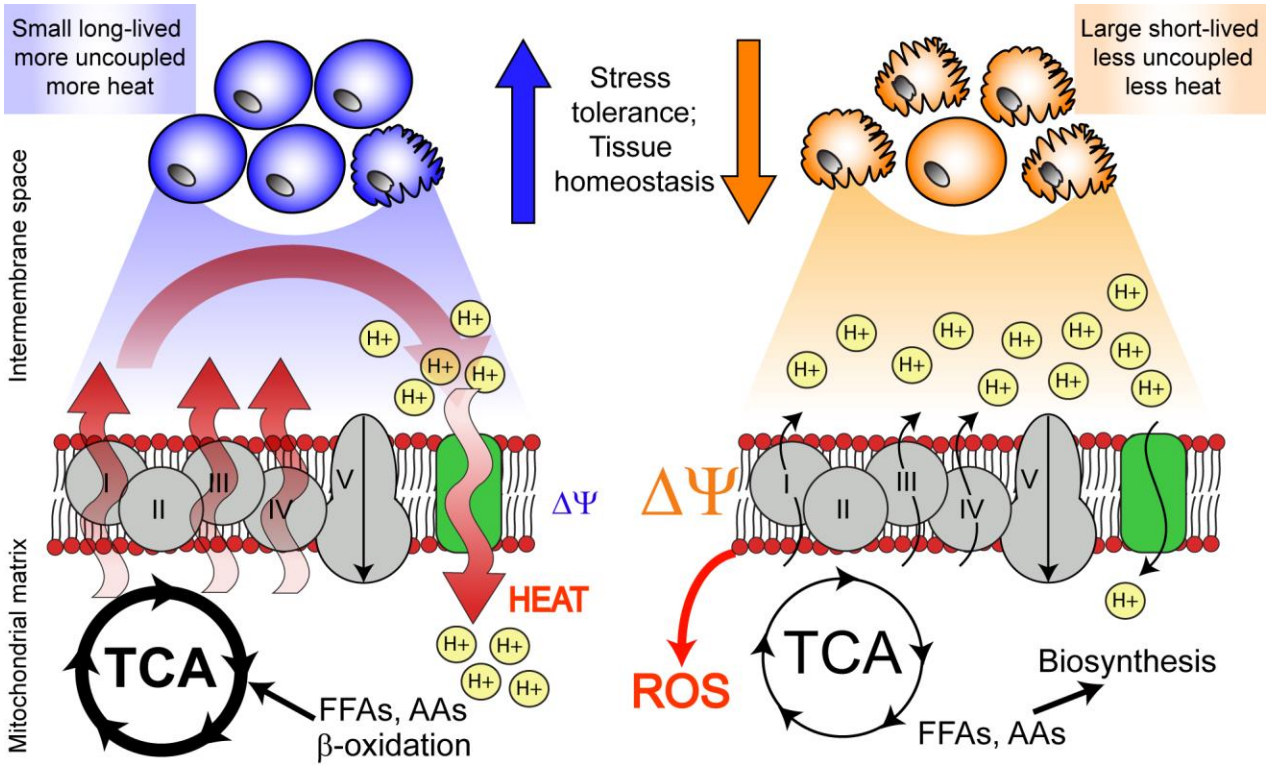

Figure 6. Model of canine aging diversity. We propose that smaller dogs, due to extra demand for thermogenesis, evolved or responded to have more uncoupled mitochondria, which in turn results in lowered electrical potential (due to proton leak), and elevated β-oxidation and catabolism (in order to fuel uncoupled mitochondria). We suggest that the secondary changes associated with these adaptations happen to be beneficial for longevity; these include decreased production of reactive oxygen species, metabolic profiles which are less favorable for tumorigenesis, increased cytoskeletal flexibility, and resistance to stress (affording superior tissue homeostasis

and longevity). Conversely, larger breeds might preferentially use energy for biosynthesis to maintain their greater mass. Overall, our data suggest that lifespan variation across canine breeds is partially regulated by innate cellular properties.

Smaller breeds have a higher metabolic rate and utilize more energy per gram of tissue than larger breeds (Speakman *et al.* 2003; National Research Council (U.S.). Ad Hoc Committee on Dog and Cat Nutrition. 2006). Small dogs need to expend more energy via uncoupling and adaptive thermogenesis to maintain homeostatic temperature. The identification of FGF5 and RSPO2, genes that regulate coat phenotypes (Housley & Venta 2006; Cadieu *et al.* 2009), to associate with breed-longevity further supports a connection between thermoregulation and canine longevity (**Table 1**, **Fig. 1D**). The fact that dogs possess strategies for thermoregulation at the organismal level (coat length) would support that cellular mechanisms, such as uncoupling, are present and or evolved. Our data suggest that smaller long-lived dogs have a higher metabolic rate to fuel uncoupled energetics and thermogenesis (**Fig. 6**). Moreover, naturally higher or induced uncoupling increases mammalian lifespan with elevated respiration and suppressed oxidative damage (Speakman *et al.* 2004; Caldeira da Silva *et al.* 2008). Furthermore, our data show a superior response to bioenergetic stress in long-lived breed cells. The increase in uncoupling and superior stress response would confer metabolic and survival advantages for cells and tissues (**Fig. 6**). This would suppress the functional decline of tissues, staving off dysfunction and disease, and help to explain why small dogs have greater longevity. Overall, our data agree with the "uncoupling to survive" and "oxidative damage" theories of aging, which respectively posit that greater uncoupling (Brand 2000) and lower ROS-induced damage (Harman

1956) promote longevity. However, the "rate of living" theory has garnered recent support in human CR trials (Redman *et al.* 2018). It may be that increased metabolism is maladaptive to longevity, but when caused by and paired with uncoupled energetics is beneficial.

In the future it will be important to investigate which pathways are responsible for bioenergetic variation between long and short-lived breeds and how they are regulated. Are cells from small long-lived breeds more uncoupled because of a thermodynamic response (that is retained *in vitro* epigenetically), or because they are hardwired at the DNA level? IGF-1 is not likely to be responsible for variation in cellular metabolism across breeds, as we observed no differences in its expression (**Fig. S3**). Additionally, examination of passive versus regulated mitochondrial uncoupling may be informative, as uncoupling proteins associate with human longevity (Rose *et al.* 2011). Modeling these bioenergetic properties in human populations with variable lifespans is similarly worth pursuing and provides a novel avenue for aging research.

SUPPLEMENTARY INFORMATION

Notes on GWAS candidates and SNPs:

Insulin-like growth factor binding protein 2 (IGFBP2) functions to inhibit IGF signaling but also has effects independent of IGF's. IGFBP2 overexpression increases lifespan in mice (Hoeflich *et al.* 2016) and can ameliorate diabetic pathology (Hedbacker *et al.* 2010). Methionine sulfoxide reductase B3 (MSRB3) is an

antioxidant enzyme that repairs proteins damaged by reactive oxygen species (ROS). Mammalian MSRB3 is localized to the endoplasmic reticulum and mitochondria, promotes cellular stress resistance (Kwak *et al.* 2012), and is important for healthy aging and longevity in *Drosophila* (Lim *et al.* 2012). Metallopeptidase and ATP synthase assembly factor homolog (ATP23) is a protease critical for ATP-synthase assembly in the mitochondria (Osman *et al.* 2007). While TRMT5, tRNA methyltransferase 5, regulates various mitochondrial functions like respiration, membrane potential, and ROS generation (Zhou *et al.* 2017). Furthermore, mutations in human TRMT5 are associated with respiratory-chain deficiencies (Powell *et al.* 2015).

	CHR	SNP	BP	n_miss	allele1	allele0	af	beta	se	P
11038	2	BICF2P1258111	59036686	0	A	C	0.058	0.048731	0.011138	1.24E-05
43317	8	BICF2S23757907	36016977	0	A	C	0.051	-0.06476	0.013774	2.67E-06
44555	8	BICF2P86355	56373545	0	A	T	0.134	-0.03416	0.007867	1.44E-05
49659	10	BICF2P633408	2185035	0	A	C	0.16	-0.04952	0.011038	7.44E-06
49660	10	BICF2P80262	2201298	0	G	A	0.16	-0.04952	0.011038	7.44E-06
49661	10	BICF2S23211324	2224239	0	A	G	0.16	-0.04952	0.011038	7.44E-06
49665	10	BICF2S23642724	2378696	0	A	G	0.099	-0.06536	0.015098	1.53E-05
49830	10	BICF2S23762663	6711713	0	C	A	0.158	0.038588	0.008049	1.69E-06
49912	10	G580f46S240	8183593	0	A	G	0.127	0.071478	0.0125	1.15E-08
49980	10	BICF2S23554577	9518669	0	T	A	0.109	0.051135	0.010641	1.6E-06
49984	10	BICF2S23611584	9566309	0	A	G	0.133	0.045435	0.00979	3.57E-06
56177	11	G697f11S121	47400651	0	G	A	0.066	-0.04374	0.010013	1.28E-05

63459	13	BICF2P1389702	8391652	0	A	G	0.177	0.057764	0.010948	1.39E-07
63480	13	BICF2P112526	8654384	0	A	G	0.293	0.059352	0.010899	5.46E-08
87972	19	BICF2G63041764	19107981	0	A	G	0.049	0.061269	0.012597	1.19E-06
129738	32	BICF2G630600871	4503644	0	A	G	0.256	-0.03015	0.006539	4.12E-06
135497	34	BICF2P1324672	18341784	0	A	C	0.332	0.029381	0.006789	1.54E-05

Table 2: Donor Information:

Experiment:	TMRE & MitoTracker Green				H2DCFDA		
	Breed	**Donor ID**	**Age (years)**		**Breed**	**Donor ID**	**Age (years)**
	Toy Poodle	CF56	6.0		Toy Poodle	CF56	6.0
	Labrador Retriever	1 lab	2		Labrador Retriever	1 lab	2
	Saint Bernard	192820	3.0		Saint Bernard	192820	3.0
	Beagle	CuteB	5.0		Beagle	CuteB	5.0
	Boxer	CF10	6.0		Boxer	CF10	6.0
	Fox Terrier (toy)	CF30	0.6		Chihuahua	CF49	1.0
	Chihuahua	CF49	1.0		Great Dane	196071	0.6
	Great Dane	196071	0.6		German Shepherd	194951	6.5
	German Shepherd	194951	6.5		Jack Russel	197757	1.1
					Border Collie	200396	2.5
					Rottweiler	199252	2.0
					Norfolk Terrier	199514	0.8

Apoptosis Analysis				Atomic Force Microscopy		
Breed	**Donor ID**	**Age (years)**		**Breed**	**Donor ID**	**Age (years)**
Toy Poodle	CF56	6.0		Labrador Retriever	200289	0.7
Labrador	1 lab	2		Saint Bernard	192820	3.0

Retriever						
Saint Bernard	192820	3.0		Beagle	CuteB	5.0
Beagle	CuteB	5.0		Great Dane	196071	0.6
Boxer	CF10	6.0				
Chihuahua	CF49	1.0				
Great Dane	196071	0.6				
German Shepherd	194951	6.5				
Jack Russel	197757	1.1				
Border Collie	200396	2.5				
Rottweiler	199252	2.0				
Norfolk Terrier	199514	0.8				
Fox Terrier (toy)	CF30	0.6				

Seahorse					**Mass Spectrometry**	
Breed	**Donor ID**	**Age (years)**		**Breed**	**Donor ID**	**Age (years)**
Toy Poodle	CF56	6.0		Boxer	CF37	0.6
Labrador Retriever	1 lab	2		Boxer	CF59	1.5
Saint Bernard	192820	3.0		Boxer	CF44	1.5
Beagle	CuteB	5.0		Boxer	CF24	5.1
Boxer	CF10	6.0		Boxer	CF10	6.0
Fox Terrier (toy)	CF30	0.6				
Chihuahua	CF49	1.0		Labrador Retriever	200289	0.7
Great Dane	196071	0.6		Labrador Retriever	196275	3.0
German Shepherd	194951	6.5		Labrador Retriever	C52	7.0
				Labrador Retriever	155085	10.5
				Labrador Retriever	196074	11.8
				Labrador Retriever	192987	12.8
				Chihuahua	CF49	1.0
				Chihuahua	CF62	1.0
				Chihuahua	CF39	4.1

				Chihuahua mix	CF55	0.7
				Chihuahua mix	CF 47	1.5
				Chihuahua mix	CF45	1.5
				Chihuahua mix	CF36	2.1

qRT-PCR		
Breed	**Donor ID**	**Age (years)**
Norfolk Terrier	199514	0.8
Jack Russel	197757	1.1
Beagle	CuteB	5.0
Border Collie	200396	2.5
English Bulldog	197747	1.0
Viszla	196110	8.0
Golden Retreiver	200253	0.5
German Shepherd	194951	6.5
Giant Schnauzer	200399	2.5
Rottweiler	199252	2.0
Saint Bernard	192820	3.0
Great Dane	196071	0.6

Breed Lifespans (years):

Chihuahuas	**16**
Norfolk Terriers	14
Toy Fox Terriers	13.75
Toy poodle	13.5
Russell Terriers	13
Beagles	12.75
Border Collies	12.75
Golden Retrievers	11.25
Labrador Retrievers	11
Vizslas	10.575
Boxers	10
English Bulldogs	10
German Shepherd Dogs	9.75
Giant Schnauzers	9.75
Rottweilers	9
St. Bernards	9

Great Danes	7.75

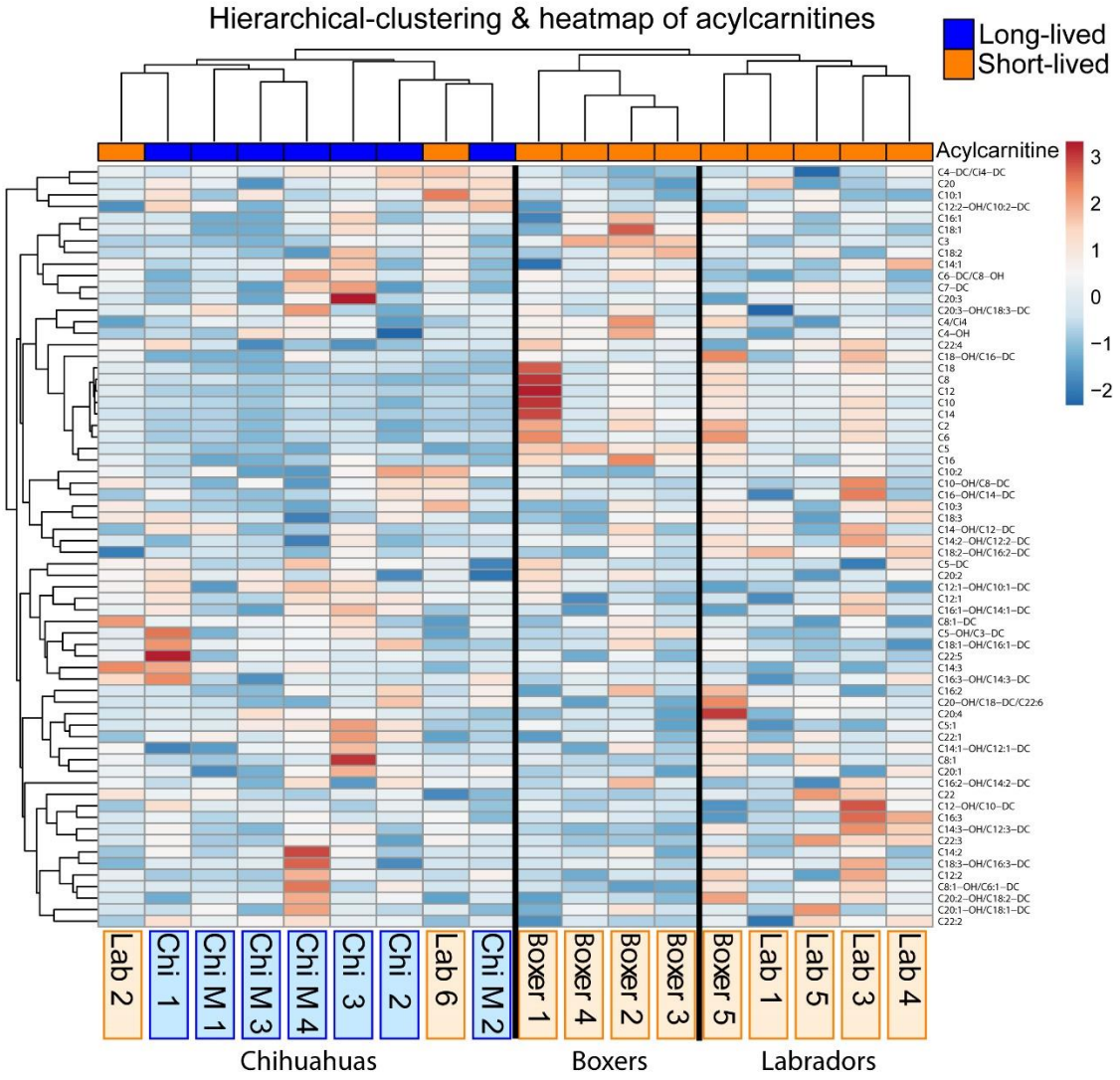

Supplemental Figure 1. **Acylcarnitine profiles have strong predictive power for canine breed.** Unbiased hierarchical-clustering of donor acylcarnitine profiles, note the clustering of donors by breed and the separation of breeds by longevity.

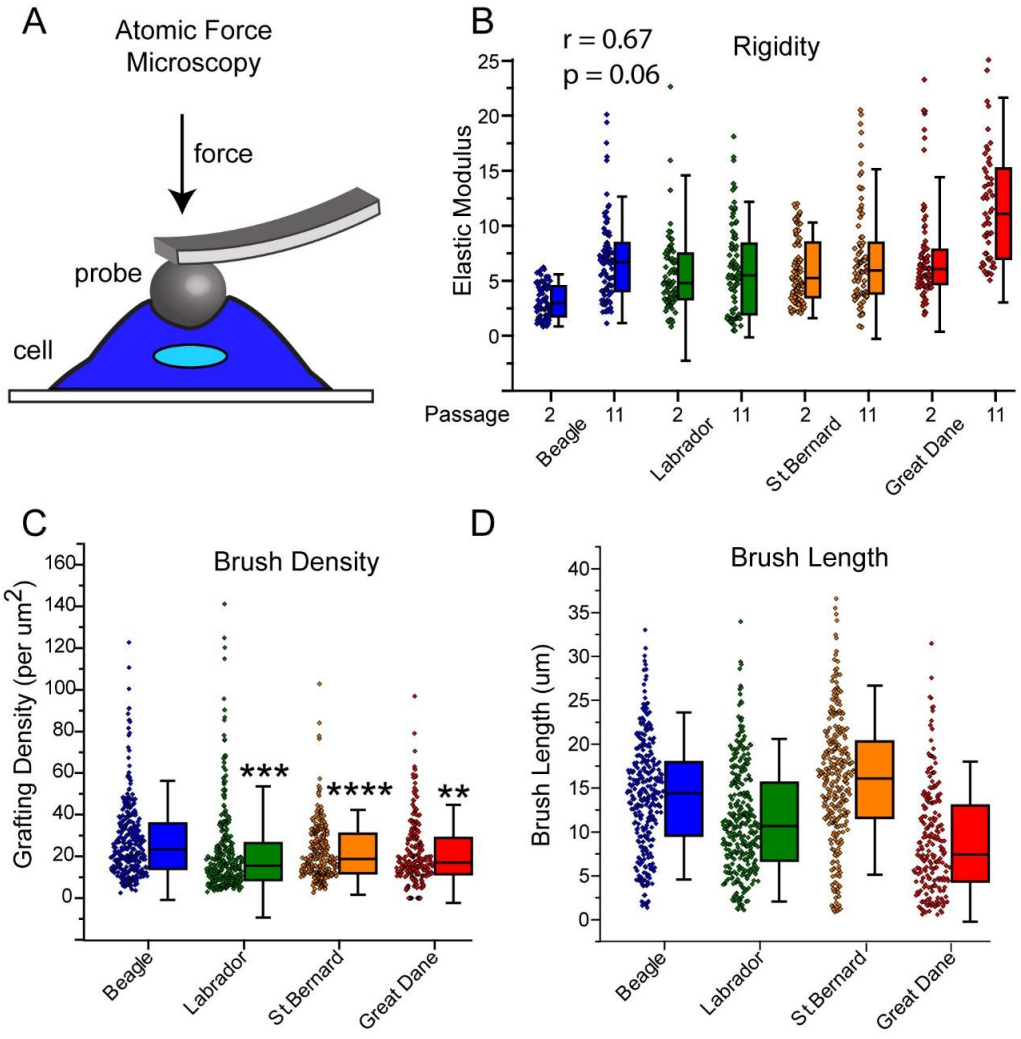

Supplemental Figure 2. **Fibroblasts from long-lived dog have a more flexible cytoskeleton than those from short-lived.** (A) Schematic representation of Atomic Force Microscopy (AFM) applied to an individual cell. (B) Boxplots of elastic modulus (rigidity) of canine fibroblasts at passages two and eleven as measured by AFM. Note the increasing rigidity of cells with decreasing breed lifespan, as well as increasing passage number. P-values for passage 2: Beagle vs Labrador = $1.5 \cdot 10^{-5}$, Beagle vs St. Bernard = $5.5 \cdot 10^{-12}$, Beagle vs Great Dane = $6.1 \cdot 10^{-12}$. (C) Boxplots of brush density for all passages as measured by AFM. Note that the

Beagle fibroblasts have the highest density. P-values: Beagle vs Labrador = 0.0006, Beagle vs St. Bernard = 0.00002, Beagle vs Great Dane = 0.002. (D) Boxplots of brush length for all passages as measured by AFM. Note the Great Dane's cells have the shortest brush length. P-values: Beagle vs Labrador = $3.8 \cdot 10^{-8}$, Beagle vs St. Bernard = $1.2 \cdot 10^{-3}$, Beagle vs Great Dane = $3.3 \cdot 10^{-19}$.

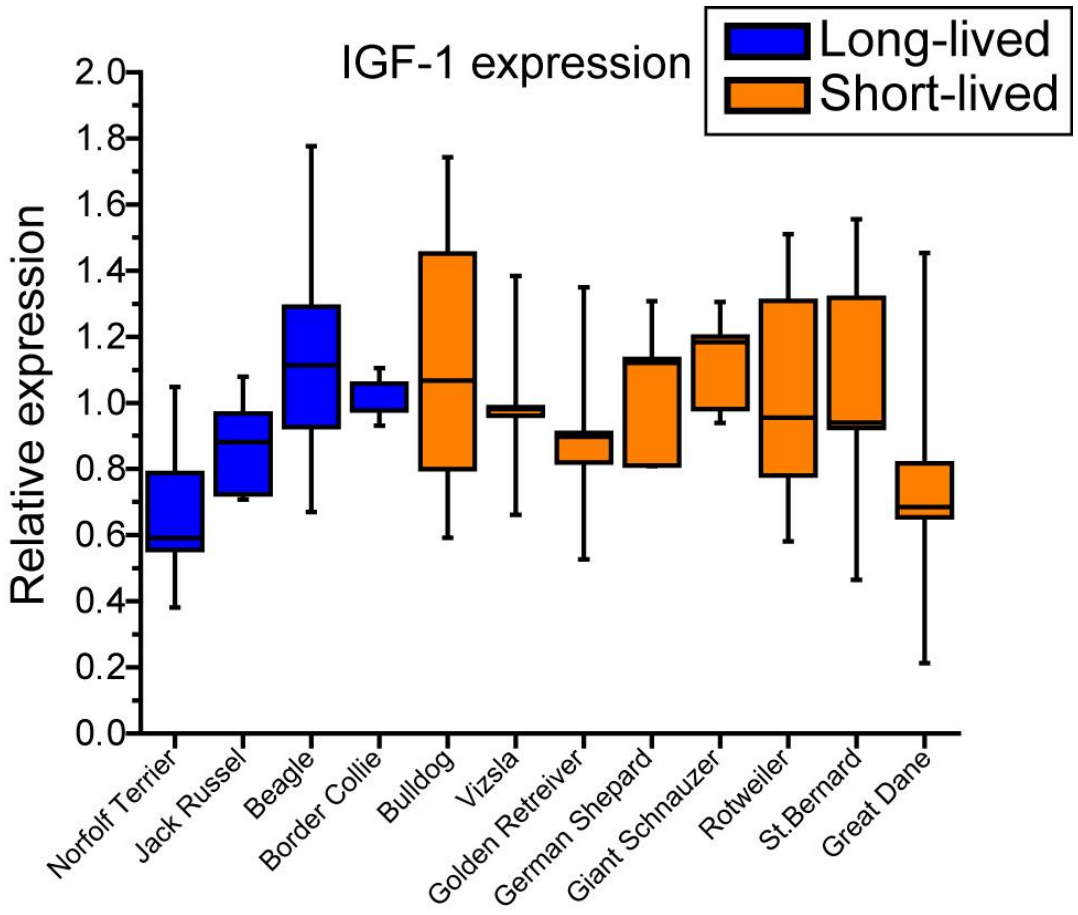

Supplemental Figure 3. **IGF-1 expression in primary fibroblasts is not different across breeds**. IGF-1 expression was assessed by qRT-PCR (n = 3 per breed), with no significant trend observed. This suggests that the variation in cellular metabolism in primary fibroblasts derived from short and long-lived breeds is

not due to IGF-1.

Table 3: Mass Spectrometry Data

Organic Acids		All averaged - Normalized to protein (uM/mg)						
		Lactate	**Pyruvate**	**Succinate**	**Fumarate**	**Malate**	**a-Kg**	**Citrate**
Boxer	Avg	37.6221	1.0299	4.8973	0.8660	2.7985	1.0380	1.9879
	SEM	1.3993	0.0332	0.1434	0.0138	0.0639	0.0210	0.0483
Lab	Avg	42.6907	0.5447	5.9339	0.7833	1.7499	0.5288	0.7450
	SEM	0.5835	0.0107	0.1884	0.0124	0.0415	0.0107	0.0196
Chi Mix	Avg	24.5704	0.3011	4.8502	0.7461	2.0828	0.6447	1.0607
	SEM	0.7744	0.0078	0.1580	0.0125	0.0416	0.0181	0.0392
Chi	Avg	30.3910	0.2077	5.3722	0.8118	1.8575	0.7283	0.8427
	SEM	1.6713	0.0090	0.3028	0.0237	0.0788	0.0237	0.0395
Amino Acids		All averaged - Normalized to protein (uM/mg)						
		Glycine	**Alanine**	**Serine**	**Proline**	**Valine**	**(Iso)Leucine**	**Methionine**
Boxer	Avg	197.2135	62.9886	164.6370	46.9447	92.0606	100.2677	32.7907
	SEM	3.9009	1.1470	1.2822	1.0283	1.4843	2.8565	0.6152
Lab	Avg	140.9738	40.3389	155.1497	28.8407	101.2904	68.0847	24.8289
	SEM	1.8426	0.5484	0.7149	0.4557	1.5063	1.2567	0.3520
Chi Mix	Avg	125.2052	40.2605	183.4545	26.8631	80.7027	63.1470	24.5550
	SEM	1.8577	0.5549	2.9109	0.4901	1.3130	1.7769	0.4403
Chi	Avg	136.2781	39.6628	176.3790	33.3384	76.5339	55.8790	21.4354
	SEM	2.9862	0.7604	4.0218	1.4612	2.5160	1.4656	0.4219
		Histidine	**Phenylalanine**	**Tyrosine**	**Asparta**	**Glutamate & Glutamine**	**Ornithine**	**Citrulline**
Boxer	Avg	29.0089	48.9691	58.9320	108.9549	418.8632	12.7505	9.6428
	SEM	0.6433	1.1948	1.3966	1.3260	10.4900	0.6576	0.5306
Lab	Avg	15.0326	28.4735	35.0428	93.3790	259.3618	5.4525	3.4895
	SEM	0.2109	0.6107	0.6302	1.4826	6.7692	0.0495	0.0605
Chi Mix	Avg	16.3264	26.9458	33.9110	99.2777	257.0307	3.9335	3.1724

	SEM	0.4059	0.6535	0.7545	1.8753	5.4124	0.0620	0.1108
Chi	Avg	13.0707	25.2599	28.6046	88.2701	280.5961	3.7053	2.7046
	SEM	0.1687	0.5161	0.9236	1.6879	7.5580	0.0562	0.0815
Boxer	Avg	**Arginine**						
	SEM	13.3534						
Lab	Avg	0.5271						
	SEM	6.7545						
Chi Mix	Avg	0.0493						
	SEM	6.4641						
Chi	Avg	0.1681						
	SEM	6.0032						
		0.1203						
Acylcarnitines		All averaged - Normalized to protein (uM/mg)						
		C2	**C3**	**C5:1**	**C5**	**C6**	**C4-DC/Ci4-DC**	**C8**
Boxer	Avg	0.6493	0.4290	0.0622	0.1465	0.0807	0.0058	0.0688
	SEM	0.2253	0.0864	0.0094	0.0127	0.0408	0.0017	0.0379
Lab	Avg	0.4237	0.2786	0.0557	0.0862	0.0579	0.0082	0.0421
	SEM	0.1491	0.0566	0.0064	0.0225	0.0181	0.0050	0.0147
Chi Mix	Avg	0.2729	0.2111	0.0652	0.0588	0.0309	0.0105	0.0263
	SEM	0.0597	0.0186	0.0074	0.0061	0.0075	0.0021	0.0049
Chi	Avg	0.2728	0.3054	0.0722	0.0836	0.0285	0.0111	0.0196
	SEM	0.1100	0.0588	0.0104	0.0047	0.0106	0.0040	0.0079
		C10	**C12**	**C14**	**C14:2-OH/C12:2-DC**	**C16**	**C18**	**C18:1-OH/ C16:1-DC**
Boxer	Avg	0.0690	0.0610	0.0804	0.0077	0.1352	0.0875	0.0035
	SEM	0.0369	0.0370	0.0301	0.0022	0.0282	0.0392	0.0019
Lab	Avg	0.0472	0.0396	0.0547	0.0076	0.0903	0.0695	0.0018
	SEM	0.0181	0.0117	0.0164	0.0036	0.0192	0.0231	0.0012
Chi Mix	Avg	0.0271	0.0180	0.0324	0.0035	0.0581	0.0340	0.0037
	SEM	0.0076	0.0044	0.0043	0.0023	0.0081	0.0043	0.0013
Chi	Avg	0.0246	0.0211	0.0343	0.0049	0.0867	0.0516	0.0065
	SEM	0.0102	0.0026	0.0014	0.0039	0.0237	0.0042	0.0023

		C18-OH/C16-DC	**C22:4**	**C22:1**	**C4/Ci4**	**C4-OH**	**C5-OH/C3-DC**	**C8:1**
Boxer	Avg	0.0047	0.0032	0.0080	0.1576	0.0204	0.0138	0.0094
	SEM	0.0023	0.0017	0.0039	0.0355	0.0051	0.0064	0.0035
Lab	Avg	0.0039	0.0038	0.0069	0.0886	0.0126	0.0076	0.0105
	SEM	0.0022	0.0010	0.0030	0.0300	0.0043	0.0053	0.0038
Chi Mix	Avg	0.0020	0.0015	0.0090	0.1262	0.0171	0.0104	0.0078
	SEM	0.0021	0.0011	0.0026	0.0189	0.0062	0.0050	0.0012
Chi	Avg	0.0021	0.0022	0.0135	0.0938	0.0097	0.0199	0.0149
	SEM	0.0012	0.0026	0.0034	0.0392	0.0088	0.0109	0.0089
		C5-DC	**C8:1-OH/C6:1-DC**	**C6-DC/C8-OH**	**C10:3**	**C10:2**	**C10:1**	**C7-DC**
Boxer	Avg	0.0171	0.0097	0.0117	0.0026	0.0026	0.0028	0.0056
	SEM	0.0050	0.0035	0.0025	0.0019	0.0014	0.0014	0.0013
Lab	Avg	0.0159	0.0125	0.0097	0.0042	0.0050	0.0041	0.0062
	SEM	0.0063	0.0026	0.0025	0.0019	0.0022	0.0032	0.0021
Chi Mix	Avg	0.0147	0.0131	0.0110	0.0013	0.0028	0.0043	0.0045
	SEM	0.0086	0.0050	0.0035	0.0008	0.0029	0.0025	0.0042
Chi	Avg	0.0206	0.0119	0.0103	0.0026	0.0058	0.0047	0.0052
	SEM	0.0013	0.0028	0.0033	0.0014	0.0033	0.0018	0.0061
		C8:1-DC	**C10-OH/C8-DC**	**C12:2**	**C12:1**	**C12:2-OH/C10:2-DC**	**C12:1-OH/C10:1-DC**	**C12-OH/ C10-DC**
Boxer	Avg	0.0027	0.0018	0.0025	0.0020	0.0018	0.0026	0.0027
	SEM	0.0014	0.0005	0.0023	0.0016	0.0012	0.0020	0.0018
Lab	Avg	0.0022	0.0027	0.0032	0.0028	0.0031	0.0026	0.0050
	SEM	0.0028	0.0017	0.0024	0.0019	0.0018	0.0016	0.0035
Chi Mix	Avg	0.0035	0.0010	0.0036	0.0029	0.0035	0.0041	0.0036
	SEM	0.0002	0.0012	0.0028	0.0015	0.0022	0.0030	0.0013
Chi	Avg	0.0033	0.0026	0.0025	0.0047	0.0039	0.0051	0.0045
	SEM	0.0020	0.0011	0.0012	0.0001	0.0020	0.0021	0.0025
		C14:3	**C14:2**	**C14:1**	**C14:3-**	**C14:1-**	**C14-**	**C16:3**

					OH/C12:3-DC	OH/C12:1-DC	OH/C12-DC	
Boxer	Avg	0.0015	0.0037	0.0040	0.0289	0.0089	0.0030	0.0019
	SEM	0.0006	0.0027	0.0025	0.0169	0.0026	0.0018	0.0012
Lab	Avg	0.0014	0.0023	0.0069	0.0495	0.0093	0.0031	0.0040
	SEM	0.0020	0.0017	0.0024	0.0215	0.0017	0.0022	0.0026
Chi Mix	Avg	0.0023	0.0051	0.0053	0.0341	0.0082	0.0029	0.0023
	SEM	0.0010	0.0047	0.0019	0.0144	0.0020	0.0017	0.0014
Chi	Avg	0.0026	0.0039	0.0055	0.0435	0.0086	0.0038	0.0027
	SEM	0.0018	0.0023	0.0039	0.0182	0.0043	0.0018	0.0006
		C16:2	**C16:1**	**C16:3-OH/C14:3-DC**	**C16:2-OH/C14:2-DC**	**C16:1-OH/C14:1-DC**	**C16-OH/C14-DC**	**C18:3**
Boxer	Avg	0.0037	0.0188	0.0034	0.0051	0.0055	0.0064	0.0025
	SEM	0.0031	0.0088	0.0004	0.0025	0.0019	0.0016	0.0012
Lab	Avg	0.0022	0.0159	0.0037	0.0050	0.0074	0.0063	0.0028
	SEM	0.0013	0.0035	0.0015	0.0025	0.0020	0.0041	0.0011
Chi Mix	Avg	0.0026	0.0127	0.0032	0.0052	0.0063	0.0045	0.0015
	SEM	0.0021	0.0054	0.0015	0.0022	0.0023	0.0009	0.0010
Chi	Avg	0.0038	0.0166	0.0044	0.0042	0.0099	0.0080	0.0029
	SEM	0.0021	0.0081	0.0021	0.0031	0.0011	0.0010	0.0012
		C18:2	**C18:1**	**C18:3-OH/C16:3-DC**	**C18:2-OH/C16:2-DC**	**C20:4**	**C20:3**	**C20:2**
Boxer	Avg	0.0055	0.0446	0.0053	0.0035	0.0040	0.0035	0.0052
	SEM	0.0023	0.0204	0.0011	0.0019	0.0027	0.0018	0.0011
Lab	Avg	0.0047	0.0339	0.0058	0.0051	0.0036	0.0044	0.0044
	SEM	0.0016	0.0094	0.0030	0.0027	0.0008	0.0007	0.0012
Chi Mix	Avg	0.0027	0.0242	0.0072	0.0029	0.0042	0.0034	0.0041
	SEM	0.0009	0.0069	0.0041	0.0008	0.0014	0.0021	0.0018
Chi	Avg	0.0052	0.0441	0.0042	0.0037	0.0043	0.0058	0.0048
	SEM	0.0025	0.0093	0.0028	0.0014	0.0004	0.0064	0.0024
		C20:1	**C20**	**C20:3-OH/C18:3-**	**C20:2-OH/C18:2-**	**C20:1-OH/C18:1-**	**C20-OH/C18-**	**C22:5**

				DC	DC	DC	DC/C22:6	
Boxer	Avg	0.0046	0.0031	0.0056	0.0068	0.0039	0.0034	0.0032
	SEM	0.0020	0.0010	0.0016	0.0036	0.0015	0.0028	0.0019
Lab	Avg	0.0057	0.0039	0.0037	0.0075	0.0041	0.0039	0.0031
	SEM	0.0018	0.0016	0.0019	0.0022	0.0020	0.0008	0.0011
Chi Mix	Avg	0.0044	0.0037	0.0070	0.0089	0.0041	0.0026	0.0034
	SEM	0.0026	0.0017	0.0022	0.0025	0.0026	0.0017	0.0012
Chi	Avg	0.0074	0.0049	0.0038	0.0067	0.0033	0.0042	0.0060
	SEM	0.0019	0.0008	0.0016	0.0024	0.0005	0.0021	0.0039
		C22:3	C22:2	C22				
Boxer	Avg	0.0041	0.0032	0.0039				
	SEM	0.0011	0.0011	0.0005				
Lab	Avg	0.0085	0.0041	0.0054				
	SEM	0.0037	0.0023	0.0022				
Chi Mix	Avg	0.0051	0.0051	0.0040				
	SEM	0.0022	0.0008	0.0012				
Chi	Avg	0.0056	0.0051	0.0049				
	SEM	0.0034	0.0009	0.0001				

METHODS:

Genome-Wide Association: A GWAS of adult life expectancy was run in GEMMA v. 0.94 using a linear mixed model as described in (Hayward *et al.* 2016). 4,169 individuals from 110 breeds were included in the analysis. Dogs were genotyped on a semicustom Illumina SNP array; see (Shannon *et al.* 2015) for detailed methods. Adjusted breed-average life expectancies (Adj. e(2)) were obtained from (Yordy *et al.*), and are based on data from the Veterinary Medical Database and other sources. Genotype data were pruned in PLINK to exclude SNPs with MAF < 0.05, leaving about 150,000 loci in the analysis. A kinship matrix was calculated in GEMMA and this matrix was included as a random effect in the association test. Top associations are given in **Table 1**, more information in **Supplementary Information.**

Coat-length classifications for breeds were sourced from (Cadieu *et al.* 2009). Sweeping by weight ten breeds at a time (moving one breed/point every sweep) and calculating the fraction of short, medium, and long hair within that sweep vs the respective total present. These fractions and the corresponding weights of breeds were then averaged over five points (moving one point every sweep) and plotted with a three-order polynomial.

TMRE & MitoTracker Green: The fibroblasts were plated at a concentration of 25K in 500ul media in a 24-well plate and incubated for 18 hours. The cells were then stained with 200nM of either MitoTracker Green (Molecular Probes) or TMRE (Abcam) for one hour or 30 minutes at 37°C, respectively. The cells were then rinsed and immediately imaged with a ZOE Fluorescent Cell Imager (Bio-Rad). 10

representative images were taken for every cell line and dye. The average intensity per image was computed and then averaged across the representative images, this was done on 3 occasions. Average MitoTracker Green intensity was used to normalize TMRE intensity to the total mitochondrial mass for each breed respectively.

Mass Spectrometry: See **Supplementary File 2** for raw data and analysis. Fibroblasts were expanded to fill 6 x 100mm plates and washed with ice cold PBS, scraped from plates in ice cold PBS then spun down in a swinging bucket centrifuge at 500g for 5 mins to pellet cells at 4°C. Cell pellets were then lysed in 300 µL 0.6% formic acid, 30 µL was then removed for protein quantification, followed by addition of 270 µL acetonitrile to give a final concentration of 0.3% formic acid and 50% acetonitrile. Amino acids, acylcarnitines and organic acids were analyzed using stable isotope dilution technique. Amino acids and acylcarnitine measurements were made by flow injection tandem mass spectrometry using sample preparation methods described previously (An *et al.* 2004; Ferrara *et al.* 2008). The data were acquired using a Waters TQD mass spectrometer equipped with AcquityTM UPLC system and controlled by MassLynx 4.1 operating system (Waters). Organic acids were quantified using methods described previously (Jensen *et al.* 2006) employing Trace Ultra GC coupled to ISQ MS operating under Xcalibur 2.2 (Thermo Fisher Scientific).

Principal Component Analysis and Hierarchical-Clustering of metabolites: PCA was performed using the web based tool ClustVis (Metsalu & Vilo 2015). PCA plots and heatmaps were exported and modified with Adobe Illustrator.

Seahorse Analyzer: We followed the protocol and used the reagents from the Agilent

XF Cell Energy Phenotype kit (103325-100) to measure Oxygen Consumption Rate (OCR) and Extracellular Acidification Rate (ECAR), which are readouts of mitochondrial respiration and glycolysis respectively. Fibroblasts were plated the night prior to assay at 45K cells in normal cell culture media (DMEM, 10% FBS) in 24-well XF seahorse plates. 1-hour prior to assay, media was washed and changed to serum free XF assay media supplemented with 2mM glutamine and 10mM glucose (adjusted to a pH of 7.4). Glucose was not added to assay media in the case of **Fig. 4D** and **E**. Cells were then incubated in a non-CO2 chamber for 1 hour before being analyzed in a XF-24 Extracellular Flux Analyzer. FCCP and oligomycin were diluted in XF assay media and used at working concentrations of 1μm.

ROS analysis: Fibroblasts were plated at 50K in 24 well plates in normal media the day prior to experiment. Media was then removed from wells, washed with warm PBS, then warm PBS containing 10μm H2DCFDA (D399, Thermo Fisher Scientific) was added. Cells were incubated for 30 minutes at 37°, after which H2DCFDA was removed and trypsin was added for two minutes. Cells were collected, centrifuged, and washed with ice cold PBS. Cells were centrifuged again and resuspended in 500uL ice cold PBS. We then proceeded to measure H2DCFDA intensity by the FITC channel on a Beckton-Dickinson LSR II. A no stain control for every breed was used for every experiment that was subtracted from the respective stained replicates.

Stress Tolerance Analysis: Fibroblasts were plated the night prior to stress at 75K in normal media in 12-well plates. 16 hours later cells were treated with either 20μM rotenone or replaced with media lacking glucose and serum. Stress conditions lasted

72 hours before being collected (including adhered and suspended cells) from wells using Trypsin digestion. Cells were washed in PBS and then suspended in 100μL of 1X binding buffer (10 mM HEPES, 140 mM NaCl, 2.5 mM $CaCl_2$, pH 7.4) with 5μL of Annexin-V conjugate and PI. After a 15-minute incubation another 400 μL of binding buffer was added and then cells were analyzed using a 3 laser/ 8 color Beckton-Dickinson LSR II. A cell was considered to survive if it was negative for both Annexin-V and PI stains.

Statistics: Pearson correlation coefficient (R) and sample size (n) used to calculate p-value for all correlations between experimental results and breed longevity. When appropriate, we grouped the breeds into long and short-lived and compared results by the two-tailed t-test. For breed lifespan values, we took data from the American Kennel Club: http://akc.com/dog-breeds/ and data available from PetcareRX: https://www.petcarerx.com/article/lifespan-of-a-dog-a-dog-years-chart-by-breed/1223 and averaged the two data sets together.

Primary Canine Fibroblasts: Fibroblasts acquired from the Miller lab were procured as described previously (Harper *et al.* 2011). Fibroblasts from the Cornell Veterinary Bank were prepared as follows (briefly): Tissue was minced in MEM and cultured in 15% FBS with 1% L-glutamine and antibiotics in T25 flasks. Fibroblasts incubated in atmospheric oxygen with 5% carbon dioxide at 37°. Once sub-confluent they were collected via trypsin and centrifugation and frozen (-70 O/N to liquid nitrogen) in 10% DMSO and 18% FBS media).

In the Libert lab: after thawing and reanimation, fibroblasts were cultured in DMEM (Corning, 10-017) supplemented with 10% FBS on culture plates treated with 0.1% gelatin (including for experiments). To prevent mycoplasma, bacterial and fungal contamination streptomycin, penicillin, and amphotericin b were used in manufacturer specified concentrations. Fibroblasts were incubated in atmospheric oxygen with 5% carbon dioxide at 37°. See **Supplementary Information** for all canine donors used in this study. Please note we attempted to match fibroblast donor age across breeds but availability was a limiting factor. Interestingly, donor age within breed appears irrelevant for most metabolite concentrations (**Supplementary Information**). While *In vitro* age (passage) of fibroblasts plays a more apparent role in the rigidity observed by AFM (**Fig. S2**).

Atomic Force Microscopy: Dimension 3100 and Dimension Icon (Bruker Nano/Veeco, Inc.) AFMs with Nanoscope V controllers and NPoint close-loop scanners (200 μm × 200 μm × 30 μm, XYZ) were used in the present study. It is important to use such a large Z-range close loop scanner because of need to detect a rather large brush layer. Standard cantilever holders for operation in liquids were employed. To obtain the distribution of the properties over the cell surface and simultaneously record cell topography, the force-volume mode of operation was utilized. The force curves were collected with the vertical ramp size of 22 μm. To minimize viscoelastic effects, force-indentation curves were recorded with a frequency of 1.1 Hz (with approach vertical speed of 27 μm/sec and retract speed of 140 μm/sec). The force-volume images of cells were collected with the resolution of 16x16 pixels within 50 x 50 μm^2 area for sparsely distributed cells and the resolution

of 32x32 pixels within 120x120 μm^2 area.

AFM probe: spherical indenter: A standard V-shaped arrow 200 μm AFM tipless cantilevers (Veeco, Santa Barbara, CA) were used throughout the study. A 5 μm diameter silica balls (Bangs Labs, Inc.) were glued to the cantilevers as described (Berdyyeva *et al.* 2005). The radius of the probe was measured by imaging the inverse grid (TGT1 by NT-NGT, Russia). The cantilever spring constant was measured using the thermal tuning method.

Cells used for Atomic Force Microscopy: Viable fibroblasts cells are imaged directly in the growth medium without any special preparation. Specifically, fibroblast samples were shipped to Tufts University (the AFM lab) in Corning flasks filled with culture media, overnight without freezing. The amount of the growth medium in the flasks was close to the maximum possible to avoid mechanical damaging of cells during transportation. After receiving, the excessive medium was removed (only 10 ml of the media was kept in each flask). Flasks with cells were placed in an incubator at 37C (5% CO_2) for 12-16 hours to let cells relax after transportation. Before the AFM imaging, the top side of the culture bottles was removed. The AFM study was done directly in the medium on the cells attached to the bottom of the culture bottle. A relatively large amount of the medium insured safety of the cell while imaging (ran about three hours; no statistical difference differences between the cell parameters derived from the measurements in the beginning and at the end of the experiments was noticed). The study of this work was done on cells far from confluency (to avoid excessively large production of collagen which may hide the pericellular coat).

Brush model. The brush model was used to separate mechanical response due to

deformation of the pericellular layer and cell body (Dokukin *et al.* 2013; Sokolov *et al.* 2013). In this model the cell body is self consistently (independent of particular AFM and indentation force) characterized with an effective Young's modulus (the modulus of elasticity), whereas the pericellular coat layer it is described with the help of two parameters, the thickness of the pericellular coat and the number of effective molecules per unit area (brush density).

Data processing notes: The models described in the next section were developed for a known geometry such as a sphere over either plane or hemisphere or sphere. Therefore, we consider only the force curves from the top area of cells (following the previous works (Sokolov *et al.* 2006; Sokolov *et al.* 2007), we take the force curves in the surface points around the top when the incline of the surface is <10-15 degrees). To identify such curves, the cell height image was used (this image was collected as a part of the force-volume data set). The radius of the cell curvature was derived from these images after correcting the cell heights for deformations (see the Supplementary materials for details). A nonlinear curve fitting of corresponding equations allows deriving both the elastic modulus of the cell body and parameters of the pericellular brush (length and grafting density).

Real-time reverse polymerase chain reaction (RT-PCR): Total RNA was extracted from primary cell culture using RNeasy kit (Qiagen, Cat# 74104). A cDNA library was prepared using Superscript III Synthesis System (Invitrogen, Cat# 18080051). Reverse polymerase reaction was performed using poly-dT primers as per manufacturers instruction. qRT-PCR was performed using CFX96 Touch™ Real-Time PCR Detection System, using the following primers: IGF-1 F:

ttcgtgtgcggagacagg, IGF-1 R: ggaggctagagatgtactgtgc, β-actin F: gacaggatgcagaaggagatca, β-actin R: ctgatccacatctgctggaaggt. All relative mRNA abundance measurements were to β-actin

CHAPTER 3

NICOTINE PROMOTES NEURON SURVIVAL AND PARTIALLY PROTECTS FROM PARKINSON'S DISEASE BY SUPPRESSING SIRT6

Author list for final publication: Justin W. Nicholatos[1], Adam B. Francisco[1], Carolyn A. Bender[1], Tiffany Yeh[1], Fraz J. Lugay[1], Jairo E. Salazar[1], Christin Glorioso[2], Sergiy Libert[1]

1. Department of Biomedical Sciences, Cornell University, Ithaca, NY, 14850, USA

2. Paul F. Glenn Laboratory, Department of Biology, Massachusetts Institute of Technology, Cambridge, MA, 02139, USA

Author Contributions: Conceptualization, J.W.N. and S.L.; Formal Analysis, J.W.N., S.L., and C.G.; Investigation, J.W.N., A.B.F., C.A.B., F.J.L., T.Y., J.S., and C.G.; Writing – Original Draft, J.W.N. and S.L.; Writing – Review & Editing, J.W.N. and S.L.; Supervision, S.L.; Funding Acquisition, J.W.N. and S.L.

SUMMARY

Parkinson's disease is characterized by progressive death of dopaminergic neurons, leading to motor and cognitive dysfunction. Epidemiological studies consistently show that the use of tobacco reduces the risk of Parkinson's. We report that nicotine reduces

the abundance of SIRT6 in neurons and brain tissue by proteasome-mediated degradation. We find that reduction of SIRT6 is partly responsible for neuroprotection afforded by nicotine. Additionally, SIRT6 abundance is greater in Parkinson's patient brains, and decreased in the brains of tobacco users. We also identify SNPs that promote SIRT6 expression and simultaneously associate with an increased risk of Parkinson's. Furthermore, brain-specific SIRT6 knockout mice are protected from MPTP-induced Parkinson's, while SIRT6 overexpressing mice develop more severe pathology. Our data suggest that SIRT6 plays a pathogenic and pro-inflammatory role in Parkinson's and that nicotine can provide neuroprotection by accelerating its degradation. Inhibition of SIRT6 may be a promising strategy to ameliorate Parkinson's and neurodegeneration.

INTRODUCTION

Parkinson's disease (PD) is an age-associated neurodegenerative disorder characterized by progressive death of dopaminergic (DA) neurons, leading to motor dysfunction, behavioral changes, and often dementia. No therapy exists to prevent neuronal death or halt advancement of PD (Obeso *et al.* 2010). Several genetic risk factors have been identified in familial cases of Parkinson's, such as mutations in α-Synuclein, *LRRK2,* and Parkin (Dawson 2000), however, it is still not clear what causes the death of DA neurons at advanced age in the majority of sporadic cases, which constitute over 93% of PD (Spataro *et al.* 2015). Epidemiological studies have identified several factors that increase prevalence of PD, such as exposure to

herbicides, certain dairy products (Hughes *et al.* 2017), traumatic brain injury (Ascherio & Schwarzschild 2016), or being overweight (Chen *et al.* 2014). Surprisingly, in 1959 a U.S. Government-sponsored study of health among 200,000 veterans reported that smoking reduced PD deaths by 64% (Dorn 1959). The negative association between tobacco use and PD and has been firmly established in over seventy independent studies (Dorn 1959; Morens *et al.* 1995; Tanaka *et al.* 2010; Wirdefeldt *et al.* 2011; Chen *et al.* 2015; Kenborg *et al.* 2015; Li *et al.* 2015). Because tobacco smoke is a potent carcinogen, the "competing death risk" theory has been investigated and rejected (Driver *et al.* 2009). Some have also suggested a reverse causation explanation, where patients are more likely to quit smoking before PD development (Ritz *et al.* 2014). However, the reduction of PD risk by tobacco is dependent on the duration and intensity of use (Chen *et al.* 2010), and second hand exposure in "never-smokers" is also protective (Searles Nielsen *et al.* 2012), further supporting a causative link. Moreover, the tobacco component nicotine is believed to be a major mediator of neuroprotection (Bencherif 2009). The mechanism of tobacco and nicotine's protective actions on PD remain unclear, but researching this phenomenon presents an opportunity to identify new therapeutic targets.

SIRT6 is a member of the sirtuin family, which comprises NAD^+-dependent enzymes that have emerged as targets of interest for age-associated disorders, including neurodegeneration (Herskovits & Guarente 2013). Both SIRT6 inhibitors (He *et al.* 2014; Parenti *et al.* 2014) and activators (Ghosh *et al.* 2015) are being developed to treat a variety of diseases, but SIRT6 has never been studied in the context of PD before. SIRT6 activity promotes apoptosis in numerous cell types (Van Meter *et al.*

2011), thus its activation is suggested to be beneficial for certain cancers (Sebastian *et al.* 2012a). However, SIRT6 activity can also promote apoptosis in non-cancer cells, including neurons (Pfister *et al.* 2008; Cardinale *et al.* 2015). In fact, SIRT6 inhibition was recently demonstrated to suppress stress-induced apoptosis (Shao *et al.* 2016; Domanskyi *et al.* 2017) and protect from retinal neurodegeneration (Zhang *et al.* 2016a). SIRT6 promotes production and secretion of inflammatory cytokines (Van Gool *et al.* 2009; Bauer *et al.* 2012; Jiang *et al.* 2013; Jiang *et al.* 2016), and chronic inflammation is thought to underlie neuronal death in PD and other neurodegenerative diseases. Tobacco smoke, a PD risk reducing factor, has been shown to decrease the abundance of SIRT6 in human lungs and in cell culture (Takasaka *et al.* 2014), while the positive risk factors, such as paraquat and fatty acid overabundance both increase SIRT6 activity (Mao *et al.* 2011; Feldman *et al.* 2013). These data suggest that SIRT6 might play a pathogenic role in PD, a topic that we investigate in this study.

SIRT6 overexpression is shown to extend longevity of mice (Kanfi *et al.* 2012), and ameliorate certain age-associated diseases in rodents (Mao *et al.* 2011; Sebastian *et al.* 2012a). Based on this logic, SIRT6 is expected to protect against most age-associated diseases, including PD. However, rodents do not naturally develop PD, even at advanced age. Based on the known SIRT6 functions, it is possible that SIRT6 activity has differential impact on different human diseases of aging, which warrants detailed investigation of the relationship between SIRT6, neurodegeneration, and environmental risk factors for PD.

RESULTS

Genetic variants and abundance of SIRT6 associate with TNFα and Parkinson's Disease in humans

To investigate the connection between SIRT6 and PD in humans, we performed a meta-analysis of published GWAS studies. First, we analyzed data from the Religious Orders Study (ROS) (Bennett *et al.* 2012) and Rush Memory and Aging Project (MAP) (Bennett *et al.* 2012) – ROS-MAP cohort, in which authors documented the medical history of participants, performed SNP genotyping, and measured genome-wide gene expression in the brain using RNA-sequencing. We analyzed thirteen SIRT6 SNPs reported in these studies and discovered that six SNPs, forming a linkage disequilibrium block in the N-terminus, have a significant impact ($p<10^{-9}$) on the expression of SIRT6 (**Fig. 1A-C**). We tested the association of these SNPs with the incidence of PD and found that SNPs that associate with elevated expression of SIRT6 strongly associate with increased risk of PD (**Fig. 1B, D**). We verified that the identified SNPs associate with the risk of PD in five additional PD GWAS studies (Pankratz *et al.* 2012), which confirmed our original discovery. It is worth noting that the SNPs with the greatest impact on SIRT6 expression associate with PD incidence most strongly (**Fig. 1D**), suggesting a functional link. Moreover, reanalysis of published genome-wide expression data from the *substantia nigra* of healthy controls and patients with sporadic PD (Moran *et al.* 2006) revealed the latter tend to have elevated levels of SIRT6 transcripts (**Fig. 1E**).

Next, we acquired mid-cortex brain tissue samples from healthy controls, PD patients, and tobacco users (Bennett *et al.* 2012). After measuring SIRT6 abundance in these

samples, we observed that SIRT6 protein levels are elevated in PD patient brains. Additionally, there is a negative correlation of SIRT6 abundance with tobacco use (**Fig. 1F, G, Supplementary Fig. 1**). Those who smoked more than three packs of cigarettes a day had the lowest SIRT6 levels. Furthermore, we found that regardless of smoking or disease status, SIRT6 positively and significantly correlates with the abundance of the pro-inflammatory cytokine tumor necrosis factor alpha (TNFα) (**Fig.1H, I, Supplementary Fig. 1**). These data suggest that elevated SIRT6 levels might increases the risk PD, and that tobacco use can suppress SIRT6 in human brain tissue.

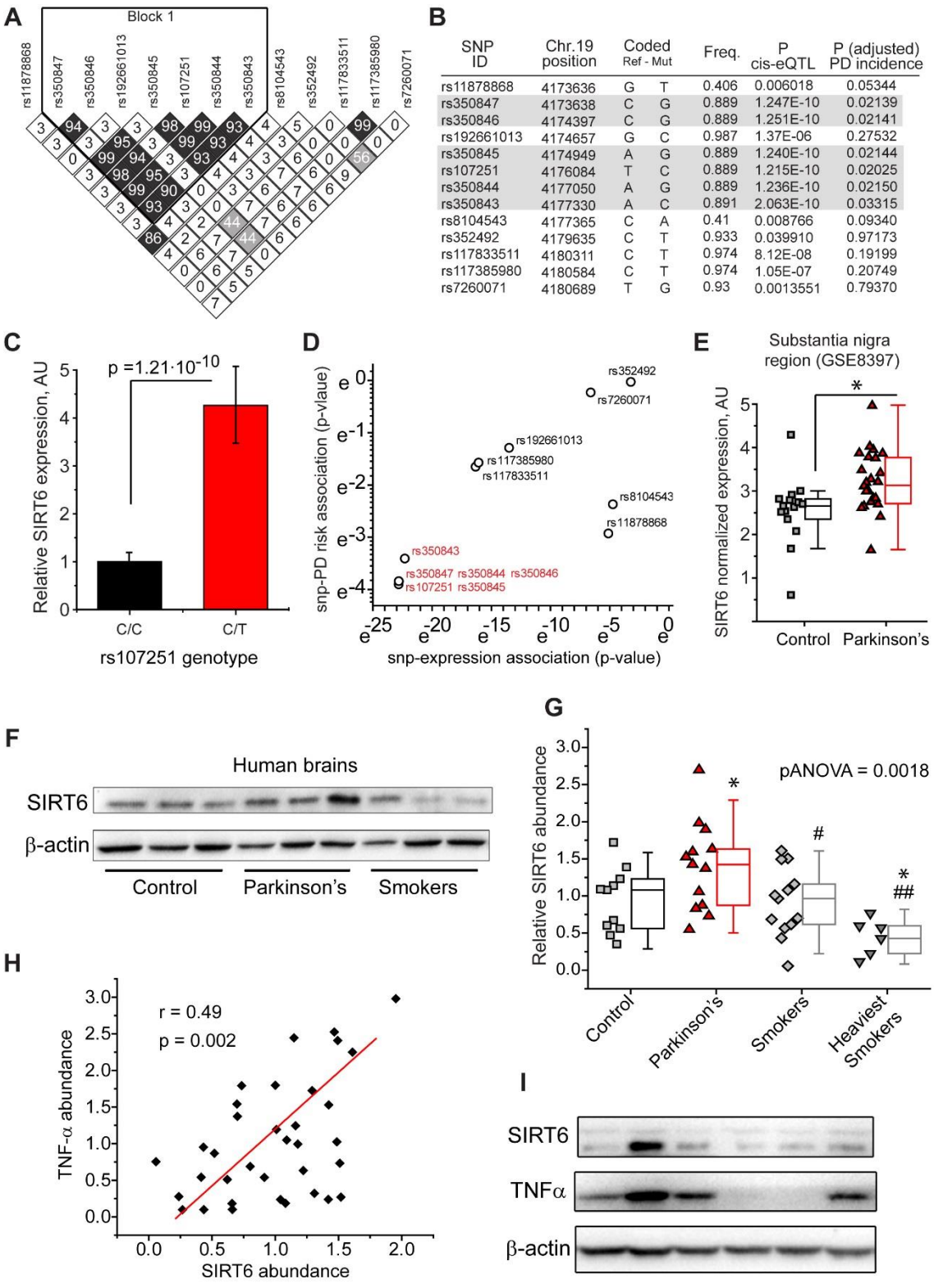

Figure 1. Higher expression of SIRT6 is associated with Parkinson's

Disease in humans. **(A)** Six N-terminus SNPs in SIRT6 are in strong linkage disequilibrium (LD). LD evaluation of genotyped SNPs in SIRT6 is shown. Shading of diamonds and numbers depict LD between markers based on the R^2 measure, where a value of "44" corresponds to $R^2 = 0.44$; **(B)** A summary of the associations between SNPs in SIRT6, SIRT6 gene expression, and Parkinson's disease prevalence. SNP ID, position, major - minor alleles and frequency (Freq.), the nominal p-value for the association of the SNP with the SIRT6 expression, and the corrected p-value for the SNP association with PD prevalence are presented. We find that SNPs associated with elevated expression of SIRT6, also associate with increased prevalence of PD. The analyzed dataset is derived from ROS-MAP cohorts(Bennett *et al.* 2012), in which all participants are organ donors. The dataset had already been assembled into RPKM values based on ENSEMBL gene ID and is publicly available through online Synapse archive (accession # syn3219045). **(C)** SNP rs107251 is associated with elevated expression of SIRT6 in human brains, bar graph showing the minor C/T genotype has ~4-fold greater expression of SIRT6 then major C/C. **(D)** The 13 SIRT6 SNPs analyzed from **A**/**B**, plotted by association with Parkinson's Disease by effect on SIRT6 expression. Note that the SNPs that associate the most significantly with expression (red) also have the strongest association with Parkinson's. **(E)** Box plot of the expression of SIRT6 in the substantia nigra region between control and PD patients, data is deposited to NCBI, accession number GSE8397. **(F)** Representative SDS-PAGE analysis of brain tissue lysates from healthy controls, Parkinson's Disease patients, and tobacco smokers. See Supplementary Figure 1 for full blots. **(G)** Box plot quantification of SIRT6 protein levels (relative to β-actin), such as those presented on

(**F**). * denotes significant difference compared from controls, # denotes significance from Parkinson's patients. Student's two tailed T-Test p-value for controls vs PD=0.04, controls vs heavy smokers=0.02, PD vs smokers=0.02, PD vs heavy smokers=0.002. One-way ANOVA between all groups p-value=0.0018. See Supplemental Figure 1 for full blots used for quantification. **(H)** Scatter plot showing the correlation between SIRT6 and TNFα protein abundance. Pearson correlation = 0.49 and the slope of regression p-value = 0.002. **(I)** Representative western blot showing the positive correlation between the levels of SIRT6 and TNFα, such as those presented in (H).

Tobacco and nicotine induce degradation of SIRT6 in vitro and in vivo

Since both tobacco and SIRT6 expression are linked to PD, we tested if tobacco smoke influences SIRT6 abundance in neurons *in vitro*. To do so, we prepared cigarette smoke extract (**Supplementary Fig. 2**) and treated primary murine neurons. We found that like in human smokers, the levels of SIRT6 can be decreased by tobacco *in vitro* (**Fig. 2A**). To test if nicotine itself reduces SIRT6 levels, we treated primary neurons with various doses of nicotine and found a dose-dependent decrease of SIRT6 abundance (**Fig. 2B**). The decrease of sirtuin levels by nicotine seems specific to SIRT6, as we observed no changes in the levels of the functionally similar SIRT1 (**Fig. 2B**). The reduction of SIRT6 in response to nicotine occurred rapidly, within 90 minutes of application, without changes in SIRT6 mRNA levels (**Fig. 2B, Supplementary Fig. 2**), all of which suggested a degradation mechanism. In support of this hypothesis, nicotine is known to regulate the ubiquitin-proteasome pathway in

neurons (Henley *et al.* 2013), and SIRT6 has been shown to be regulated in a proteasome-dependent manner (Kanfi *et al.* 2008; Thirumurthi *et al.* 2014). To test this mechanism, we treated primary neurons with nicotine and the proteasome inhibitor MG132. We found that neurons with inhibited proteasome function do not decrease SIRT6 abundance in response to nicotine exposure (**Fig. 2D, E**). These data suggest that nicotine and NR can accelerate proteasome-mediated degradation of SIRT6.

Next, we tested if nicotine in smoking-relevant concentrations can suppress SIRT6 abundance *in vivo*. To do so, we provided adult mice with drinking water supplemented with nicotine. We measured serum cotinine, an indicator of nicotine exposure, and found an average concentration of 26±4 ng/mL in the nicotine-exposed mice (**Fig. 2G**), which is in the range of a typical human smoker (Benowitz *et al.* 2009). Brain lysate analysis revealed that mice exposed to nicotine had ~50% reduction of SIRT6 levels (**Fig. 2H**), supporting our *in vitro* data. Importantly, both nicotine exposure and SIRT6 inhibition are known to activate AKT by phosphorylation at S473 (Abbott *et al.* 2008), and we observed this in both *in vitro* and *in vivo* experiments (**Fig. 2B, H**), supporting validity of our experiments. Taken together, these data demonstrate that nicotine in smoking-relevant concentrations can induce SIRT6 degradation in brain tissue *in vivo*.

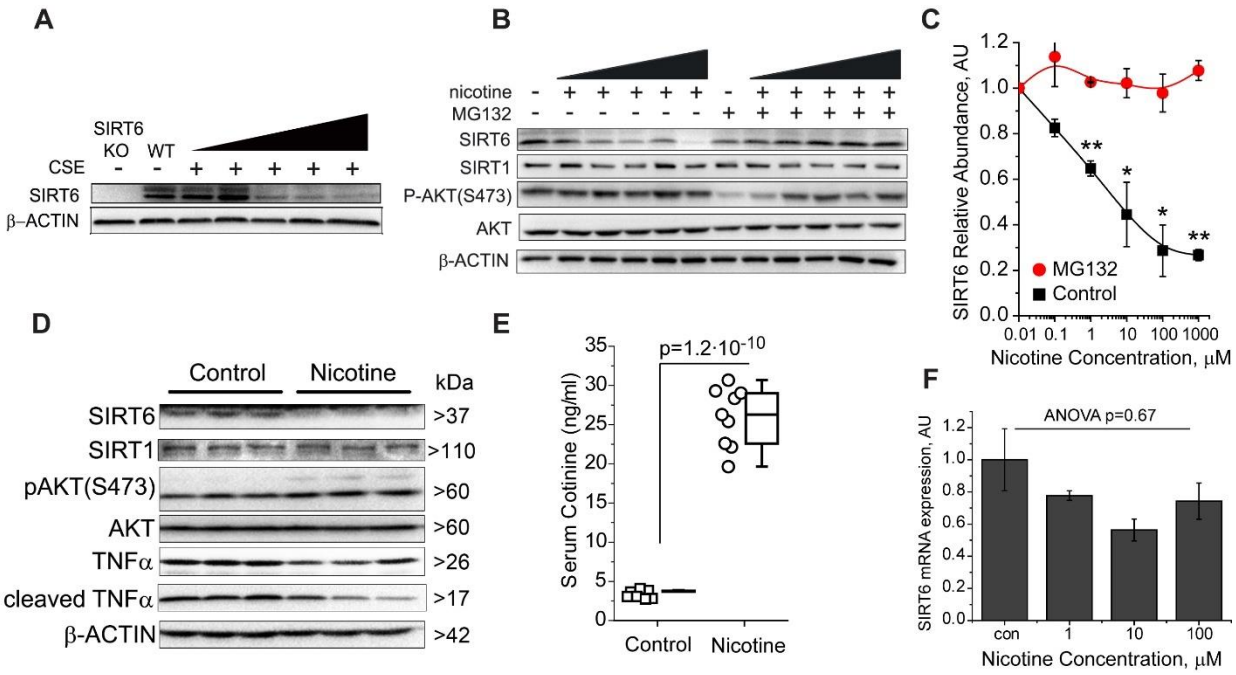

Figure 2. Nicotine suppresses SIRT6 through proteasome-mediated degradation. (A) Typical SDS-PAGE analysis of primary murine neurons treated for 24 hours with increasing concentrations of cigarette smoke extract (0.5, 1, 2, 5, and 10%). **(B)** Representative SDS-PAGE analysis of primary neurons treated for 90 minutes with nicotine at a range of concentrations - (0.1, 1, 10, 100, and 1000 □M); note the dose dependent decrease of SIRT6 abundance. Neurons pretreated with 10 μm MG132 were exposed for 2 hours. **(C)** Quantification of SIRT6 protein levels from B, n= 3 independent experiments. Note a dose-dependent decline of SIRT6 protein levels in response to nicotine, and elimination of this effect by proteasome inhibition (mean±SEM, one-way ANOVA:

*$p^{nicotine}$=0.008). **(D)** Representative SDS-PAGE analysis of brain lysates from animals treated with nicotine and vehicle-treated controls (same animals as shown in E). **(E)** Box plot of the concentration of serum cotinine in mice subjected to nicotine-supplemented water, n>9 per treatment, two tailed t-test $p<10^{-9}$. **(F)** Neurons treated with nicotine (1,10,100 μM) for 24 hours, RNA was isolated and qRT-PCR was performed for SIRT6, two-tailed t-test performed between treatment and control groups. Note no significant difference in SIRT6 transcript levels (mean±SEM, P-ANONA=0.67).

Loss of SIRT6 protects neurons from stress-induced apoptosis

To examine the causative relationship between SIRT6 and neuronal survival, we engineered brain-specific transgenic mice that either lack functional SIRT6 (BSKO, **Fig. 3A**), or overexpress SIRT6 by about four-fold (BSOX, **Fig. 3B, C, Supplementary Fig. 3A**) specifically in the brain. Noteworthy, the magnitude of SIRT6 overexpression in the brains of BSOX mice is comparable to SIRT6 increase in humans with PD-associated SNPs (**Supplementary Fig. 3B**). We isolated primary neurons from WT, BSKO, BSOX mice, and challenged them with a broad range of insults relevant to PD pathology. Following challenge, neurons were stained with the apoptotic markers Annexin-V and propidium iodide (PI), and their survival was measured using flow cytometry. Overall, SIRT6 KO neurons are better able to survive mitochondrial, oxidative, nutrient, and proteotoxic stress (**Fig. 3D-F**). Conversely,

neurons that overexpress SIRT6 tend to have higher rates of apoptosis following these insults.

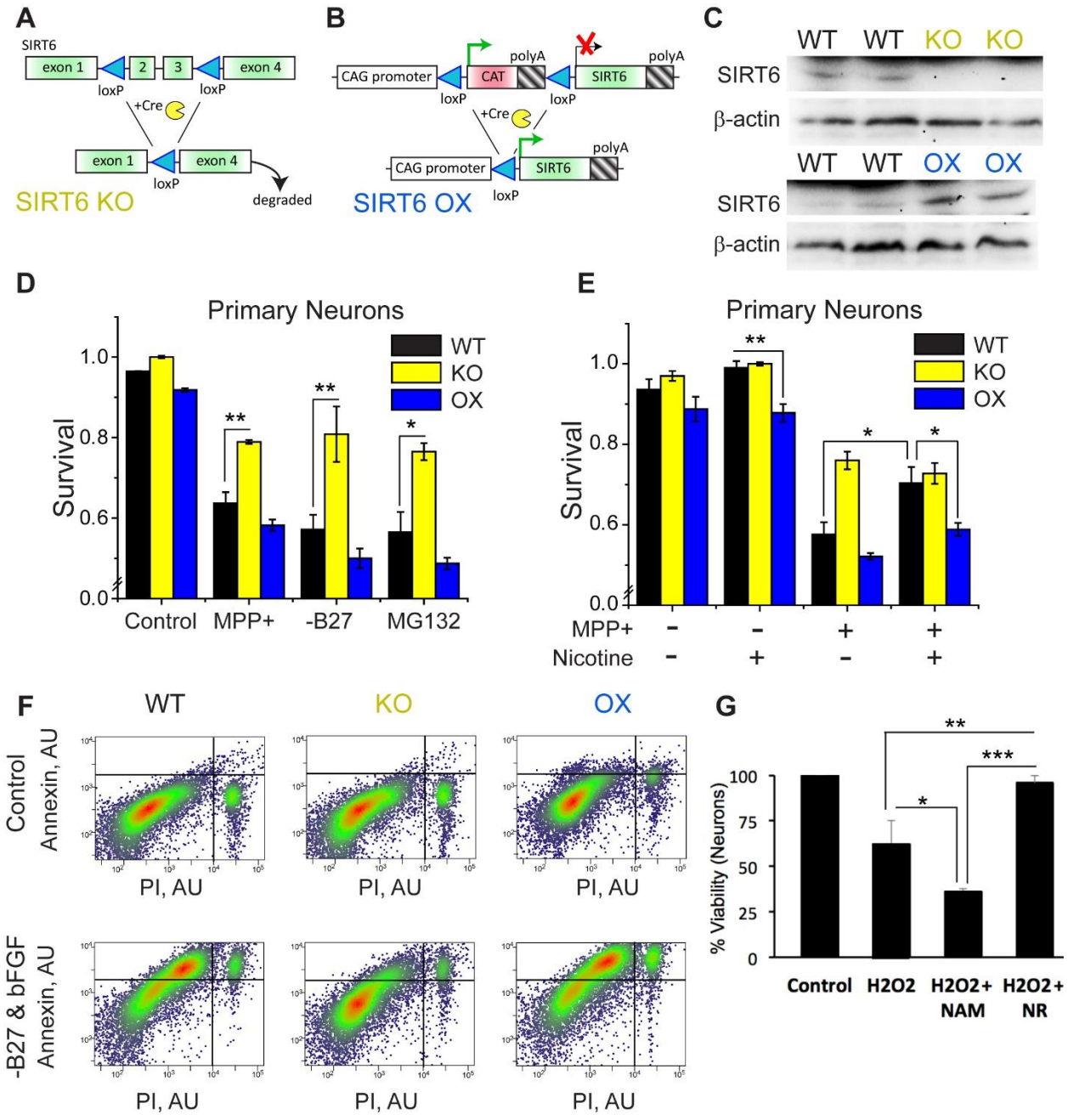

Figure 3. SIRT6 knockout neurons resist apoptosis and the effects of nicotine. (A) Schematic representation of the SIRT6 conditional strain of mice.

Exons 2 and 3 (which comprise the enzymatic active site) of SIRT6 are flanked with *lox-P* sites, and when *cre-recombinase* is expressed, these exons are excised. **(B)** Schematic representation of SIRT6 conditional overexpressing (OX) transgenic allele. The chicken β-actin promoter is followed by a *lox-P* flanked stop site in all six reading frames, followed by SIRT6 gene cDNA and poly-A signal. For both KO and OX schemes, *cre-recombinase* is expressed from the *nestin* promoter, which allows creation of brain-specific SIRT6 knockout (BSKO) or brain-specific overexpression (BSOX) animals. **(C)** Typical western blot analysis of cortex lysates from BSKO or BSOX mice and their WT littermates. **(D)** Bar graphs representing surviving fraction of primary WT, KO, and OX neurons, cultured *in vitro*, 24 hours after their stress with various insults. Neurons lacking SIRT6 resist apoptosis after stress. Con – control, MPP^+ – 1-methyl-4-phenylpyridinium (500 μM), SS – starvation (in case of primary neurons, B27 serum and bFGF were withheld), MG – proteasome inhibitor MG132 (10 μM). Survival of cells was measured using flow cytometry, after cells had been stained with the apoptotic markers– Annexin-V and propidium iodide (PI). A cell was considered "alive" if it was negative for both Annexin-V and PI staining. Mean±SEM, n=3 independent experiments with at least 10,000 cells analyzed in each experiment for each treatment; two-tailed t-test analysis *$p<0.05$, **$p<0.01$, ***$p<0.001$. **(E)** Survival of KO and OX neurons, respectively, pre-treated with 1 μM nicotine for two hours before MPP^+ stress. WT cells pre-treated with nicotine had improved survival under stress, while SIRT6 KO and OX cells did not benefit further from nicotine pretreatment. **(F)** Representative flow cytometry plots showing WT, SIRT6 KO, and OX neurons starved and stained with Annexin-V and PI, included in analyses depicted

in **D.** Each dot represents a single cell. Dot coloring reflects local cell density in the given area of the graph. **(G)** WT primary rat neurons treated with 50uM hydrogen peroxide (H_20_2) stress for 24 hours and 1mM NR or NAM (Mean±SEM, n=3 independent experiments, two-tailed t-test analysis). NAM decreases neuron survival and NR rescues survival under H_20_2 stress. Note that NR also decreases SIRT6 and NAM increases SIRT6 levels (Fig. 2F). Viability was measured by the MTT assay.

Nicotine is known to protect neurons from stress-induced apoptosis (Liu & Zhao 2004). Given our preliminary data (**Fig. 2**), we hypothesized that the neuroprotective effect of nicotine might depend on SIRT6. To test this, we exposed WT neurons, and those with knocked out (KO) or overexpressed (OX) SIRT6 to nicotine and MPP^+ (1-methyl-4-phenylpyridinium) - a molecule used to model PD-associated neuron death (Venderova & Park 2012). We found that after MPP^+ challenge, nicotine improved survival of WT neurons; however, SIRT6 KO neurons did not receive protection from nicotine treatment (**Fig. 3E**). The neurons with enforced expression of SIRT6 had a marginal increase in survival after nicotine treatment (**Fig. 4E**), likely because nicotine-induced SIRT6 degradation was counteracted by the SIRT6 overexpressing transgene, dampening nicotine efficacy. The link between SIRT6 and neuron survival was further strengthened by the fact that neurons treated with NR, which effectively depletes SIRT6 (**Fig. 2F**), had improved survival after oxidative stress (**Fig. 3G**).

We repeated the experiments testing the impact of SIRT6 and nicotine on cellular stress resistance in independently derived WT and SIRT6 KO fibroblast cell lines. As

before, we found that SIRT6 KO fibroblasts have superior stress tolerance (**Fig. 4A, B**), and that nicotine protects cells from apoptosis in part through SIRT6 (**Fig. 4C, D**), confirming our initial observations.

SIRT6 activity had been associated with cellular stress before, and it was reported that SIRT6 abundance increases in cells after stress (Mao *et al.* 2011). Our data is consistent with these reports. We find that after cellular stress, SIRT6 abundance is increased in both fibroblasts (**Fig. 4E, F**) and neurons (**Fig. 4G, H**). We also show that nicotine can reverse this stress-induced accumulation of SIRT6 and mitigate the downstream consequences (**Fig. 4G, H, I, J**), such as elevation of the pro-inflammatory cytokine TNFα. Taken together, these data demonstrate that the loss of SIRT6 enhances cellular survival under stress, and that nicotine at least partially functions through SIRT6 suppression to promote protection from apoptosis.

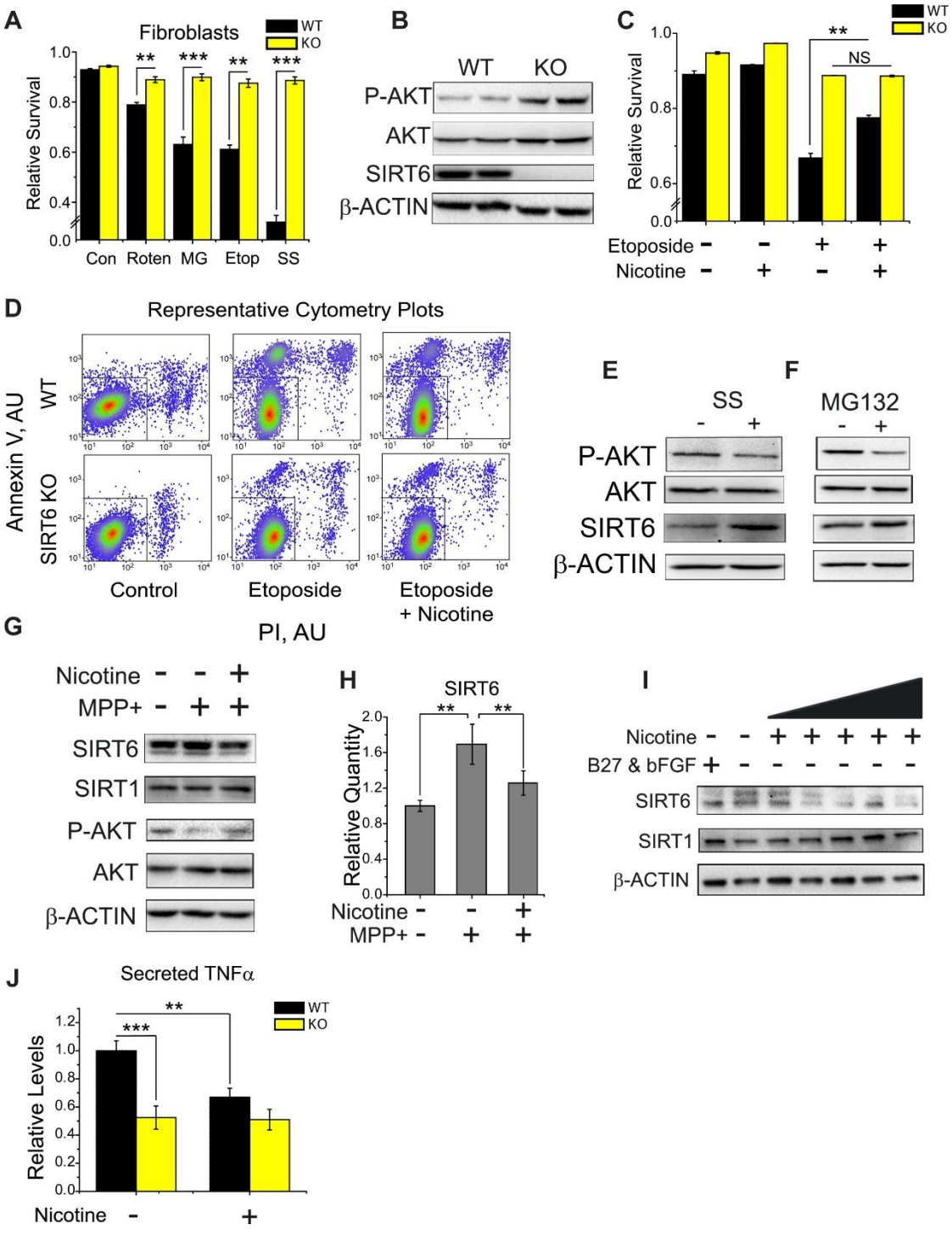

Figure 4. Nicotine reverses stress induced SIRT6 activity and inflammation. **(A)** Bar graph representing surviving fraction of WT and SIRT6 KO

fibroblasts, cultured *in vitro*, 24 hours after their stress with various insults. Fibroblasts lacking SIRT6 resist apoptosis after stress. Con – control, MPP^+ – 1-methyl-4-phenylpyridinium (500 μM), SS – starvation (fetal bovine serum was withheld), MG – proteasome inhibitor MG132 (10 μM), Roten – rotenone (10 μM), Etop – etoposide (20 μM). Survival of fibroblasts was measured using flow cytometry, after cells had been stained with the apoptotic markers– Annexin-V and propidium iodide (PI). A cell was considered "alive" if it was negative for both Annexin-V and PI staining. Mean±SEM, n=3 independent experiments with at least 10,000 cells analyzed in each experiment for each treatment; two-tailed t-test analysis *$p<0.05$, **$p<0.01$, ***$p<0.001$. **(B)** Typical western blot analysis of WT and SIRT6 KO fibroblasts. KO fibroblasts have higher levels of pAKT (S473) at baseline. **(C)** Bar graph representing survival of fibroblasts pre-treated with 1 μM nicotine for two hours before etoposide stress. WT cells pre-treated with nicotine had improved survival under stress, while SIRT6 KO cells did not benefit further from nicotine pretreatment. **(D)** Representative flow cytometry plots showing WT and SIRT6 KO fibroblasts stained with Annexin-V and PI, included in analyses depicted in **C**. Each dot represents a single cell. Dot coloring reflects local cell density in the given area of the graph. Survival of WT cells but not SIRT6 KO cells is improved by nicotine. **(E)** Typical western blot analysis of WT fibroblasts stressed with serum starvation. **(F)** Western blot analysis of WT fibroblasts stressed with MG132 (10 μM). SIRT6 increases under both SS and MG132 stress with a concomitant decrease in pAKT. **(G)** Typical western blot analysis of WT neurons treated with nicotine and or MPP^+, as depicted in Fig.3E. Note the increase in SIRT6 from MPP^+ stress and the lower levels

under nicotine treatment**. (H)** Bar graph quantification of SIRT6 levels as depicted in **G**. **(I)** Typical western blot of WT neurons starved (of B27 and FGF) and treated with nicotine for 1.5 hours (0.1, 1, 10, 100, and 1000 μM). SIRT6 increases after starvation but decreases upon nicotine exposure. **(J)** Bar graphs showing secretion of TNFα by primary neurons, measured by ELISA, 24 hours after incubation with 1 μM nicotine. SIRT6 KO neurons secrete less TNFα than WT and are unaffected by nicotine. Mean±SEM, n=4 independent experiments, two-tailed T-test analysis for *, two-way ANOVA: $p^{genotype}=8.5\bullet10^{-6}$, $p^{nicotine}=8.8\bullet10^{-3}$, $p^{genotype\ x\ nicotine}=1.6\bullet10^{-2}$.

SIRT6 regulates the pro-apoptotic TNFα pathway and pro-survival AKT signaling in the brain

We next explored the impact of SIRT6 dosage on brain physiology by profiling cortical gene expression by RNA-sequencing in BSKO, BSOX, and their respective WT littermates. Subsequent overrepresentation analysis showed that groups of genes involved in dopamine signaling and nicotine pharmacodynamics were significantly altered (**Fig. 5A, B**). These unbiased associations further strengthened SIRT6-nicotine-cell death connection. Another category impacted by SIRT6 was "immune-related processes" (**Table 7**). This is intriguing, since neuroinflammation and cytokines, namely TNFα, have been implicated in PD (Wang *et al.* 2015; Alam *et al.* 2016). Moreover, *in vitro* experiments have shown that SIRT6 regulates the production (Van Gool *et al.* 2009) and secretion (Jiang *et al.* 2013) of TNFα. To investigate this link further, we measured the secretion of TNFα from primary neurons isolated from BSKO, BSOX, or WT brains. We found that SIRT6 KO cultures secrete

less TNFα into the media (**Fig. 4J**), while OX cells secrete more than cells derived from WT littermates (**Supplementary Fig. 4A**). Moreover, we found that nicotine suppresses TNFα secretion in WT cultures but does not affect it in KO neurons (**Fig. 4J**), which is consistent with a SIRT6-mediated action of nicotine. We also measured levels of TNFα *in vivo* and found that SIRT6 deletion leads to decreased levels of brain TNFα (**Fig. 5C, D**). Surprisingly, we did not observe the upregulation of TNFα abundance in naïve BSOX mice, suggesting that additional players might be regulating this pathway. Supportive of the link between nicotine and SIRT6, we observed a significant drop of TNFα (full and cleaved forms) in brains of mice treated with nicotine (**Fig. 2H**).

In addition to inflammation, we investigated AKT signaling in the brains of SIRT6 transgenic animals. The PI3K-AKT axis is a canonical pro-growth and pro-survival pathway (Dudek *et al.* 1997), often disrupted in the brains of PD patients (Timmons *et al.* 2009; Greene *et al.* 2011). Suppression of SIRT6 has been shown to increase AKT expression and signaling (Sundaresan *et al.* 2012; Takasaka *et al.* 2014; Shao *et al.* 2016). We found that AKT phosphorylation is increased in the brains of BSKO mice and KO fibroblasts (**Fig. 5C, E, Fig. 4B**), and is lower in brains of BSOX mice (**Fig. 5C, E**). Overall, these data demonstrate that SIRT6 upregulates the pro-apoptotic TNFα pathway and suppresses pro-survival AKT signaling, which supports a pathogenic role for SIRT6 in PD.

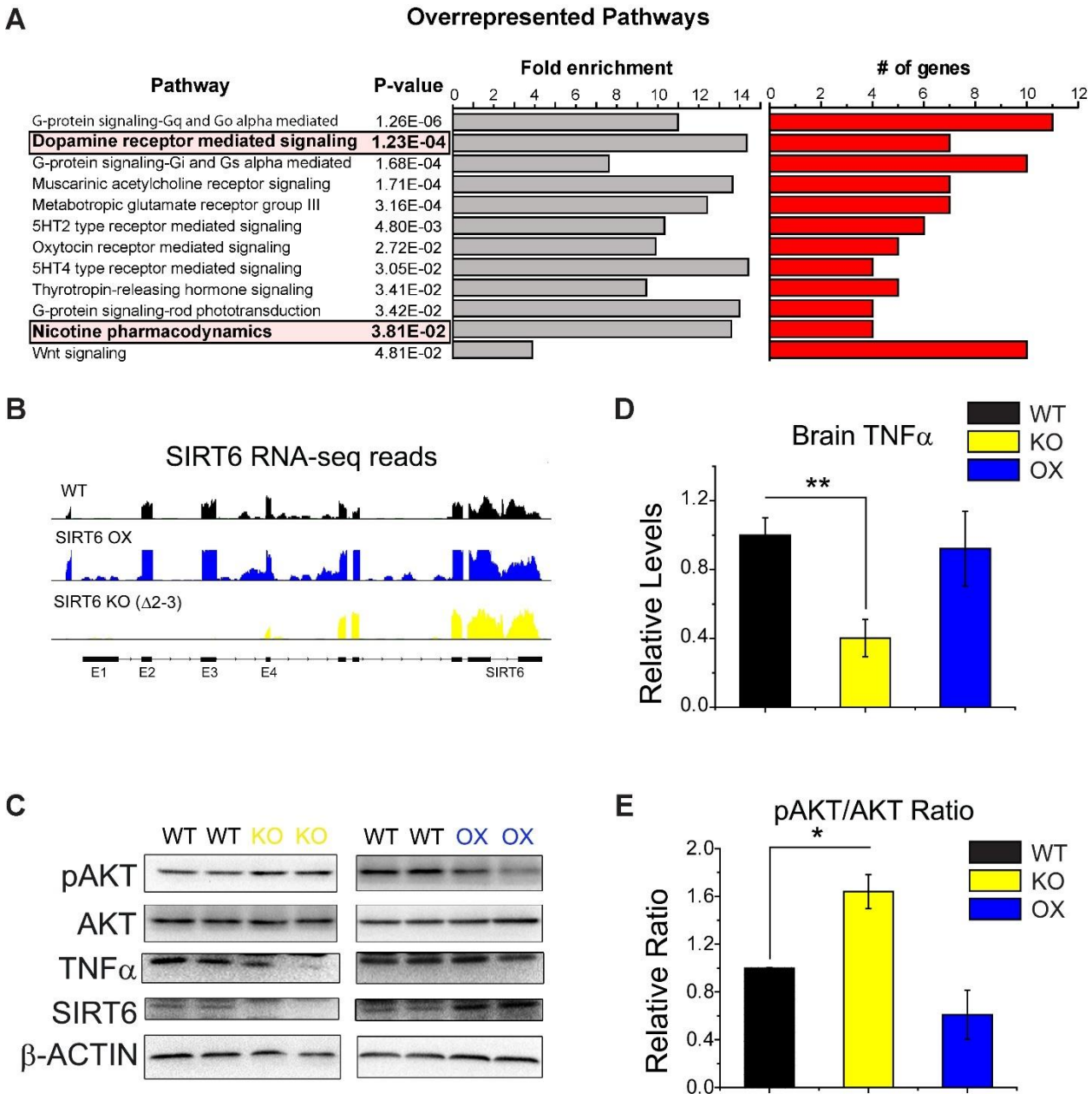

Figure 5. Characterization of brain-specific SIRT6 knockout and overexpressing mice. **(A)** Graphical representation of overrepresented pathways from RNA-sequencing analysis of BSKO, BSOX, and WT brains. All pathways shown were significantly altered after Bonferroni correction ($p<0.05$). The number of genes affected from each pathway and the pathway fold enrichment is shown. See also

Tables 4-9 for complete data analysis. **(B)** Pile-up reads of SIRT6 from the RNA-seq analysis. BSKO mice lack reads for exons 2 and 3, while BSOX mice have increased reads at all exons. **(C)** Representative SDS-PAGE analysis of brain cortex lysates from BSKO, BSOX, and WT animals is shown. **(D)** Bar graph quantification of TNFα analysis, such as on **C**, show lower abundance of full length TNFα in KO brains (mean±SEM, n≥3, **p<0.01). **(E)** Bar graph quantification of the ratio of phosphorylated (S473) AKT to total AKT from SDS-PAGE analysis, such as on **c**, showing a higher ratio (greater AKT activation) in BSKO brains (mean±SEM, n≥3, *p<0.05).

SIRT6 suppression confers neuroprotection in the MPTP model of Parkinson's Disease

To investigate the impact of SIRT6 on neurodegeneration *in vivo*, we utilized our brain-specific SIRT6 transgenic mice and the MPTP-based model of PD. MPTP (1-methyl-4-phenyl-1,2,3,6-tetrahydropyridine) selectively induces death of DA neurons and produces pathologies that closely mimic human PD; these include: neuroinflammation, nigrostriatal damage, changes in behavior and physical activity (Meredith & Rademacher 2011). After BSKO, BSOX, and WT littermates were treated with MPTP, we assessed their behavior and activity using an open field test. Compared to WT littermates, BSKO animals were protected from physical activity decline (**Fig. 6A-C**) and anxiety increase (**Fig. 6A, B**) induced by MPTP. Subsequent immuno-histochemical analysis demonstrated that BSKO mice suffered less nigrostriatal damage: they had significantly more surviving DA neurons in the

substantia nigra (**Fig. 6D-E**) and greater DA neuron dendrite density in the *striatum* relative to WT (**Fig. 6F-G**). Conversely, BSOX mice showed exaggerated PD-like symptoms– they had increased susceptibility to behavioral changes and elevated DA neuron death compared to WT littermates.

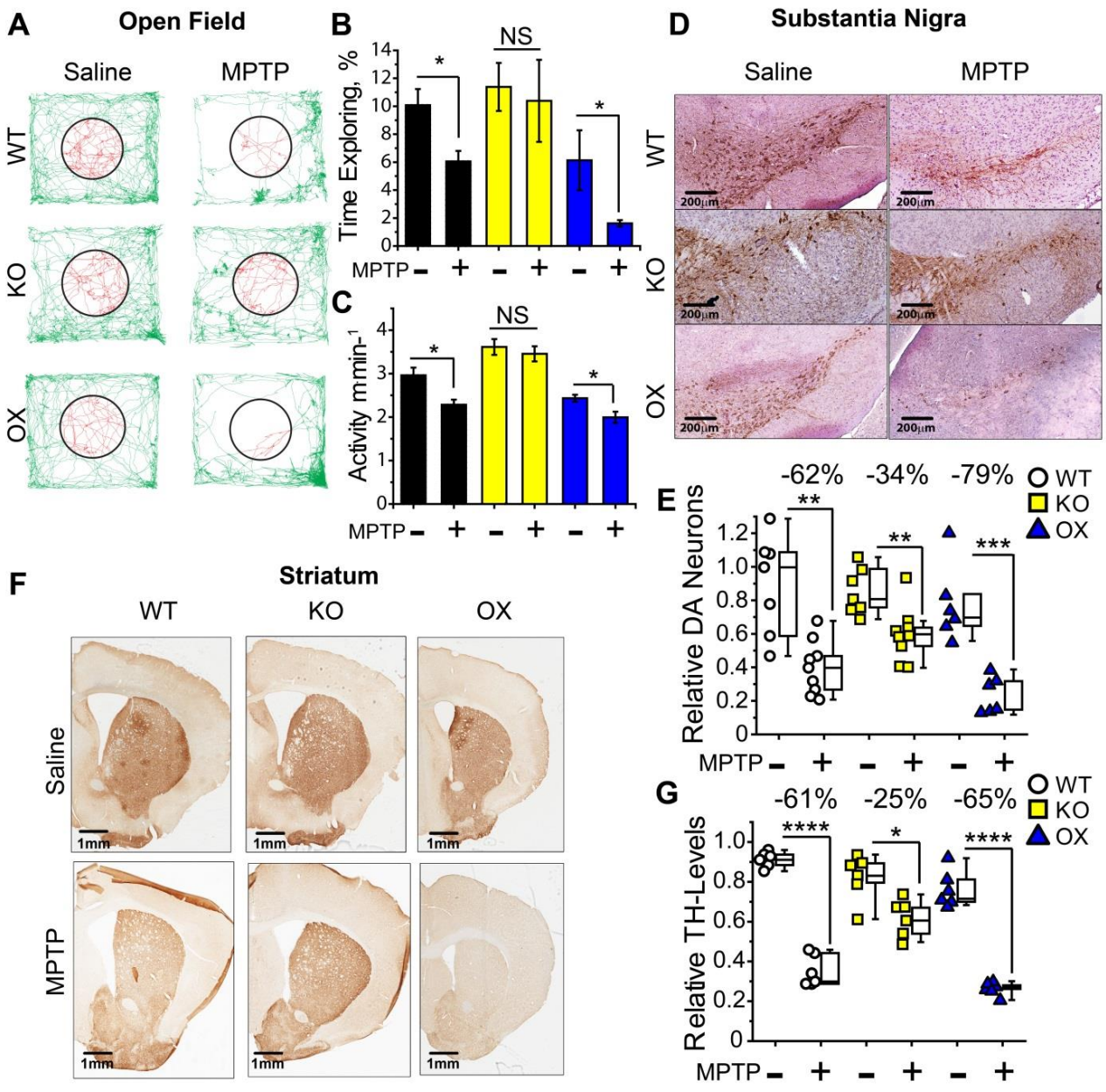

Figure 6. *In vivo* SIRT6 suppression protects from experimentally

induced Parkinson-associated pathologies. **(A)** Representative movement traces from open field test of WT, BSKO, and BSOX mice treated with MPTP or saline. BSKO mice are more resistant to MPTP-induced motor dysfunction. **(B)** Mice are naturally afraid of open spaces and prefer to be next to a wall; the fraction of time the animal explores the center of the arena (red-shaded area in **a** is inversely related to the animal's anxiety, which is induced in PD and by MPTP treatment. Quantification of exploratory behavior of SIRT6 transgenic mice treated with MPTP or saline is presented (Mean±SEM, $n \geq 6$, $^{*}p<0.05$ by two-tailed t-test. Two-way ANOVA: $p^{genotype}=6.6 \bullet 10^{-5}$, $p^{MPTP}=3.8 \bullet 10^{-3}$, $p^{MPTP\ x\ Gen}=4.8 \bullet 10^{-2}$). **(C)** Quantification of motor function of SIRT6 transgenic mice treated with MPTP or saline is presented via bar graphs (average distance covered per minute, mean±SEM). BSKO animals are protected from PD-associated mobility decline ($n \geq 6$, $^{*}p<0.05$ by two-tailed t-test. Two-way ANOVA: $p^{genotype}=4.8 \bullet 10^{-8}$, $p^{MPTP}=8.9 \bullet 10^{-3}$, $p^{MPTP\ x\ Gen}=0.675$). **(D)** Representative immuno-histochemical analysis of *substantia nigra pars compacta* of WT, BSKO, and BSOX mice treated with MPTP or saline. 15 μM sections were stained with anti-Tyrosine Hydroxylase to visualize dopaminergic neurons (brown stain) and counterstained with hematoxylin (purple stain). BSKO animals demonstrate reduced reduction of DA neurons after MPTP treatment, and BSOX animals have exaggerated neuronal death. **(E)** Quantification of histochemical analysis presented on **d**. Boxplots illustrate mean values and standard deviation of the relative abundance of DA neurons; box whiskers represent 5^{th} and 95^{th} percentiles of data distribution. Each circle is a separate animal. Black boxes – WT, green – BSKOs, and red – BSOX animals ($n \geq 6$, $^{**}p<0.01$, and $^{***}p<0.001$ by two-tailed t-test, two-way ANOVA:

$p^{genotype}=6.2\bullet10^{-2}$, $p^{MPTP}=8.2\bullet10^{-11}$, $p^{MPTP\ x\ Gen}=4.4\bullet10^{-3}$). **(F)** Representative immuno-histochemical analysis of *striatum* of WT, BSKO, and BSOX mice treated with MPTP or saline. DA neuron projections are visualized with anti-TH antibody. Drop in the density of dopaminergic projections after MPTP injections is mitigated in BSKO animals, and is exaggerated in BSOX mice. **(G)** Quantification of histochemical analysis, such as those presented on (**F**). Boxplots illustrate the mean density of dopaminergic projections in *striatum* of experimental animals; the box structure and coloring is the same as in **e**, ($n\geq6$, *$p<0.05$, and ****$p<0.0001$ by two-tailed t-test, two-way ANOVA: $p^{genotype}=2.3\bullet10^{-6}$, $p^{MPTP}=3.5\bullet10^{-16}$, $p^{MPTP\ x\ Gen}=1.1\bullet10^{-5}$).

To examine the relationship between SIRT6, nicotine, and neuroprotection *in vivo*, we challenged WT and BSKO mice with MPTP, while simultaneously co-treating them with nicotine. WT mice treated with nicotine received partial protection from MPTP-induced DA neuron death, while BSKO mice did not benefit from nicotine (**Fig. 7A, B**). These data support our *in vitro* findings (**Fig. 3D & 4C**) and suggest that SIRT6 inhibition partially mediates nicotine's neuroprotective action.

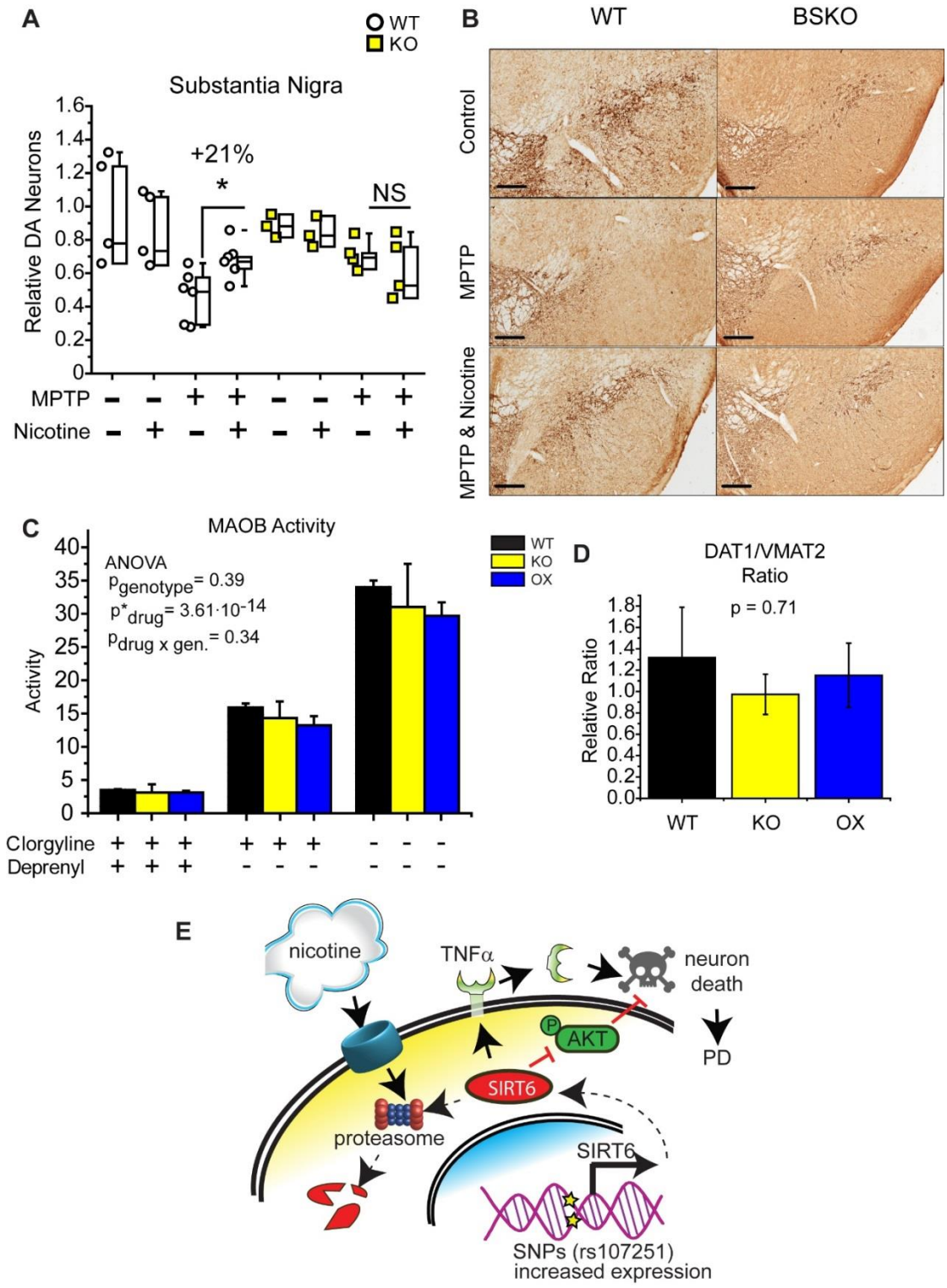

Figure 7. Nicotine does not rescue MPTP-induced DA neuron death

in SIRT6 brain-specific knockout mice. **(A)** Quantification of histochemical analysis presented on (**B**). Boxplots display the relative density of DA neurons in the *substantia nigra pars compacta* assessed by stereological counting. Three-way ANOVA analysis: $p^{genotype}=0.57$, $p^{MPTP}<0.0001$, $p^{nicotine}=1.0$. **(B)** Representative immuno-histochemical analysis of *substantia nigra pars compacta* of WT and BSKO mice treated with MPTP and or nicotine. Stained with TH to visualize DA neurons. **(C)** Bar graph of MAOB enzymatic activity from cortex homogenates. Total MAO activity was not different; residual MAOB activity was not different when MAOA was inhibited with clorgiline; nor residual MAOA activity was different when MAOB was inhibited with deprenyl. Mean±SEM, N≥3, $p^{genotype}=0.39$, $p^{inhibitors}=3.61\bullet10^{-14}$, $p^{genotype\ x\ inhibitors}=0.34$ by two-way ANOVA). Together these data suggest that SIRT6 does not alter the metabolism of the neurotoxin MPTP. **(D)** Relative DAT1/VMAT2 ratio calculated from individual expression data from WT, BSKO, and BSOX brains. See also Supplementary figure 3. One-way ANOVA p value shown. **(E)** A schematic of the mechanistic link between nicotine, SIRT6, and PD is illustrated. Our data demonstrates that SIRT6 plays a pathogenic role in initiation and progression of PD by stimulating TNFα release and suppressing AKT signaling, all of which promote neuronal apoptosis. SNPs associated with an increased risk of PD, such as rs107251 significantly increase SIRT6 abundance and therefore increase likelihood of neuronal apoptosis. Nicotine promotes proteasome-dependent degradation of SIRT6, which in turn protects cells from stress-induced apoptosis and prevents or ameliorates neurodegenerative pathologies. Selective targeting of SIRT6 might have a therapeutic effect against PD.

The neurotoxicity of MPTP depends on the activity of monoamine oxidase B (MAOB), vesicular monoamine transporter 2 (VMAT2), and the dopamine transporter 1 (DAT1) (Sai *et al.* 2013). We measured the expression of MAOB, VMAT2, and DAT1 and enzymatic activity of MAOB in the brains of BSKO, BSOX, and WT mice. We found that the DAT1/VMAT2 ratio and enzymatic activity of MAOB were unaltered by SIRT6 dosage (**Fig. 7C, D**). The expression of MAOB, VMAT2, and DAT1 were also not significantly different between WT and transgenic mice, corroborating the RNA-seq expression results (**Supplementary Fig. 3C-E, Supplemental File 2 & 3**). Additionally, we performed a motor assessment before sacrificing the mice (**Supplementary Fig. 6**), which corroborates the partial protection afforded by nicotine. These data suggest that BSKO animals resist MPTP-induced damage via enhanced DA neuron survival and not by alterations in MPTP metabolism.

DISCUSSION

Our study provides a new mechanistic link between nicotine, PD risk, and SIRT6. We suggest that SIRT6 is a plausible therapeutic target against PD. As far as we understand, genetic predisposition or cellular stresses that result in SIRT6 induction promote neuroinflammation and cell death (**Fig. 7E**), accelerating neurodegeneration. Nicotine, NR, or other molecules that can inhibit SIRT6 activity or prevent SIRT6 accumulation might enhance neuronal survival under stress (**Fig. 3**). Our data demonstrate that nicotine can induce SIRT6 degradation by proteasomes, which is consistent with previous reports that nicotine can alter proteasome activity (Rezvani *et al.* 2007; Henley *et al.* 2013). Specifically, we postulate that nicotine redirects the

activity of proteasomes to preferentially degrade certain proteins, such as SIRT6. The mechanism of this redirection is currently unknown and might be an interesting topic for future studies.

The pro-survival kinase AKT is reported to regulate SIRT6 degradation (Thirumurthi *et al.* 2014); however, our experiments suggest an alternative mechanism, since we do not observe a correlation between AKT activity (phosphorylation of AKT is saturated at 0.1 μM nicotine) and the degree of SIRT6 reduction (**Fig. 2B**). Our data also support the conclusion that AKT signaling itself is regulated by SIRT6 activity.

It is fascinating that tobacco use reduces the prevalence of PD, while almost universally being detrimental to other diseases. Tobacco smoke consists of thousands of compounds, some of which might have very strong anti-PD properties. We and others suggest that nicotine is one of these molecules. Nicotine has been shown to have beneficial effects in animal models of PD and clinical trials have been encouraging, but more work is needed to determine the proper administration and efficacy (Kelton *et al.* 2000; Schapira *et al.* 2006; Thiriez *et al.* 2011). Future studies might identify additional tobacco components that regulate sirtuins, neuronal survival, and neurodegeneration. Interestingly, we found that the NAD+ precursor molecule – nicotinamide riboside, which was shown to be effective against neurodegeneration (Gong *et al.* 2013), also suppresses abundance of SIRT6 and improves neuronal stress tolerance. These findings support the therapeutic potential of SIRT6 in PD.

In agreement with previous reports (Van Gool *et al.* 2009; Sundaresan *et al.* 2012; Jiang *et al.* 2013), we find that suppression of SIRT6 increases AKT signaling and

reduces the secretion of TNFα, both of which likely mediate the impact of SIRT6 on DA neuron survival and PD pathology (**Fig. 7E**). Our data show that nicotine can reduce the abundance and secretion of TNFα in a SIRT6 dependent manner. SIRT6 levels also positively correlate with TNFα abundance in human brain tissue, further supporting an inflammatory and pathogenic role for SIRT6 in PD and corroborating a connection between SIRT6 and TNFα (**Fig. 1H**).

Previous studies have also demonstrated a pro-apoptotic role for neuronal SIRT6 in culture (Pfister *et al.* 2008; Cardinale *et al.* 2015), supporting our results. We find that four-fold overexpression of SIRT6 is sufficient to alter gene expression and enhance MPTP-induced pathology and neuron death *in vivo* (**Fig. 6**). Human SNPs that associate with a similar four-fold increase in SIRT6 expression significantly elevate PD risk (**Fig. 1A-D**). Additionally, brain tissue from PD patients have elevated levels of SIRT6 protein (**Fig. 1F, G, Supplementary Fig. 1**), further supporting a PD-SIRT6 association.

Recent studies have reported that SIRT6 protects from DNA-damage associated with Alzheimer's disease (AD) (Jung *et al.* 2016; Kaluski *et al.* 2017); more specifically, Kaluski *et al*. showed that cells without SIRT6 succumbed to apoptosis faster, following DNA-damage induced by ionizing radiation. We find SIRT6 KO cells (fibroblast lines and primary neurons) are more resistant to apoptosis induced by oxidative damage, proteotoxicity, and nutrient shortage, which is supported by other independent studies (Van Meter *et al.* 2011; Shao *et al.* 2016; Zhang *et al.* 2016a) and our previous work (Domanskyi *et al.* 2017) . It is possible that the effect of SIRT6 on

stress-induced survival depends on the nature of the stress. It is also possible that there is a fundamental difference between AD and PD pathogenesis and stress, which lends SIRT6 as protective in one and pathogenic in the other. On this note, it is intriguing that DA neurons were shown to have extremely high levels of NAD+ (Tucker *et al.* 2016), which could make these cells more sensitive to SIRT6 induced cell death..

Several studies propose that SIRT6 is an attractive target for activation, as it is shown to suppress survival of cancer cells (Thirumurthi *et al.* 2014; Ioris *et al.* 2017) and extend longevity in whole body overexpressing mice (Kanfi *et al.* 2012). Our data support the role of SIRT6 in the regulation of cell death, but add caution to potential therapies promoting its activity, because it may exacerbate death of DA neurons (among other cell types) and accelerate PD-associated degeneration. In the same regard, the implementation of inhibition therapies to promote cellular or neuronal survival must consider a potential carcinogenic pitfall. While there are many studies detailing the positive effects of sirtuin activity in aging and disease states, our data suggests that (at least for SIRT6) the outcome is context, cell-type, and disease dependent.

Finally, it should be noted that SIRT6 has at least three reported enzymatic activities: deacetylation (Sundaresan *et al.* 2012), de-fatty acylation (Jiang *et al.* 2013), and ADP-ribosylation (Mao *et al.* 2011). A compelling topic for future studies would be to investigate if any of these activities have a dominant impact on SIRT6's role in neuronal and cellular survival, as well as to investigate the efficacy of transient SIRT6 suppression on PD (mimicking a clinical therapy). A detailed analysis of the

relationship between SIRT6 and nicotine's receptors and associated neuroprotective pathways should also be carried out (Srinivasan *et al.* 2016) (**Supplementary File 4**). Such experiments will inform the development of activity-specific SIRT6 inhibitors that could be used for the treatment of PD.

SUPPLEMENTARY INFORMATION

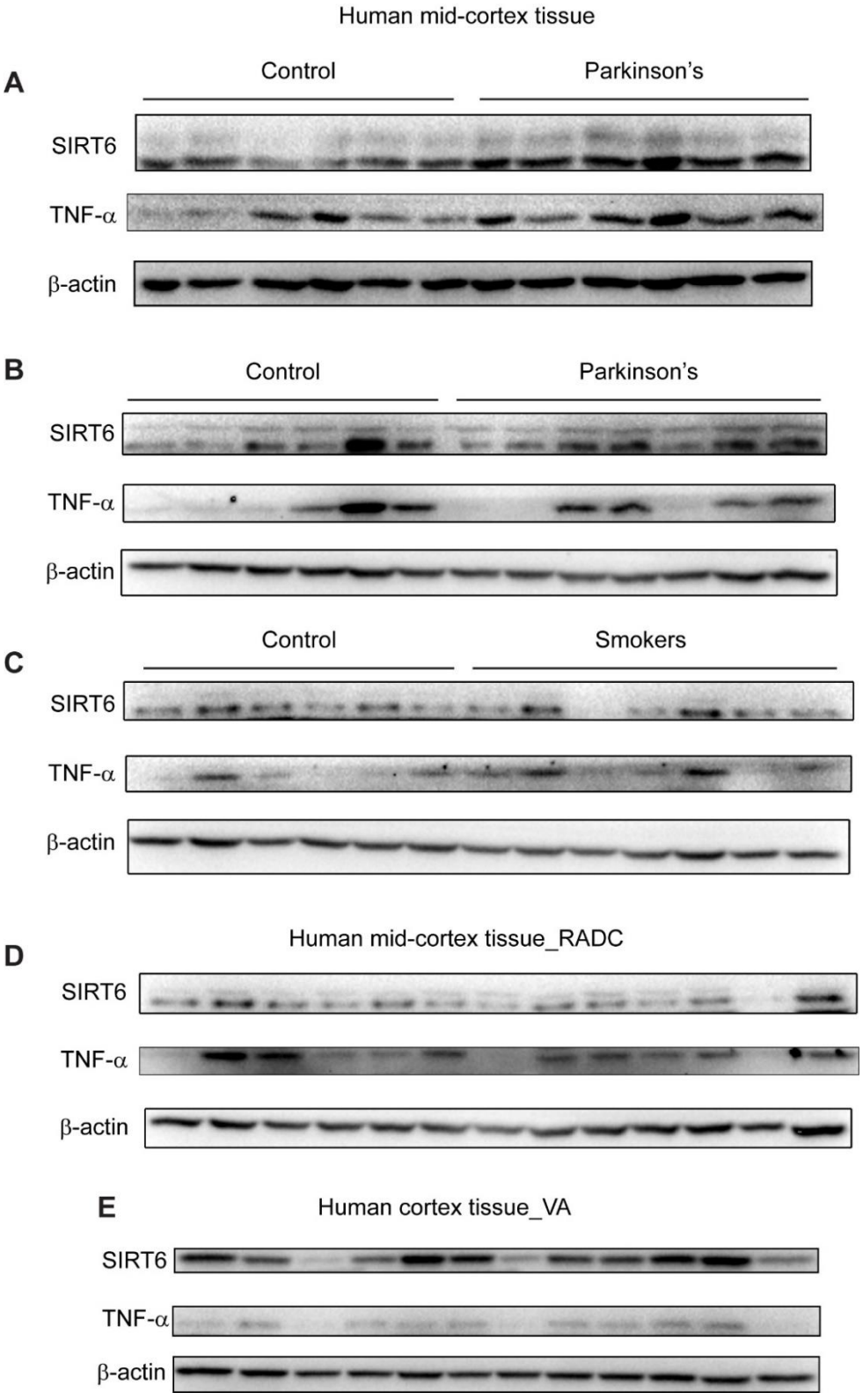

Supplementary Figure 1. Human brain tissue analysis by SDS-PAGE.

(A-E) Western blot analysis of human brain tissues showing abundance of SIRT6, TNFα, and β-actin. Each lane is an individual bio-specimen. Blots were used for quantifications showed in Figure 1G and H. RADC (Rush Alzheimer's Disease Center), VA (Veteran's Affairs), See Methods for details of brain tissue analysis.

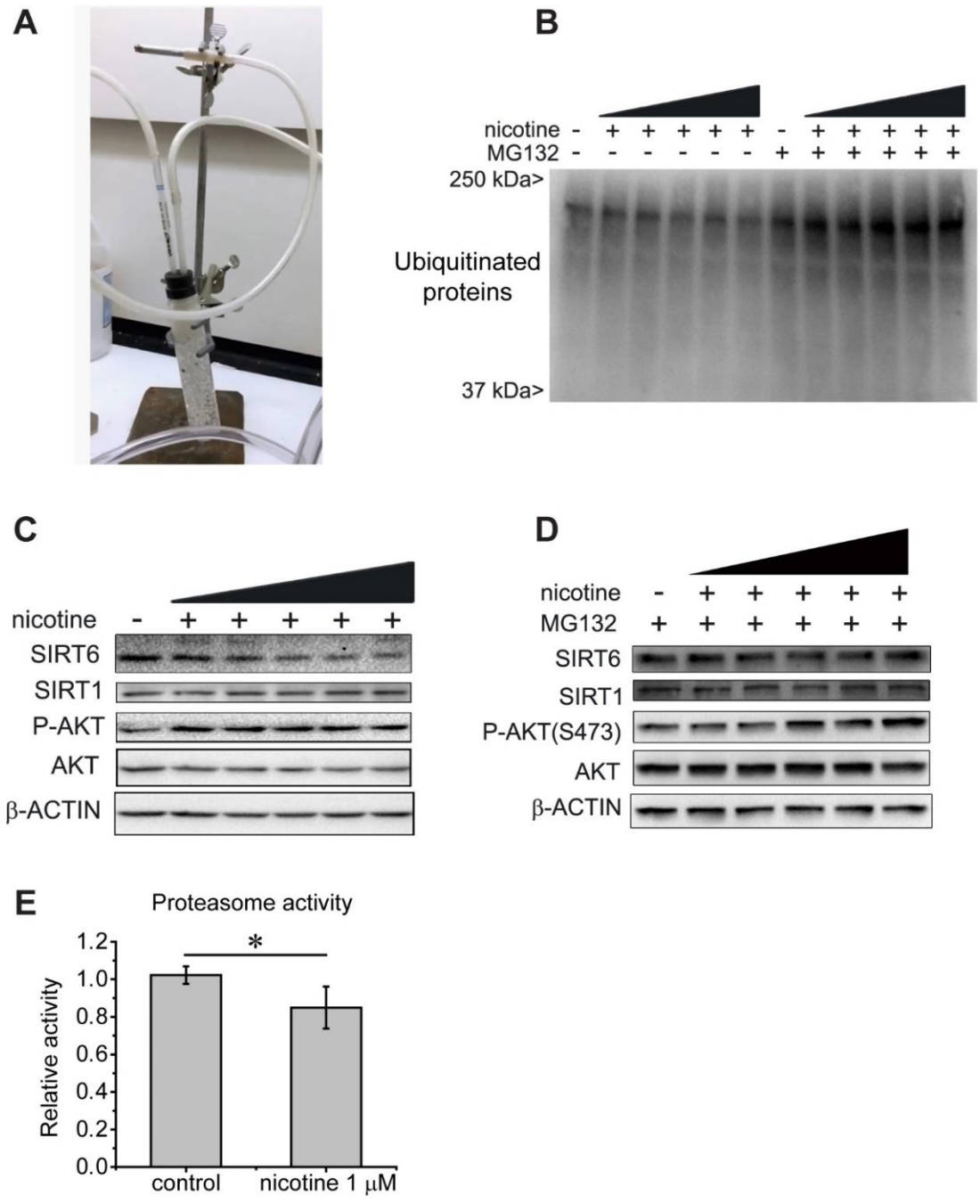

Supplementary Figure 2. Cigarette smoke extract apparatus, nicotine blots, and proteasome activity. (A) Picture of cigarette smoke extract apparatus used in our studies and for data presented on Figure 2A. **(B)**

SDS-PAGE analysis of samples as shown in Figure 2B blotted for ubiquitin. Note the increase in ubiquitinated proteins with the proteasome inhibitor MG132 treatment. **(C)** Representative SDS-PAGE analysis of primary neurons treated for 90 minutes with nicotine at a range of concentrations - (0.1, 1, 10, 100, and 1000 μM); note the dose dependent decrease of SIRT6 abundance. **(D)** Representative SDS-PAGE analysis of primary neurons treated for 90 minutes with nicotine at a range of concentrations - (0.1, 1, 10, 100, and 1000 μM), and pretreated with MG132 for 2 hours. **(E)** Overall proteasome activity of primary neuronal cultures treated with nicotine as in C.

.

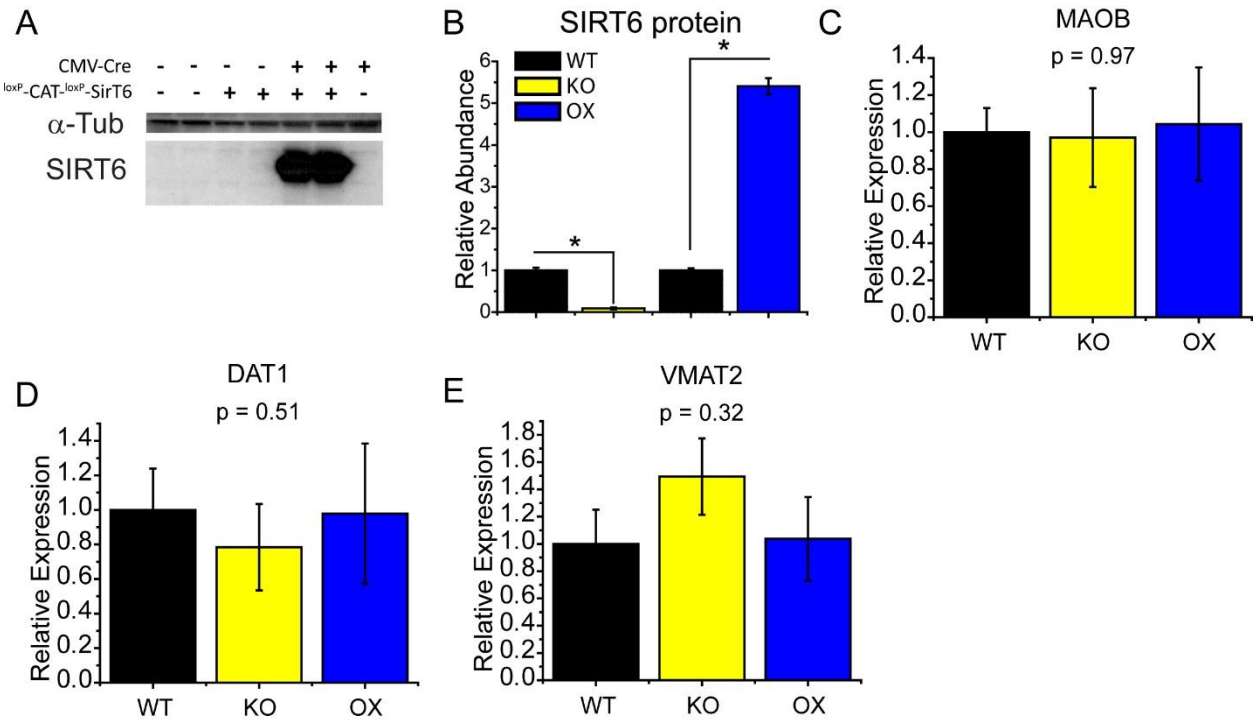

Supplementary Figure 3. Transgenic mice. (A) Typical western blot analysis of SIRT6 overexpressing transgenic cassette, which was used in creation of BSOX mice. Note that cassette does not normally express SIRT6, however in presence of *Cre*-recpmbinase, when STOP-signal is excised, overexpression ensues. **(B)** Bar graph of quantification of SIRT6 protein from brain lysates of the transgenic mice (WT, BSKO, and BSOX) (mean±SEM, N=4, *p<0.05 by two-tailed t-test). **(C, D, E)** Expression of MAOB, DAT1, and VMAT2 from the brains of WT, BSKO, and BSOX mice quantified by qRT-PCR. P value of one-way ANOVA shown (n = 8), note no significant effect from genotype.

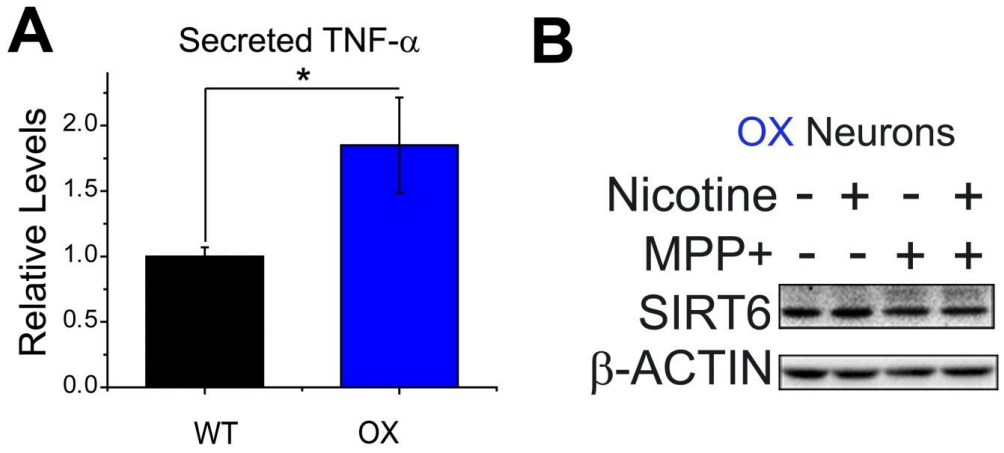

Supplementary Figure 4. SIRT6 OX neurons secrete more TNFα than WT. (A) Bar graph showing secretion of TNFα by primary SIRT6 overexpressing neurons, measured by ELISA. At baseline, SIRT6 OX neurons secrete more TNFα than their WT counterparts (mean±SEM, n=3 independent experiments, two-tailed t-test analysis shown, one-way ANOVA: $p^{genotype}$=0.003). **(B)** Representative western blot analysis of SIRT6 OX neurons stressed with MPP^+ (500 μM) for 24 hours with and without nicotine (1 μM) pre-treatment, as depicted in **Fig. 3E**. SIRT6 increases upon MPP^+ stress and remains elevated when nicotine is present.

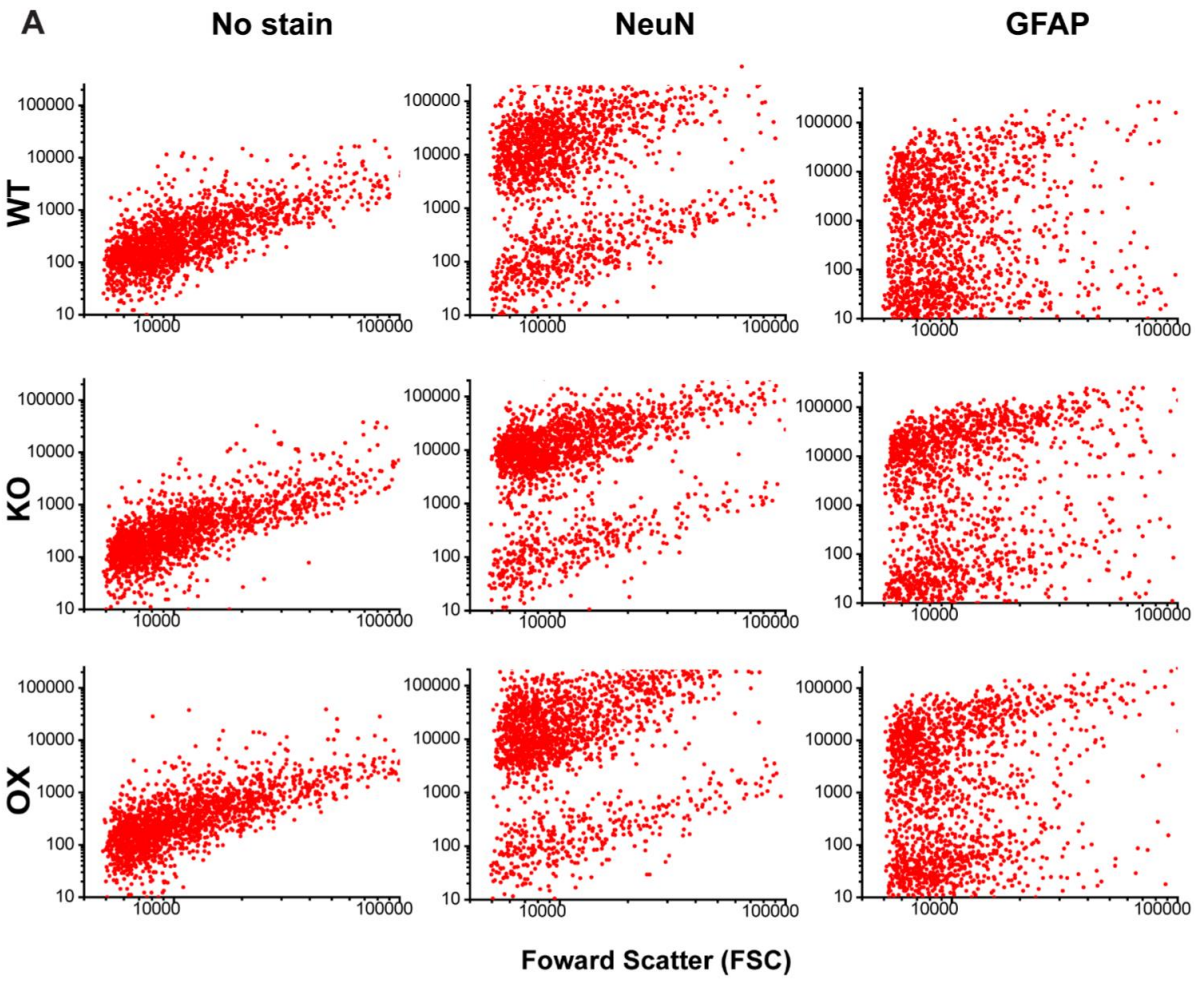

Supplementary Figure 5. Primary neuronal culture composition. (A) Representative flow cytometry plots of WT, SIRT6 KO, and OX neuronal cultures stained with NeuN (neurons), GFAP (astrocytes), or unstained. Note that all cultures proportions of neurons and astrocytes are equivalent and that cells stained with NeuN constitute the majority. **(B)** Western blot analysis of WT and KO primary neuronal

cultures. Note the complete absence of SIRT6 in KO lanes, even when overloaded for total protein compared to WT. This indicates the absence of microglia in these cultures since few if any neonatal microglia express nestin, which is the driver of CRE in our transgenic model.

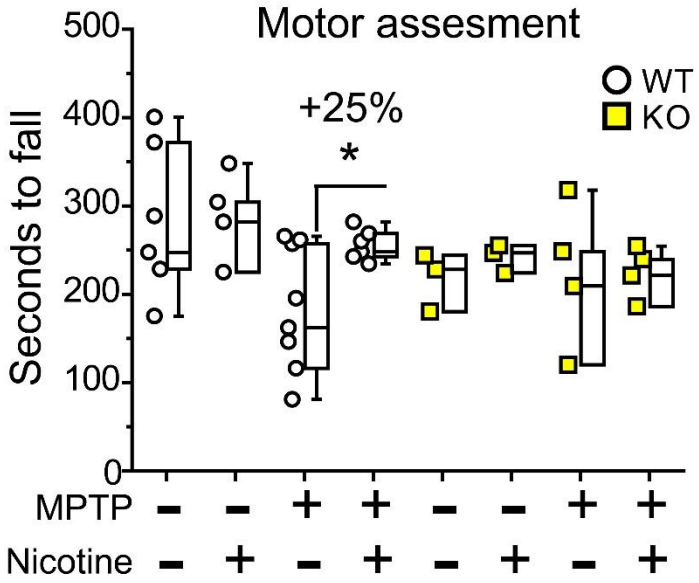

Supplementary Figure 6. Nicotine does not rescue MPTP-induced rotarod motor performance in SIRT6 brain-specific knockout mice.

Boxplots display the latency until fall (in seconds) from the rotarod performance test with forced motor activity (see methods for details). Three-way ANOVA analysis: $p^{genotype}=0.33$, $p^{MPTP}=0.02$, $p^{nicotine}=0.17$

Table 4: RNA-seq in the brain of WT and SIRT6 overexpressing

(BSOX) mice.

gene	WT's	OX's	Adj_p_value	Expression in OX
St18	1.88657	7.34393	0.010113	Up
Tfap2b	0.450395	3.29078	0.010113	Up
Fzd7	2.13542	6.07905	0.037311	Up
Rgs8	27.3288	79.6271	0.010113	Up
Stk17b	3.1185	10.3675	0.010113	Up
Slc1a6	5.44708	38.2359	0.010113	Up
Cnksr3	3.07216	9.55306	0.030744	Up
Col18a1	1.62146	8.56704	0.010113	Up
Mybpc1	1.1559	4.70234	0.010113	Up
Slc16a11	7.35416	20.6135	0.043099	Up
Atp2a3	2.79948	21.9599	0.010113	Up
Slc6a4	0.312934	5.47782	0.010113	Up
1500016L03Rik	1.14267	23.6889	0.017468	Up
Hoxb3	0	1.54516	0.010113	Up
Hoxb2	0	1.2402	0.010113	Up
Gprc5c	1.23142	11.1902	0.010113	Up
Meis1	2.07143	7.0271	0.030744	Up
Gabra6	0.194306	74.6769	0.010113	Up
Slc22a4	3.39481	14.778	0.010113	Up
Fat2	0.112394	23.5375	0.010113	Up
Epn3	0.890008	3.88246	0.024019	Up
Grin2c	14.6741	44.2379	0.010113	Up
Hpcal1	34.2063	105.23	0.010113	Up
3830431G21Rik	1.83307	10.6256	0.010113	Up
Sp8	2.30804	0.292869	0.024019	Down
Ltbp2	0.210466	3.07683	0.010113	Up
Prl2c3	0	0.825328	0.010113	Up
Gdf10	3.28165	26.4032	0.010113	Up
Zic2	6.79184	36.1848	0.010113	Up
Sncg	7.66875	41.547	0.010113	Up
Cdhr1	8.85336	1.69996	0.010113	Down
Cbln3	0.351381	96.204	0.010113	Up
Prph	1.05319	6.44187	0.017468	Up
Hoxc5	0	0.803352	0.010113	Up
Tssk5	0	0.576961	0.010113	Up
Pvalb	54.8473	329.303	0.010113	Up
Mapk12	3.56421	11.5167	0.024019	Up
B3gnt5	0.303872	1.72791	0.024019	Up
Sh3bgr	0.894357	8.21256	0.010113	Up

Gng13	71.3296	253.621	0.010113	Up
Adamts10	6.44843	23.4828	0.010113	Up
D17H6S56E-3	0.273391	2.66093	0.010113	Up
Arhgef33	0.306676	11.8866	0.010113	Up
Grm4	10.0118	43.7893	0.010113	Up
Mdfi	0.344902	4.70023	0.043099	Up
Stap2	1.50336	8.16358	0.010113	Up
Ttr	192.192	1029.02	0.010113	Up
Zfp521	2.5241	8.37694	0.010113	Up
Aqp4	29.4804	71.6326	0.030744	Up
D0H4S114	43.45	248.726	0.010113	Up
Arhgef37	0.548116	2.59511	0.043099	Up
Cep76	2.28544	11.6865	0.010113	Up
Doc2g	15.461	3.62771	0.010113	Down
Cabp2	0	0.862713	0.010113	Up
Cdc42bpg	1.41745	6.53877	0.010113	Up
Lbx1	0	1.84921	0.010113	Up
Afap1l2	3.53162	13.0733	0.010113	Up
Fam107b	4.46503	18.2641	0.010113	Up
Mybpc3	0.164758	7.27086	0.010113	Up
Pax6	4.74089	14.9919	0.010113	Up
Neb	0.147159	0.74118	0.017468	Up
Neurod1	4.14225	56.1997	0.010113	Up
Shf	16.261	44.4684	0.030744	Up
Paqr6	5.06093	18.5512	0.017468	Up
Rorc	0.61883	2.86884	0.017468	Up
Casq2	1.69637	6.26047	0.043099	Up
Bcl2l15	0.262968	7.28902	0.010113	Up
Ptpn22	0.274017	8.28747	0.010113	Up
Chd7	2.34044	9.18549	0.010113	Up
Inadl	4.97313	21.542	0.010113	Up
Trim62	9.65649	28.5548	0.017468	Up
Car8	2.79222	81.8494	0.010113	Up
Svep1	0.191756	1.6101	0.010113	Up
Epb4.1	8.01427	24.1094	0.010113	Up
Rps6ka1	5.28383	18.9574	0.010113	Up
Hes3	0.22598	9.39332	0.017468	Up
En2	0.580433	14.3702	0.010113	Up
Dao	0.288194	14.4031	0.010113	Up
Uncx	0.429429	6.87409	0.049817	Up
Hopx	29.1309	96.7511	0.010113	Up
Barhl2	0.427454	7.72101	0.010113	Up
Chn2	20.6106	82.3562	0.010113	Up
Ppp1r17	0.612981	47.573	0.010113	Up

Grid2	3.7053	12.0859	0.017468	Up
A2m	0.932882	8.87356	0.010113	Up
Hoxa2	0	0.81436	0.010113	Up
Pde1c	2.8219	10.1192	0.010113	Up
Tspan9	15.1872	40.2762	0.024019	Up
Mrgprf	0.624884	4.58798	0.017468	Up
Il16	1.01201	18.0947	0.010113	Up
Ebf3	0.646877	2.77198	0.037311	Up
Ank1	9.88838	26.7877	0.017468	Up
Gm2694	1.83401	26.9391	0.010113	Up
Cdh15	0.937179	8.38387	0.010113	Up
Cbln1	7.53551	134.417	0.010113	Up
Calb2	46.1265	189.243	0.010113	Up
Kcng4	2.81045	14.9168	0.010113	Up
Agt	17.3221	50.3013	0.024019	Up
Exph5	2.56513	7.36256	0.024019	Up
AI118078	3.65487	12.657	0.010113	Up
Megf11	6.01404	15.511	0.037311	Up
Zic4	1.24943	4.3263	0.017468	Up
Kank2	3.68872	13.4901	0.010113	Up
Rgl3	1.45828	8.78896	0.010113	Up
Zic1	10.5151	61.3595	0.010113	Up
Il20rb	0.388915	8.92963	0.010113	Up
LOC100862004	11.4641	37.5481	0.024019	Up
Frmd7	2.4823	0.315185	0.017468	Up

Table 5: RNA-seq in the brain of WT and SIRT6 knockout (BSKO) mice.

gene	WT's	KO's	Adj_P_value	significant	Expression in KO
Fat2	21.3444	0.065496	0.009071	yes	Down
Cbln3	122.346	0.382333	0.009071	yes	Down
Gabra6	97.7576	0.681489	0.009071	yes	Down
En2	16.7269	0.307049	0.009071	yes	Down
Car8	107.353	2.80684	0.009071	yes	Down
Ppp1r17	43.8025	1.27433	0.009071	yes	Down
Arhgef33	17.0481	0.630474	0.009071	yes	Down
Kcng4	21.7647	0.90919	0.009071	yes	Down

Glra1	15.8763	0.802628	0.009071	yes	Down
Tfap2b	3.85248	0.210133	0.009071	yes	Down
Cbln1	135.458	7.90819	0.009071	yes	Down
Neurod1	55.6205	4.65728	0.009071	yes	Down
Klk6	26.8327	2.61487	0.009071	yes	Down
Grid2ip	8.12322	0.792406	0.009071	yes	Down
Pvalb	373.352	36.9315	0.009071	yes	Down
Atp2a3	25.0933	2.48296	0.009071	yes	Down
Il16	14.9382	1.61729	0.009071	yes	Down
H2-Ab1	21.474	2.64332	0.009071	yes	Down
A2m	8.4734	1.0729	0.009071	yes	Down
3830431G21Rik	12.5947	1.62833	0.009071	yes	Down
Syt2	51.6976	6.93292	0.009071	yes	Down
Zic1	77.3074	10.6081	0.009071	yes	Down
Cd74	63.9988	9.43807	0.009071	yes	Down
Mybpc3	7.53329	1.16938	0.009071	yes	Down
Cep76	13.638	2.31316	0.009071	yes	Down
Col18a1	8.13016	1.38405	0.009071	yes	Down
D0H4S114	236.822	41.2284	0.009071	yes	Down
Gdf10	23.4499	4.08887	0.009071	yes	Down
Zic2	40.2421	7.09771	0.009071	yes	Down
Grid2	20.9506	3.76872	0.009071	yes	Down
Slc1a6	34.2663	6.1822	0.009071	yes	Down
Spp1	57.3749	10.4958	0.009071	yes	Down
Inadl	23.4758	4.70171	0.009071	yes	Down
Fam107b	22.891	5.12685	0.009071	yes	Down
Gng13	210.184	47.5246	0.009071	yes	Down
Ret	6.13065	1.45929	0.009071	yes	Down
Exph5	9.43823	2.32305	0.009071	yes	Down
Rps6ka1	18.7917	4.99202	0.009071	yes	Down
Chd7	8.59972	2.31418	0.009071	yes	Down
Grm4	41.668	11.2571	0.009071	yes	Down
Trpc3	16.671	4.60902	0.009071	yes	Down
Stk17b	12.2074	3.4382	0.009071	yes	Down
H2-K1	65.6019	18.8382	0.009071	yes	Down
Prkcd	22.9324	6.66041	0.009071	yes	Down
Tmem145	33.9936	10.0036	0.009071	yes	Down
Plxdc1	16.0279	4.80403	0.009071	yes	Down
Grin2c	32.6322	10.481	0.009071	yes	Down
Cdkl5	6.40557	19.2672	0.009071	yes	Up
Pde1b	68.8485	232.389	0.009071	yes	Up
Lrrc7	4.01655	14.095	0.009071	yes	Up
2900052N01Rik	10.227	37.4537	0.009071	yes	Up
Pde10a	18.1124	66.7676	0.009071	yes	Up

Adcy5	31.6869	118.402	0.009071	yes	Up
Tmem90a	13.2047	49.5831	0.009071	yes	Up
Rasd2	31.7629	121.392	0.009071	yes	Up
Rxrg	5.74313	23.6767	0.009071	yes	Up
Adora2a	9.54036	41.4322	0.009071	yes	Up
Gpr26	5.26345	24.5928	0.009071	yes	Up
Rgs9	16.4261	78.1484	0.009071	yes	Up
Drd1a	4.80366	24.4326	0.009071	yes	Up
Drd2	7.11747	37.2461	0.009071	yes	Up
Gng7	39.854	221.226	0.009071	yes	Up
Grin2b	1.9785	11.1192	0.009071	yes	Up
Gpr88	25.4306	145.998	0.009071	yes	Up
Zranb3	1.72713	12.7301	0.009071	yes	Up
Serpina9	1.47654	13.9447	0.009071	yes	Up
Esr1	0.712713	9.51112	0.009071	yes	Up
Cdhr1	0.94688	13.3648	0.009071	yes	Up
Myo3b	0.1786	4.50093	0.009071	yes	Up
Cacng1	0	1.03596	0.009071	yes	Up
1700121N20Rik	0	0.835734	0.009071	yes	Up
Iltifb	2.77306	0	0.009071	yes	Down
Hoxb8	1.6225	0	0.009071	yes	Down
Hoxb6	1.92169	0	0.009071	yes	Down
Hoxb3	2.12654	0	0.009071	yes	Down
Hoxb2	1.85402	0	0.009071	yes	Down
Tlx3	3.05016	0	0.009071	yes	Down
Hcrt	7.14666	0	0.009071	yes	Down
Hoxc4	2.51059	0	0.009071	yes	Down
Tgm5	0.706298	0	0.009071	yes	Down
Sycp1	2.0993	0	0.009071	yes	Down
Ambp	1.16415	0	0.009071	yes	Down
Phox2b	0.910403	0	0.009071	yes	Down
Hoxa2	0.951669	0	0.009071	yes	Down
Slc6a5	15.1909	0	0.009071	yes	Down
Barhl2	7.05782	0.641247	0.015735	yes	Down
Sncg	39.5883	4.62507	0.015735	yes	Down
Mybpc1	4.70278	0.725623	0.015735	yes	Down
Epn3	4.87242	0.757577	0.015735	yes	Down
Mreg	7.78086	1.67449	0.015735	yes	Down
Rnf152	9.18658	2.43885	0.015735	yes	Down
Hopx	91.5364	25.2379	0.015735	yes	Down
Bcl11b	7.5818	25.69	0.015735	yes	Up
Lrrc10b	11.7865	61.4355	0.015735	yes	Up
Sec14l3	0.686405	4.65504	0.015735	yes	Up
Pgam2	3.48032	34.2697	0.015735	yes	Up

Serpina1c	1.01619	0	0.015735	yes	Down
Uts2d	1.11097	0	0.015735	yes	Down
Gm2694	23.4956	2.22175	0.020838	yes	Down
Gbp6	3.06394	0.467761	0.020838	yes	Down
H2-Eb1	15.3776	2.68621	0.020838	yes	Down
St18	9.69948	2.46025	0.020838	yes	Down
Trim67	4.5294	1.19208	0.020838	yes	Down
Megf11	16.4076	4.85341	0.020838	yes	Down
Kank2	13.1785	3.9616	0.020838	yes	Down
Cpne9	22.5003	6.87089	0.020838	yes	Down
Anln	14.9538	4.99135	0.020838	yes	Down
Fosl2	3.67774	11.0892	0.020838	yes	Up
Ppp1r1b	125.032	407.363	0.020838	yes	Up
Gm1337	4.87087	19.7408	0.020838	yes	Up
Rps15a-ps8	0	1.22827	0.020838	yes	Up
Ebf3	3.46043	0.513162	0.025488	yes	Down
Afap1l2	10.125	2.80236	0.025488	yes	Down
Zfp521	10.1302	3.06005	0.025488	yes	Down
Ndst3	12.0939	4.40557	0.025488	yes	Down
Gng4	13.3135	38.4778	0.025488	yes	Up
Meis2	17.9795	53.4886	0.025488	yes	Up
Gabra2	12.6345	40.1313	0.025488	yes	Up
Actn2	3.83756	16.8644	0.025488	yes	Up
Kcna5	1.47963	7.5377	0.025488	yes	Up
Hpd	0.819984	0	0.025488	yes	Down
Prph	5.77769	0.212922	0.028346	yes	Down
Chn2	82.4358	20.1955	0.028346	yes	Down
Cdc42bpg	5.54009	1.42691	0.028346	yes	Down
Flt3	6.51705	1.71316	0.028346	yes	Down
Steap2	6.73271	2.06297	0.028346	yes	Down
Tprn	22.4551	7.43383	0.028346	yes	Down
Adamts10	14.5109	4.8852	0.028346	yes	Down
Kcnq3	6.91835	19.6641	0.028346	yes	Up
Syt6	5.77394	17.1342	0.028346	yes	Up
Mn1	3.41338	10.9638	0.028346	yes	Up
Accn4	5.80713	20.7627	0.028346	yes	Up
Slc35d3	2.08725	8.55645	0.028346	yes	Up
9030224M15Rik	0.666732	5.15906	0.028346	yes	Up
Prl2c3	0.891015	0	0.028346	yes	Down
Fabp1	2.56372	0	0.028346	yes	Down
C3	3.43823	0.175216	0.031903	yes	Down
H2-Aa	28.3508	3.59396	0.031903	yes	Down
Ttll5	16.2795	5.53225	0.031903	yes	Down
Ermn	38.8387	14.1375	0.031903	yes	Down

Dclk3	8.77294	24.4725	0.031903	yes	Up
Tmem158	24.2101	74.7761	0.031903	yes	Up
Nr4a3	2.41994	10.4632	0.031903	yes	Up
Lamb3	0.62161	3.15374	0.031903	yes	Up
Pcsk9	1.02207	6.16753	0.031903	yes	Up
Rgl3	8.31617	1.48456	0.036222	yes	Down
S100b	223.452	69.9074	0.036222	yes	Down
4930485B16Rik	0.79599	3.08777	0.036222	yes	Up
Gm2373	0.442777	3.49861	0.036222	yes	Up
Ank1	35.4469	9.03213	0.039794	yes	Down
Vamp1	189.806	50.4076	0.039794	yes	Down
Plcb4	32.7968	10.2698	0.039794	yes	Down
Pde7b	7.3915	19.9974	0.039794	yes	Up
Cpne5	10.8682	37.2303	0.039794	yes	Up
Cryba2	0.676829	0	0.039794	yes	Down
Igj	13.9809	0.226451	0.043642	yes	Down
Svep1	1.3585	0.276255	0.043642	yes	Down
Cdh15	5.84997	1.41484	0.043642	yes	Down
Foxp1	8.66953	21.7492	0.043642	yes	Up
Psmb8	8.99415	1.43001	0.047593	yes	Down
Ldlrap1	6.24261	1.33359	0.047593	yes	Down
Th	4.1424	15.9186	0.047593	yes	Up

Table 6: Panther pathway analysis of significant genes from RNA-seq.

Analysis Type:	PANTHER Overrepresentation Test (release 20170413)
Annotation Version and Release Date:	PANTHER version 12.0 Released 2017-07-10
Analyzed List:	Client Text Box Input (Mus musculus)
Reference List:	Mus musculus (all genes in database)
Bonferroni correction:	TRUE
Bonferroni count:	158

PANTHER Pathways	Mus musculus - REFLIST (22221)	Client Text Box Input (187)	Client Text Box Input (expected)	Client Text Box Input (fold Enrichment)	Client Text Box Input (P-value)
Unclassified (UNCLASSIFIED)	19621	141	165.12	0.85	0.00E+00

Heterotrimeric G-protein signaling pathway-Gq alpha and Go alpha mediated pathway (P00027)	119	11	1	10.98	1.26E-06
Dopamine receptor mediated signaling pathway (P05912)	58	7	0.49	14.34	1.23E-04
Heterotrimeric G-protein signaling pathway-Gi alpha and Gs alpha mediated pathway (P00026)	156	10	1.31	7.62	1.68E-04
Muscarinic acetylcholine receptor 1 and 3 signaling pathway (P00042)	61	7	0.51	13.64	1.71E-04
Metabotropic glutamate receptor group III pathway (P00039)	67	7	0.56	12.41	3.16E-04
5HT2 type receptor mediated signaling pathway (P04374)	69	6	0.58	10.33	4.80E-03
Oxytocin receptor mediated signaling pathway (P04391)	60	5	0.5	9.9	2.72E-02
5HT4 type receptor mediated signaling pathway (P04376)	33	4	0.28	14.4	3.05E-02
Thyrotropin-releasing hormone receptor signaling pathway (P04394)	63	5	0.53	9.43	3.41E-02
Heterotrimeric G-protein signaling pathway-rod outer segment phototransduction (P00028)	34	4	0.29	13.98	3.42E-02
Nicotine pharmacodynamics pathway (P06587)	35	4	0.29	13.58	3.81E-02
Wnt signaling pathway (P00057)	306	10	2.58	3.88	4.81E-02

Table 7: Panther process analysis of significant genes from RNA-seq.

Analysis Type:	PANTHER Overrepresentation Test (release 20170413)
Annotation Version and Release Date:	GO Ontology database Released 2017-08-14
Analyzed List:	Client Text Box Input (Mus musculus)
Reference List:	Mus musculus (all genes in database)
Bonferroni correction:	TRUE
Bonferroni count:	8483

GO biological process complete	Mus musculus - REFLIST (22221)	Client Text Box Input (187)	Client Text Box Input (expected)	Client Text Box Input (over/under)	Client Text Box Input (fold Enrichment)	Client Text Box Input (P-value)
Unclassified (UNCLASSIFIED)	1678	5	14.12	-	0.35	0.00E+00

biological regulation (GO:0065007)	11376	147	95.73	+	1.54	7.48E-11
regulation of biological process (GO:0050789)	10867	141	91.45	+	1.54	1.02E-09
regulation of cellular process (GO:0050794)	10275	134	86.47	+	1.55	1.44E-08
cellular developmental process (GO:0048869)	3496	67	29.42	+	2.28	1.36E-07
cell differentiation (GO:0030154)	3427	66	28.84	+	2.29	1.69E-07
multicellular organismal process (GO:0032501)	7032	102	59.18	+	1.72	7.00E-07
regulation of multicellular organismal process (GO:0051239)	2747	56	23.12	+	2.42	1.33E-06
locomotory behavior (GO:0007626)	230	15	1.94	+	7.75	1.37E-05
developmental process (GO:0032502)	5122	80	43.1	+	1.86	1.57E-05
anatomical structure development (GO:0048856)	4795	76	40.35	+	1.88	2.80E-05
behavior (GO:0007610)	631	23	5.31	+	4.33	4.21E-05
positive regulation of biological process (GO:0048518)	5342	81	44.96	+	1.8	4.84E-05
chemical synaptic transmission (GO:0007268)	338	17	2.84	+	5.98	5.08E-05
anterograde trans-synaptic signaling (GO:0098916)	338	17	2.84	+	5.98	5.08E-05
trans-synaptic signaling (GO:0099537)	345	17	2.9	+	5.86	6.84E-05
synaptic signaling (GO:0099536)	347	17	2.92	+	5.82	7.44E-05
positive regulation of cellular process (GO:0048522)	4836	75	40.7	+	1.84	1.03E-04
regulation of biological quality (GO:0065008)	3281	58	27.61	+	2.1	1.22E-04
system development (GO:0048731)	3943	65	33.18	+	1.96	1.70E-04
regulation of transport (GO:0051049)	1855	40	15.61	+	2.56	2.53E-04
generation of neurons (GO:0048699)	1486	35	12.51	+	2.8	2.64E-04
synaptic transmission, dopaminergic (GO:0001963)	22	6	0.19	+	32.41	3.75E-04
neurogenesis (GO:0022008)	1586	36	13.35	+	2.7	4.08E-04
multicellular organism development (GO:0007275)	4506	70	37.92	+	1.85	4.13E-04
regulation of nervous system development (GO:0051960)	912	26	7.67	+	3.39	5.48E-04
regulation of multicellular organismal development (GO:2000026)	1841	39	15.49	+	2.52	6.25E-04
central nervous system	747	23	6.29	+	3.66	8.85E-04

development (GO:0007417)						
regulation of cell differentiation (GO:0045595)	1673	36	14.08	+	2.56	1.51E-03
cell communication (GO:0007154)	5067	74	42.64	+	1.74	1.81E-03
positive regulation of nucleic acid-templated transcription (GO:1903508)	1404	32	11.82	+	2.71	2.36E-03
positive regulation of transcription, DNA-templated (GO:0045893)	1404	32	11.82	+	2.71	2.36E-03
positive regulation of RNA biosynthetic process (GO:1902680)	1405	32	11.82	+	2.71	2.40E-03
animal organ development (GO:0048513)	2807	49	23.62	+	2.07	3.60E-03
regulation of neurogenesis (GO:0050767)	816	23	6.87	+	3.35	4.10E-03
response to amphetamine (GO:0001975)	18	5	0.15	+	33.01	4.73E-03
positive regulation of gene expression (GO:0010628)	1760	36	14.81	+	2.43	5.08E-03
response to organic substance (GO:0010033)	2255	42	18.98	+	2.21	5.82E-03
nervous system development (GO:0007399)	2093	40	17.61	+	2.27	6.01E-03
response to amine (GO:0014075)	19	5	0.16	+	31.27	6.15E-03
regulation of ion transport (GO:0043269)	649	20	5.46	+	3.66	6.28E-03
positive regulation of RNA metabolic process (GO:0051254)	1477	32	12.43	+	2.57	7.10E-03
regulation of developmental process (GO:0050793)	2357	43	19.84	+	2.17	7.19E-03
anatomical structure morphogenesis (GO:0009653)	2031	39	17.09	+	2.28	7.62E-03
sarcomere organization (GO:0045214)	37	6	0.31	+	19.27	7.65E-03
signaling (GO:0023052)	4958	71	41.72	+	1.7	8.23E-03
positive regulation of nucleobase-containing compound metabolic process (GO:0045935)	1727	35	14.53	+	2.41	9.28E-03
antigen processing and presentation of exogenous peptide antigen (GO:0002478)	21	5	0.18	+	28.29	1.00E-02
neuromuscular process (GO:0050905)	122	9	1.03	+	8.77	1.01E-02
rhombomere development (GO:0021546)	9	4	0.08	+	52.81	1.06E-02
regulation of neuron	674	20	5.67	+	3.53	1.12E-02

differentiation (GO:0045664)						
cognition (GO:0050890)	289	13	2.43	+	5.35	1.13E-02
cellular process (GO:0009987)	13735	146	115.59	+	1.26	1.25E-02
regulation of cell development (GO:0060284)	941	24	7.92	+	3.03	1.31E-02
regulation of developmental growth (GO:0048638)	346	14	2.91	+	4.81	1.50E-02
positive regulation of cellular biosynthetic process (GO:0031328)	1780	35	14.98	+	2.34	1.84E-02
learning or memory (GO:0007611)	258	12	2.17	+	5.53	2.08E-02
response to stimulus (GO:0050896)	7620	95	64.13	+	1.48	2.15E-02
response to oxygen-containing compound (GO:1901700)	1110	26	9.34	+	2.78	2.18E-02
positive regulation of biosynthetic process (GO:0009891)	1814	35	15.27	+	2.29	2.80E-02
antigen processing and presentation of exogenous antigen (GO:0019884)	26	5	0.22	+	22.85	2.81E-02
muscle contraction (GO:0006936)	178	10	1.5	+	6.68	2.88E-02
regulation of neurotransmitter levels (GO:0001505)	180	10	1.51	+	6.6	3.17E-02
negative regulation of biological process (GO:0048519)	4650	66	39.13	+	1.69	3.49E-02

Table 8: Panther cellular component analysis of significant genes from RNA-seq.

Analysis Type:	PANTHER Overrepresentation Test (release 20170413)
Annotation Version and Release Date:	GO Ontology database Released 2017-08-14
Analyzed List:	Client Text Box Input (Mus musculus)
Reference List:	Mus musculus (all genes in database)
Bonferroni correction:	TRUE
Bonferroni count:	1311

GO cellular component complete	Mus musculus - REFLIST (22221)	Client Text Box Input (187)	Client Text Box Input (expected)	Client Text Box Input (over/under)	Client Text Box Input (fold Enrichment)	Client Text Box Input (P-value)

Unclassified (UNCLASSIFIED)	1433	3	12.06	-	0.25	0.00E+00
neuron part (GO:0097458)	1579	43	13.29	+	3.24	7.63E-09
somatodendritic compartment (GO:0036477)	889	30	7.48	+	4.01	1.46E-07
organelle (GO:0043226)	12286	145	103.39	+	1.4	2.56E-07
neuron projection (GO:0043005)	1308	36	11.01	+	3.27	4.27E-07
synapse (GO:0045202)	921	29	7.75	+	3.74	1.49E-06
cell periphery (GO:0071944)	4887	77	41.13	+	1.87	4.15E-06
cell part (GO:0044464)	15167	162	127.64	+	1.27	6.84E-06
cell (GO:0005623)	15171	162	127.67	+	1.27	7.04E-06
plasma membrane bounded cell projection (GO:0120025)	1975	43	16.62	+	2.59	7.77E-06
plasma membrane (GO:0005886)	4765	75	40.1	+	1.87	8.15E-06
cell projection (GO:0042995)	2147	44	18.07	+	2.44	2.97E-05
neuronal cell body (GO:0043025)	646	22	5.44	+	4.05	4.73E-05
membrane-bounded organelle (GO:0043227)	11357	132	95.57	+	1.38	6.18E-05
axon (GO:0030424)	500	19	4.21	+	4.52	8.13E-05
plasma membrane part (GO:0044459)	2560	48	21.54	+	2.23	9.03E-05
synapse part (GO:0044456)	733	23	6.17	+	3.73	9.80E-05
axon part (GO:0033267)	233	13	1.96	+	6.63	1.60E-04
intracellular part (GO:0044424)	12888	142	108.46	+	1.31	2.88E-04
cell body (GO:0044297)	725	22	6.1	+	3.61	3.38E-04
intracellular (GO:0005622)	13001	142	109.41	+	1.3	5.83E-04
axon terminus (GO:0043679)	185	11	1.56	+	7.07	8.29E-04
MHC class II protein complex (GO:0042613)	9	4	0.08	+	52.81	1.64E-03
neuron projection terminus (GO:0044306)	200	11	1.68	+	6.54	1.75E-03
MHC protein complex (GO:0042611)	23	5	0.19	+	25.83	2.40E-03
presynapse (GO:0098793)	358	14	3.01	+	4.65	3.43E-03
synaptic membrane (GO:0097060)	311	13	2.62	+	4.97	3.87E-03
plasma membrane	224	11	1.89	+	5.84	5.12E-03

protein complex (GO:0098797)							
dendrite (GO:0030425)	600	18	5.05	+		3.56	5.18E-03
plasma membrane region (GO:0098590)	936	23	7.88	+		2.92	6.24E-03
intracellular organelle (GO:0043229)	11257	125	94.73	+		1.32	7.22E-03
terminal bouton (GO:0043195)	114	8	0.96	+		8.34	8.88E-03
postsynaptic membrane (GO:0045211)	243	11	2.04	+		5.38	1.09E-02
Z disc (GO:0030018)	118	8	0.99	+		8.06	1.14E-02
postsynapse (GO:0098794)	472	15	3.97	+		3.78	1.76E-02
vesicle (GO:0031982)	3853	56	32.42	+		1.73	2.11E-02
I band (GO:0031674)	133	8	1.12	+		7.15	2.66E-02
cell projection part (GO:0044463)	1103	24	9.28	+		2.59	2.82E-02
plasma membrane bounded cell projection part (GO:0120038)	1103	24	9.28	+		2.59	2.82E-02

Table 9: Panther molecular function analysis of significant genes from RNA-seq.

Analysis Type:	PANTHER Overrepresentation Test (release 20170413)
Annotation Version and Release Date:	GO Ontology database Released 2017-08-14
Analyzed List:	Client Text Box Input (Mus musculus)
Reference List:	Mus musculus (all genes in database)
Bonferroni correction:	TRUE
Bonferroni count:	3061

GO molecular function complete	Mus musculus - REFLIST (22221)	Client Text Box Input (187)	Client Text Box Input (expected)	Client Text Box Input (over/under)	Client Text Box Input (fold Enrichment)
Unclassified (UNCLASSIFIED)	1859	2	15.64	-	< 0.2
binding (GO:0005488)	#####	152	106.1	+	1.43
protein binding (GO:0005515)	8402	118	70.71	+	1.67
cation binding (GO:0043169)	3480	59	29.29	+	2.01
RNA polymerase II regulatory region sequence-specific DNA binding (GO:0000977)	677	22	5.7	+	3.86

RNA polymerase II regulatory region DNA binding (GO:0001012)	683	22	5.75	+	3.83
sequence-specific DNA binding (GO:0043565)	1047	27	8.81	+	3.06
metal ion binding (GO:0046872)	3384	56	28.48	+	1.97
transcription regulatory region sequence-specific DNA binding (GO:0000976)	748	22	6.29	+	3.49
RNA polymerase II core promoter proximal region sequence-specific DNA binding (GO:0000978)	414	16	3.48	+	4.59
core promoter proximal region sequence-specific DNA binding (GO:0000987)	426	16	3.58	+	4.46
sequence-specific double-stranded DNA binding (GO:1990837)	780	22	6.56	+	3.35
core promoter proximal region DNA binding (GO:0001159)	428	16	3.6	+	4.44
neurotransmitter receptor activity (GO:0030594)	96	8	0.81	+	9.9
ion binding (GO:0043167)	5283	73	44.46	+	1.64
transmitter-gated channel activity (GO:0022835)	46	6	0.39	+	15.5
transmitter-gated ion channel activity (GO:0022824)	46	6	0.39	+	15.5
double-stranded DNA binding (GO:0003690)	862	22	7.25	+	3.03
transcription factor activity, RNA polymerase II core promoter proximal region sequence-specific binding (GO:0000982)	432	15	3.64	+	4.13
protein dimerization activity (GO:0046983)	1305	28	10.98	+	2.55
transcription regulatory region DNA binding (GO:0044212)	892	22	7.51	+	2.93
regulatory region DNA binding (GO:0000975)	894	22	7.52	+	2.92
regulatory region nucleic acid binding (GO:0001067)	898	22	7.56	+	2.91
transcriptional activator activity, RNA polymerase II core promoter proximal region sequence-specific binding (GO:0001077)	291	12	2.45	+	4.9
calcium ion binding (GO:0005509)	583	17	4.91	+	3.46
molecular_function (GO:0003674)	#####	185	171.4	+	1.08

MATERIALS AND METHODS

All resources generated from this study will be or already are openly shared with the research community.

In vitro cell culture experiments

Immortalized fibroblasts

Mouse embryonic fibroblasts were cultured in DMEM supplemented with 10% fetal bovine serum and penicillin/streptomycin antibiotics. The immortalized WT and SIRT6 null fibroblasts were previously generated in the laboratory of and are a generous gift from Dr. Raul Mostoslvasky.

Primary neuronal cultures

Primary neurons were isolated from P0 pups by a standard protocol (Brewer & Torricelli 2007) modified for our study. Briefly, after dissection of neonatal brains, cortices were minced and digested in papain for 30 minutes at 30C^{o} temperature. After that the solution was filtered through a 100 μm filter and then fractionated in a sucrose gradient. The gradient fractions containing neurons were collected and re-suspended in Neuro Basal Media, and cells were counted and plated on poly-D-lysine coated plates. The neurons were cultured in Neuro Basal Media with physiological concentrations of glucose (2.5 mM) at physiological concentrations of oxygen (5%) and supplemented with bFGF and B27. Cultures were treated and analyzed 7 days after plating.

Histochemical analysis performed on every batch of cells confirmed that cells were comprised of 75% neurons and 25% astrocytes. Proportions were identified by flow cytometry with the markers- NeuN and GFAP respectively (**Supplementary Fig. 5**). The neuron population included tyrosine hydroxylase expressing cells confirmed by SDS-PAGE analysis. Proportion of neural cell types were not changed between WT, SIRT6 KO, and OX cultures.

To prevent mycoplasma, bacterial and fungal contamination streptomycin, penicillin, and amphotericin b were used in manufacturer specified concentrations.

For Fig. 2F and Fig. 3G only: Cortical neurons extracted from E18 Sprague Dawley embryos were seeded at a cell density of 10,000 cells/well in a poly-D-lysine coated 96 well plate using NBActive 1 as culture medium with growth supplement N21

Flow cytometry

Primary neurons or fibroblasts were collected from wells using Trypsin digestion. Cells were washed in PBS and then suspended in 100 μL of 1X binding buffer (10 mM HEPES, 140 mM NaCl, 2.5 mM $CaCl_2$, pH 7.4) with 5 μL of Annexin-V conjugate and PI. After a 15-minute incubation another 400 μL of binding buffer was added and then at least 10,000 cells were analyzed using a 3 laser/ 8 color Beckton-Dickinson LSR II. In the case of NeuN and GFAP markers, primary cultures were permeabilized with triton to allow intracellular staining.

MTT assay

MTT assay was used to assess the number of viable cells in each treatment condition by measuring fluorescence at 570nm and 690nm (Fig. 3G only)

Nicotine

-(-) nicotine was used for all cell culture experiments (Sigma, Cat# N3876). Fresh dilutions were made for every experiment.

MG132

((R)-MG132, Cayman, Cat# 13697-1). Diluted in DMSO.

Cigarette smoke extract

Cigarette smoke was extracted by a custom vacuum device. Briefly, two 100 mm Marlboro cigarettes were burnt completely, and their smoke vacuum collected and bubbled through 20 mL of Neuro Basal Media for 1 minute. This media was considered 100% cigarette smoke extract (CSE), which was later diluted and applied to cells at various concentrations.

Human GWAS meta-analysis

The ROS-MAP cohorts are community-based cohort studies of aging in which all participants are organ donors(Bennett *et al.* 2012). We used 438 brains from subjects aged 67-108 years old with transcriptomic data including subjects with and without a variety of clinical diagnoses and phenotypes. Subjects were 2/3 female and predominantly Caucasian. Cohort characteristics can be found in the table below. In

the original study, RNA was extracted from fresh frozen cortex sections and processed and analyzed using standard commercial RNA sequencing methods. RNA integrity was between 5.0 and 9.9, and postmortem intervals were 0-41 hours. The dataset had already been assembled into RPKM values based on ENSEMBL gene ID. Data is available at https://www.synapse.org/#!Synapse:syn3219045.

Further normalization and quality control procedures were applied to each of the datasets. First, outlier values for each gene were removed (standard deviation > 4). There were several samples for which many genes were outliers (>300). These samples were removed. Overall, these samples had lower than average RIN scores. After removing those samples, the remaining outlier values were imputed with a K-nearest neighbor algorithm[40]. To put the datasets on a comparable scale, we scaled the dataset by mean (0-normalized) and standard deviation (normalized so the standard deviation for each gene is 1).

For continuous variables in ROS-MAP such as PD symptoms, we used a linear regression model subtracting *APOE ε4*, age, sex, race, and population principle components, study number, RNA integrity, and batch. Logistic regression was used in the case of binary variables such as PD diagnosis.

ROS-MAP characteristics

ROS-MAP Cohort Characteristics	n=438

Age range	67-108 years
Sex female	275 subjects
Average education	16.5 years
Race white	437 subjects
Race black	1 subject
Average post mortem interval	7.1 hrs
Past medical history of AD	170 subjects
Pathological diagnosis of AD	261 subjects
Past medical history of PD	31 subjects
Past medical history of Lewy body dementia	11 subjects
Self report history of thyroid problems	73 subjects
Self report history of heart problems	72 subjects
Self report history of stroke	43 subjects
Self report history of cancer	143 subjects
Self report history of hypertension	203 subjects

Human brain tissue analysis

Brain tissue specimens was acquired from participants in the Religious Orders Study and provided by the Rush Alzheimer's Disease Center, Rush University Medical Center in Chicago. Samples were taken from the mid-temporal cortex for every specimen. Samples were homogenized and protein was isolated as described in **SDS-PAGE, Western**.

Brain tissue specimens were also obtained from the Human Brain and Spinal Fluid Resource Center, VA West Los Angeles Healthcare Center, Los Angeles, CA 90073 which is sponsored by the NINDS/NIMH, National Multiple Sclerosis Society, and Department of Veteran Affairs. Tissue samples were taken from the frontal cortex (coronal slab #4) for every specimen. Samples were homogenized and protein was isolated as described in **SDS-PAGE, Western**.

Sodium-dodecyl-sulfate polyacrylamide gel electrophoresis (SDS-PAGE, Western) immunoblots

Tissues or cells were lysed in RIPA buffer (50 mM Tris at pH 7.4, 150 mM NaCl, 1M EDTA, 0.25% deoxy chloric acid, and 1% NP-40) supplemented with protease inhibitor cocktail (Roche, Cat# 4693116001) and phosphatase inhibitors (20mM sodium fluoride, 1mM sodium orthovanadate). The mixture was centrifuged, and supernatant was taken. Protein levels were standardized using a Bradford protein assay. Protein was mixed with sodium dodecyl sulfate and electrophoresed in a 13% or 12% acrylamide gels. Proteins were transferred to a PVDF membrane (0.45uM) and

the membrane was then immunoblotted with antibodies, diluted at concentrations recommend by the manufacturer, against the specific proteins being examined. In this study we used the following **Antibodies**: anti-SIRT1 (rabbit polyclonal, gift from Imai Shin (Satoh *et al.* 2010)), anti-SIRT6 (rabbit polyclonal, Sigma-Aldrich, Cat# S4322), anti-SIRT6 (rabbit monoclonal, Cell Signaling Technology, Cat# 12486, used only for Fig. 2F), anti-AKT (rabbit monoclonal, Cell Signaling Technology, Cat# 4691), anti-pAKT-S473 (rabbit monoclonal, Cell Signaling Technology, Cat# 4060), anti-Tyrosine Hydroxalase (rabbit polyclonal, Abcam, Cat# ab112), anti-NeuN (rabbit monoclonal, Abcam, Cat# ab177487), anti-TNF alpha (rabbit polyclonal, Abcam, Cat# ab9739), anti-β-actin (mouse monoclonal, Abcam, Cat#ab8226), anti-GFAP (mouse monoclonal, ThermoFisher Scientific, Cat# 50-9892). Band intensities were quantified using ImageJ.

TNFα analysis

Commercial TNFα ELISA kits were used: Mouse TNFα DuoSet ELISA (R&D Systems, Cat# DY410). Media samples were analyzed in a Biotek Synergy 2 Multi-Mode Reader. Reads were normalized to cell number and amount of media present in the respective well.

Proteasome activity assay

Protocol was followed from Proteasome Activity Fluorometric Assay Kit (BioVision, Cat# K245-100). Primary neuronal cultures were treated with nicotine 90 minutes before assessment. Samples were analyzed in a Biotek Synergy 2 Multi-Mode Reader

Real-time reverse polymerase chain reaction (RT-PCR)

Total RNA was extracted from tissues or cell culture using RNeasy kit (Qiagen, Cat# 74104). A cDNA library was prepared using Superscript III Synthesis System (Invitrogen, Cat# 18080051). Reverse polymerase reaction was performed using poly-dT primers as per manufacturers instruction. qRT-PCR was performed using CFX96 Touch™ Real-Time PCR Detection System, using the following primers: MAOB-F: ATGAGCAACAAAAGCCATGTCA; MAOB-R: TCCTAATTGTGTAAGTCCTGCCT; DAT1 F: AAATGCTCCGTGGGACCAATG; DAT1 R: GTCTCCCGCTCTTGAACCTC; VMAT2-F: AGGGGACACCTCTTACGACC; VMAT2-R: CTGCCACTTTCGGGAACACA; SIRT6-F: CTGAGAGACACCATTCTGGACT; SIRT6-R: GGTTGCAGGTTGACAATGACC; β-ACTIN-F: GACAGGATGCAGAAGGAGATCA; β-ACTIN-R: CTGATCCACATCTGCTGGAAGGT. All primers target mouse transcripts spanning exon junctions to eliminate DNA contribution to message quantification. All relative mRNA abundance measurements were to β-actin.

MAO-B activity

MAO-B activity was analyzed by the commercial MAO-Glo™ Assay, Promega, Cat# V1401. Briefly, brain cortex homogenates were made in 100 mM HEPES 5% gylcerol buffer pH ~7.4. Homogenates were treated per MAO-Glo protocol and were treated

with clorgyline (MAOA inhibitor, Abcam, Cat# ab145646) and or deprenyl (MAOB inhibitor, Abcam, Cat# ab120604). Samples were analyzed in a Biotek Synergy 2 Multi-Mode Reader

Animal experiments and transgenic mice

All procedures were performed according to guidelines and under supervision of the Institutional Animal Care and Use Committee (IACUC) of Cornell University. For all tests, we used both male and female 3-month-old mice. All transgenic animals were compared to corresponding wild-type littermates. Based on variability of prior collected data, necessary sample sizes were estimated using power analysis. No animals were excluded from the analysis; assignment to treatment groups was done at random using animals ear-tag numbers and done separately for males and females. All mice were handled daily for two weeks prior to the behavioral tests to eliminate the influence of stress and anxiety on their behavior due to human handling. In all the tests, animal behavior was filmed and analyzed later with the help of custom-written software.

Conditional SIRT6 mice

SIRT6 conditional deletion allele has been described previously(Sebastian *et al.* 2012b). To obtain brain-specific SIRT6 knockout animals (BSKO), we crossed these mice, which have exons 2 and 3 of SIRT6 flanked by loxP sites (**Supplementary Fig. 2 A-D**), to a nestin-cre line of mice (JAX Stock# 003771).

To create conditional SIRT6 overexpressing mice (BSOX), chicken actin promoter

(CAG) was cloned in front of chloramphenicol acetyltransferase (CAT) gene, flanked by loxP cites. Mouse SIRT6 cDNA with added polyA signaling sequence was cloned in after the second loxP site. This construct normally expresses reporter gene – CAT, upon exposure to Cre-recombinase, the CAT gene would be excised and SIRT6 will be expressed (**Supplementary Fig. 2 A-D**). Linearized construct was injected into mouse embryo pronucleus, after which embryos were transferred into pseudo-pregnant dames. Pups were screened for the transgene presence by PCR and backcrossed into C57/BL for 8 generations. To overexpress SIRT6 specifically in the brain, resulting transgenic mice were crossed to nestin-cre line of mice (JAX Stock# 003771).

RNA sequencing and Overrepresentation Analysis

RNA was purified from dissected cortices of 3-month-old male BSKO, and BSOX mice, as well as their corresponding WT littermates (2 WT vs 2 BSKO, 2 WT vs 2 BSOX). Total purified RNA was depleted of cytoplasmic and mitochondrial rRNA using beads conjugated to oligonucleotides with sequences complimentary to those of ribosomal RNA. Purified and riboRNA-depleted RNA was fragmented and assessed for its quality and fragment size. cDNA library synthesis and adaptor/bar code ligation was done using Illumina TruSeq RNA Library Prep Kit, according to manufacturer instructions. The library was sequenced on an Illumina HiSeq instrument employing the 100bp single-ended run regime. This configuration routinely resulted in ~200 million reads per run. Obtained reads were mapped onto *Mus musculus* genome using the open source software programs – Bowtie2 and TopHat. Expression of various loci (both coding RNA, and short and intragenic long non-coding RNA) was assessed

across different genotypes using a related open source software program – Cufflinks and the R statistical package. Significantly altered genes were determined by p-values equal to or less than 0.05 after correction for false discovery. For overrepresentation analysis, genes significantly altered in BSKO and BSOX mice were combined and run with the Panther Classification System (http://www.pantherdb.org/). Separate analysis was performed for: Pathways, Biological Process, Cellular Component, and Molecular Function (**Tables. 4-9**). *Mus musculus* was used for the gene reference list, and Bonferroni correction for multiple testing was performed.

MPTP

In vivo MPTP and nicotine mouse experiments: MPTP was delivered by intraparietal injection at 10 mg/kg four times a day for four days a week (two weeks' total). Mice were scarified for immunohistochemistry 1 month after the completion of MPTP administration. Mice were 3 months of age at the start of treatment.

Nicotine

For *in vivo* administration, -(-) nicotine tartrate (MP Biomedicals, Cat# 0215355491) was added to tap water to create a concentration of free base nicotine at 200 μg per milliliter. Dilutions also contained 2% saccharin sodium salt hydrate (Oakwood Chemical, Cat# 098769). Control animals received only 2% saccharin. Nicotine dilutions were given in light protective bottles and made fresh 3 times a week. After 3 weeks of treatment mice were sacrificed and their tissues were analyzed. Mice were 3 months of age at the start of treatment.

MPTP & nicotine cotreatment

Mice received nicotine and MPTP as described above, nicotine was given throughout the trial starting two weeks prior to MPTP injections. Mice were scarified for immunohistochemistry 1 month after the completion of MPTP administration. Animals were 3 months of age at the start of the trial.

Behavior

Behavior was measured in experimental animals two weeks after MPTP administration. In this period, animals were attended daily, to insure their wellbeing, as well as to habituate them to human handling to eliminate the influence of stress and anxiety on their behavior in the open field test paradigm. In this paradigm, a single animal was introduced to a novel square (90 cm by 90 cm), well-lit arena, cleaned of any familiar scents and filmed for 5 minutes. To take into consideration circadian changes in the behavior, all the experiment were performed in the same time of the day, and no longer than 3 hours in a row. Each mouse was recorded for at least five minutes. Muse movement and statistics were analyzed automatically using custom-written tracking software, freely available upon request. At the time of data acquisition, identity of mouse genotype and treatment was not available to the person performing the analysis. Un-blinding was done only during statistical data analysis. The software and its code are available upon request.

Immunohistochemistry

Before brain sample collection animals underwent cardiac perfusion with PBS for 5

minutes, and with 4% paraformaldehyde for 10 minutes. After perfusions, brain samples were quickly harvested and further fixed in 4% phosphate buffered paraformaldehyde solution for 16 hours. After fixing, samples were cryo-protected in 30% sucrose for 30 hours, embedded in OCT (Tissue-Tek) and stored at −80°C until use. Serial sections at 15 μm thickness were made on a cryostat and mounted on Superfrost Plus slides. Before staining, sections were dehydrated in acetone at 20°C for 30 minutes, followed by three TBS washes before blocking in 1% normal goat serum for 2 hr. Primary antibodies were diluted in TNT buffer (50 mM Tris at pH 7.5, 150 mM NaCl and 0.05% Tween 20; 1:500) and allowed for overnight incubation at 4°C. Further staining steps were carried out with Vectastain Elite ABC HRP Kit (Vector Laboratories, now part of Maravai LifeSciences) according to the manufacturer's instructions. Microscopic images were obtained using Aperio ScanScope SC2 system of total slide capture. Intensities of stain and cell counting were done using ImageJ software, macro functions were created for automatic quantification. Stereological assessment was also performed on tissue slides using Stereology Analyzer v 4.3.3 by ADCIS. A region of interest was outlined around *the substantia nigra pars compacta* on section slides, then a point grid was generated (100 x 100 pixels sampling and pattern, 1 pixel = 0.5μm), if a grid point intersected a DA neuron it was counted, the volume fraction was subsequently computed. For each genotype/treatment, at least 5 sections from at least five mice were obtained and found to give a consistent pattern. Representative sections are shown in each case.

Experimental Statistical Analysis

For pairwise comparisons, relevant to data analysis two-tailed Student's t-test was used and is usually reported on figures using "*"-representations, where *$p<0.05$, **$p<0.01$, ***$p<0.001$, and ****$p<0.001$. T-test was calculated assuming "equal variance" if variance of compared samples was similar. In cases, where several conditions are being tested, one-way ANOVA was used, and performance and results of such analysis is described in figure captions. In cases were serval variables are influencing the same measured values, such as genotype and stress are influencing survival of cells; two-way ANOVA analysis was performed. In this case three p-values are reported in figure legends, such as p-value for the influence of genotype on survival, p-value for the influence of drug on the survival and interaction p-value, which is a statistical measure representing the confidence that genotype influenced the way drug influenced the measured value. Where appropriate, further pot-hoc statistical tests were performed. Calculations were preformed using licensed and registered copy of Microsoft Excel or the open source free statistical software R, with Bioconductor package.

For genotype association studies, a combination of R and p-link software was used, to create a linear regression model, where statistics was corrected for individual APOE ε4 status, age, sex, race, population principle components, RNA integrity, and batch as covariates. Bonferroni correction was used to account for multiple testing.

CHAPTER 4

CONCLUSIONS & FUTURE DIRECTIONS

PART 1: Using the novel canine model system, we have demonstrated that there are intrinsic cellular properties that correlate with breed longevity, which likely underlie aging diversity. Overall, our data support the hypothesis that the main driving force behind longevity diversity in dogs is thermogenesis. Due to extra demand for thermogenesis, smaller dogs evolved (or potentially responded) to have more uncoupled mitochondria, which in turn resulted in lowered electrical potential (due to proton leak), and elevated β-oxidation and catabolism (due to extra demand to fuel leaky mitochondria). We suggest that secondary changes associated with these adaptations happen to be beneficial for longevity; these include decreased production of reactive oxygen species, metabolic profiles which are less favorable for tumorigenesis, changes to cytoskeleton dynamics, and stress resistance.

What regulates the uncoupling differences between cells from long-lived and short-lived breeds? One outstanding question is how the fibroblasts from the many different dog breeds are maintaining breed-specific differences. One possibility is that small long-lived breeds are more uncoupled because of a thermodynamic response, smaller dogs initiating uncoupling to maintain heat (that is retained *in vitro* epigenetically). A second possibility is that these properties evolved with the breeds, are hardwired, and would persist regardless of breed size. We could test this by

epigenetic clearing compounds/techniques in culture and see if the cells are able to rederive their differences. If they do, then it suggests the differences are deriving from their DNA code, if not then it suggests a thermodynamic response that is carried over from the breed to culture.

Regardless we want to figure out the genes and regions of the DNA responsible for these property differences. One method to probe this is with ATAC-seq (Assay for Transposase-Accessible Chromatin using sequencing) and RNA sequencing in parallel. We can identify the differences in chromatin architecture and accessibility, which should align well with differences in transcription/gene expression. Importantly, this will give us a candidate list of longevity regulators/regions that govern the cellular properties we discovered. This list can be compared to the candidate genes generated by our GWAS. In fact, we have carried out a similar analysis already with published canine genomic methylation levels (Koch *et al.* 2016), where we identified significant regions with differential methylation that correlate with breed longevity. Nearby genes to these regions were also scanned and noted, with DIP2C as the strongest example (**Fig. 1**).

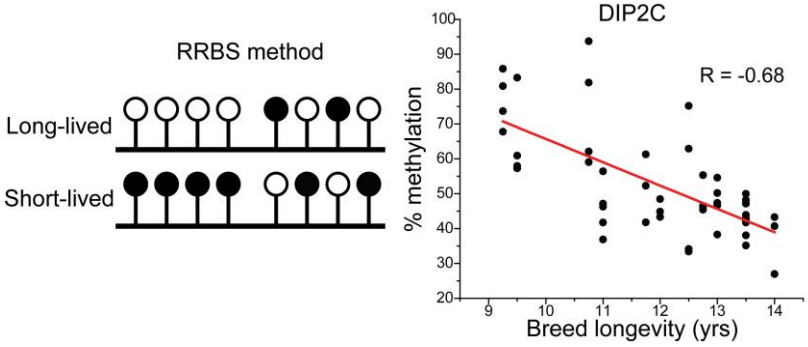

nearby gene	FDR p value	R	chr	start	end
DIP2C	0.0005	-0.68	2	34462000	34463000
TIA1A	0.0005	0.68	10	68759000	68761000
COL8A2	0.025	0.60	15	6108000	6109000
NRP2	0.033	0.59	37	14364000	14365000
PAX9	0.038	-0.57	8	15236000	15237000
UQCRFS1	0.038	0.57	1	122092000	1.22E+08
	0.038	-0.57	34	41401000	41402000
IFITM1	0.038	0.57	18	25491000	25492000
ADARB2	0.038	-0.56	2	33811000	33812000
ARHGEF10	0.049	0.55	16	54611000	54612000
B3GAT1	0.049	-0.55	5	748000	749000
ASB1	0.049	-0.55	25	48916000	48917000
MYT1L	0.049	0.55	17	1058000	1060000
CDH4	0.049	-0.55	24	45840000	45841000

Figure 1. Differential methylation states correlate with breed

longevity. Schematic of differential methylation state between short and long-lived dog breeds. Top candidate gene (DIP2C) and region where the tightest significant correlation exists between breed longevity and methylation percentage. Table showing significant hits (after correction for false discovery), Pearson correlation (R) for breed longevity and methylation status of a respective region.

Is β-oxidation fueling long-lived breed uncoupling (source of electrons)?

Based on our mass spectrometry data, we believe that cells from long-lived breeds preferentially utilize β-oxidation to fuel their uncoupled energetics. One way to confirm this would be through isotope labeling of glucose and fat derivates with flux analysis by mass spectrometry to track the carbon movement through metabolic pathways. This will tell us how the cells preferentially shuttle metabolites and which catabolic processes are favored.

Differences in cellular lactate concentrations in long and short-lived breeds was an interesting observation, especially since we did not observe breed longevity correlation in glycolysis (**PART 1**: **Fig. 3 & 5**). This seeming contradiction may arise from the fact that mass spectrometry measured intracellular lactate levels, whereas the Seahorse Analyzer measured extracellular lactate levels as a proxy for glycolysis. This should be confirmed and followed up as it suggests fascinating metabolic differences between long and short-breeds. Are short-lived breeds producing more lactate, but not necessarily performing more glycolysis, and how? The isotope labeling and tracking

of carbon through flux experiments should elucidate what is happening. Increasing the number of breeds for mass spectrometry will be crucial too.

Passive versus regulated uncoupling in the mitochondria.

Another area to explore in the future is if the higher degree of proton uncoupling in longer-lived breeds is a passive-diffuse process or is more tightly regulated by uncoupling proteins (proton transporters, like UCP1-3). Although no proton transporters were identified from our GWAS, it does not mean they are not involved.

Do the cellular profiles of long-lived breeds mimic that of caloric restriction?

Our data overall support a metabolic profile similar to that of CR, the higher degree of β-oxidation in particular. We should analyze ATP/ADP, NAD+, and other energy metabolites. An analysis of the expression of genes involved in the CR response (such as sirtuins and AMPK activity) should also be carried out. Perhaps the source of long-lived breed cells superior stress resistance is from a classical CR response.

What about whole dogs? How much do the cellular differences (particularly energetics) scale up to the organismal level? Cellular characteristics are fascinating but ultimately we want to know if these properties manifest in live dogs. Measuring energetics and oxygen consumption on live dogs of various long and short-lived breeds would answer this. This type of analysis has been performed but on a small scale (only three breeds) (Speakman *et al.* 2003). A more comprehensive examination with more breeds would confirm altered energetics between long and short-lived

breeds.

Does mitochondrial uncoupling variation take place within other species and humans with diversity in size?

There are data supporting that shorter people live longer than those who are tall (Kabat *et al.* 2013), as well as a wealth of data showing that those who are heavier or obese have reduced lifespans. We could isolate cells from humans of large and small size and measure their rates of uncoupling. This could show if innate cellular properties, such as uncoupling, influence tissue dynamics and aging in humans

Interestingly, exposure to cold (Holloszy & Smith 1986), as well as heat stress (Olsen *et al.* 2006) have been shown to extend lifespan in various animal models. Taken together with our data, it suggests that multiple thermogenic mechanisms influence longevity, where cold induced promotion of lifespan likely stems from uncoupling and increased energy expenditure.

PART 2: There are two major findings from the SIRT6-PD project. First, we identify the enzyme SIRT6 as a pathogenic factor and a possible therapeutic target for suppression of Parkinson's disease (PD) associated pathologies. Second, we demonstrate that the PD-protective properties of the tobacco component nicotine partly function through the degradation of SIRT6. A significant role of SIRT6 in cellular and neuronal survival is also demonstrated. Taken together our research results provide a mechanistic link for the negative correlation of tobacco use and the

incidence of PD and identify new potential therapeutic targets and a novel line of research.

Determine nicotine's mechanism of action on SIRT6

We demonstrate that nicotine can induce proteasome mediated degradation of SIRT6, but what are the upstream signals that nicotine is acting on? The neuroprotective effects of nicotine have mainly been attributed to action through the alpha-7 nicotinic receptor (Bencherif 2009; Barreto *et al.* 2014). To test whether alpha-7 receptors are involved in mediating the degradation of SIRT6, we can treat primary neuronal cultures with the alpha-7 agonist PNU282987 (PNU) or antagonist methyllycaconitine (MLA). These compounds should respectively mimic or block the actions of nicotine on SIRT6. Other nicotinic receptors can be similarly checked.

Determine the contribution of glial cell types to the pro-survival neuronal phenotype upon loss of SIRT6. Our transgenic mice lack or overexpress SIRT6 in all cells of neural origin. Thus, the relative contribution of glial and neuronal cell types to the differences in AKT, TNFα, and survival of neurons is unknown. Microglia and astrocytes regulate neuroinflammation, neuronal survival, and are implicated in PD pathogenesis. The presence of 75% NeuN and 25% GFAP positive cells indicates a majority neuronal population with astrocytes also present from our experiments. Furthermore, the majority of neonatal microglia do not express Nestin (Wlodarczyk *et al.* 2017) and thus would still carry SIRT6 in our transgenic model. There is no

detectable SIRT6 via western blot in our cultures. Thus, our data suggest that our cultures do not possess microglia. Further suggesting that, at least in our cultures, that it is the neurons and astrocytes that are important. Another possibility is that the neuronal pro-survival phenotype is due to an intrinsic property, increased AKT signaling in the neurons themselves for example. To elucidate the contribution of glia to neuronal survival we will carry out a series of primary co-culture experiments. We will measure the survival of WT neurons co-cultured with SIRT6 KO or OX glial cells (including microglia, astrocytes, and oligodendrocytes) after exposure to PD associated stressors. Microglia are still of interest because, although neurons can produce it, they synthesize the majority of TNFα in the brain (Welser-Alves & Milner 2013), KO/OX microglia can be made with a CRE-virus. Correspondingly, SIRT6 KO and OX neurons will be co-cultured with WT glial cells. These cultures can be compared to fully WT, KO, and OX cultures. We will learn the specific cell types where loss of SIRT6 is required for the improvement of neuronal survival. In addition, by measuring the secretion of TNFα and activation of AKT in these cultures, we can deduce the cellular contribution to the differences in these pathways.

Determine whether TNFα and or AKT are mediating survival downstream of SIRT6: SIRT6 regulates TNFα by de-fatty acylation which induces its cleavage and secretion. Secreted (or soluble) TNFα is critical for spreading the inflammatory and apoptotic signal through binding of the TNFα receptors (Micheau & Tschopp 2003). Importantly, total levels of TNFα are decreased in SIRT6 KO brains (**PART 2: Fig.5C, D**). Thus, to specifically test the involvement of TNFα we will utilize

inhibitors in our primary culture system. The TNFα inhibitor pirfenidone robustly reduces levels of membrane bound and secreted form and is effective on neuronal cells (Grattendick *et al.* 2008). Cells that are overexpressing SIRT6 have a pro-apoptotic phenotype; we will test if pirfenidone (TNFα inhibition) alleviates this predisposition. Conversely, we will overexpress total or introduce recombinant soluble TNFα to KO cultures to suppress the pro-survival phenotype. If true, this would demonstrate TNFα controlled survival downstream of SIRT6.

SIRT6's histone deacetylation activity can regulate the pro-survival AKT pathway. When SIRT6's deacetylation function is suppressed, levels of AKT phosphorylation at sites T308 and S473 increase (Sundaresan *et al.* 2012). These phosphorylation sites are critical for full AKT activation and the promotion of cell survival (Sarbassov *et al.* 2005; Manning & Cantley 2007). Importantly, our data shows upregulation of AKT signaling in SIRT6 KO brains (**PART 2: Fig.5C, E**), thus we will utilize AKT signaling inhibitors in our cell culture model. Specifically, inhibition of AKT in SIRT6 KO cultures will demonstrate whether its signaling is required for the pro-survival phenotype. The highly specific AKT inhibitor MK-2206 2HCl will be used since it is effective in neuronal culture models (Santo *et al.* 2013). Conversely, overexpression or constitutive AKT signaling may alleviate the pro-apoptotic phenotype of OX cells. Constitutive AKT signaling will be accomplished by the introduction of a phospho-mimetic mutant (Manning & Cantley 2007). If these observations are true, this would demonstrate the involvement of AKT controlled survival downstream of SIRT6.

Identify the enzymatic functions of SIRT6 that influence neuronal survival. Knowing which functions of SIRT6 regulate cellular survival will not only direct to the downstream effectors involved (TNFα, AKT, among others) but will also be important for future therapeutic applications. It is possible that multiple activities, including a structural (non-enzymatic) function, are involved. Studying both enzymatic and structural functions of SIRT6 will help us to define unbiasedly its mechanism and downstream effectors. To identify these functions, we will utilize SIRT6 mutants that due to point mutations in the enzymatic core of the protein can only perform defatty acylation, ADP-ribosylation, or no enzymatic activities (Mostoslavsky *et al.* 2006; Kugel *et al.* 2015; Zhang *et al.* 2016b). Respective addback of these SIRT6 enzymatic mutants and normal SIRT6 into KO cells with stress and apoptosis analysis will reveal which functions influence survival. No SIRT6 mutant exists that can only perform deacetylation. However, comparing addback of WT and defatty acylase only SIRT6 will reveal the relative contribution of both activities. Addback of enzymatic null SIRT6 will reveal if any structural or scaffolding role is present. Within these experiments we will also isolate RNA and protein for qRT-PCR and immunoblotting analysis. From these we can measure expression, abundance, and activation of TNF-α, AKT, and other inflammatory and apoptotic associated molecules. These experiments will demonstrate whether SIRT6 is influencing survival through transcription via histone deacetylation, post translational modification via defatty acylation, and or a structural element.

Test the efficacy of in vivo SIRT6 deletion on the progression and outcome in a

Lewy body-based PD model.

We have demonstrated that SIRT6 BSKO mice are protected from MPTP induced PD (**PART 2**: **Fig.6**). However, the MPTP model does not fully recapitulate the neuropathology of PD. Lewy bodies are intraneuronal protein aggregates whose principal component is alpha-synuclein. The contribution of Lewy bodies and alpha-synuclein to the etiology of PD is still being elucidated but their importance is underscored by their occurrence in 90% of sporadic cases (Lee & Trojanowski 2006). In addition, there are mutations in the alpha-synuclein gene itself known to cause inherited forms of PD (Lesage & Brice 2009). Lewy bodies are absent with MPTP administration, which is a drawback of toxin-based PD models. Considering Lewy bodies occur in sporadic, genetic, and the overall majority of PD cases, accounting for this pathological feature is critical for developing relevant therapeutics. Thus, we will utilize the transgenic mouse model that expresses the human Alpha-Synuclein (A53T) mutation (α-syn(A53T)), which are available from the Jackson Laboratories. This model develops intraneuronal Lewy bodies, progressive motor deficits, and neuronal loss eventually leading to death in an age-dependent manner (Lee *et al.* 2002). SIRT6 BSKO and BSOX mice will be crossed with α-syn(A53T) mice. A cross sectional analysis will assess the development of Lewy bodies, behavioral and motor deficits, and neuronal loss. Time points, which are consistent with observing significant differences, for assessment and tissue collection include 8 and 14 months of age (Lee *et al.* 2002; Oaks *et al.* 2013). Behavioral and motor tests to run include the open field, rotarod, and wire hang test. All these tests are commonly used to measure behavioral and motor deficits in central nervous system disease models like

PD. After behavioral assessment, mice will be sacrificed for immunohistochemical analysis of dopaminergic neuron abundance in the *substantia nigra* and dendrite density in the *striatum*. Staining and measurement of alpha-synuclein based protein aggregates will be done on regions sensitive to their formation (Giasson *et al.* 2002; Tsika *et al.* 2010). We will measure expression, abundance, and activation of TNF-α, AKT, and other inflammatory and apoptotic molecules. Importantly we can check the cellular localization of these molecules on tissue sections; here we can also asses the reactivity and involvement of microglia and astrocytes.

α-syn(A53T) mice have a mean lifespan of 14 months, far shorter compared to WT, we will assess whether SIRT6 manipulation can alter the lifespan of these mice. The characterization of these transgenic crosses will reveal whether SIRT6 status can alter disease progression and outcome in a Lewy body-based PD model, and strengthen the relevance of SIRT6 based therapies to human PD.

Test the effectiveness of *in vivo* SIRT6 inhibition as a Parkinson's disease intervention.

To propose SIRT6 inhibition as a viable therapy we must demonstrate effective PD amelioration by practical means. Our transgenic models are encouraging but genetic engineering therapies are not common enough in the clinic yet, and total SIRT6 ablation may not be desired. Testing the effectiveness of small molecule SIRT6 inhibitors for the treatment of PD would be the next step. The thiomyristoyl peptide BHJH-TM3 (TM3) is the most potent cell permeable SIRT6 inhibitor to date (He *et al.*

2014). TM3 exploits SIRT6's affinity for de-fatty acylation (such as the removal of myristoyl groups), and was created by our collaborator Dr. Hening Lin. Another potent inhibitor of SIRT6 is EX527 (Kokkonen *et al.* 2014), which is less specific than TM3 but has been researched extensively, including *in vivo* in our laboratory. TM3 and EX527 will be administered to both the MPTP and α-syn(A53T) PD models to account for the full range of pathology. The use of two models and inhibitors will validate the results generated from one another.

For the MPTP model we will administer the inhibitor compounds concurrently with the start of MPTP injections. The compounds will be delivered by intraperitoneal injection (IP) along with MPTP 3 times per week throughout the 3 week treatment period. Only adult WT mice will be utilized with treatment and corresponding control groups. For the α-syn(A53T) model we will administer the inhibitor compounds starting at 8 months and continue to 14 months of age. Similarly, to the MPTP model the compounds will be delivered by IP 3 times per week for the duration of the trial. EX527 will be delivered at 10mg/kg, which is an effective concentration to inhibit neuronal sirtuins demonstrated by our lab and others (Dietrich *et al.* 2010). Even though the pharmacodynamics of TM3 has not specifically been studied, therapeutic peptides in general are well researched. An effective concentration of this peptide to inhibit 50% of SIRT6 is ~1.5μM (He *et al.* 2014), which would correspond to daily injections of 49.2μg of peptide. 49.2μg of protein per injection is relatively small amount, which can easily be scaled up (or down) if necessary.

Although improvements in the potency and specificity of SIRT6 inhibitors are rapidly advancing (Sukumar *et al.* 2016), compounds like TM3 may not be effective *in vivo*. In that case other inhibitory compounds that exploit different SIRT6 properties may be used, such as quercetin analogs (Ravichandran *et al.* 2014; Rahnasto-Rilla *et al.* 2016). In addition, if *in vivo* treatments prove unreliable, we can analyze any of these compound's effects in our *in vitro* primary culture system. The MPTP model can be mimicked by delivery of its toxic metabolite (MPP+) in cell culture (Zhang *et al.* 2014), and primary neural cultures from the α-syn(A53T) mice would effectively mimic the *in vivo* model (Li *et al.* 2013).

REFERENCES

Abbott JJ, Howlett DR, Francis PT, Williams RJ (2008). Abeta(1-42) modulation of Akt phosphorylation via alpha7 nAChR and NMDA receptors. *Neurobiol Aging*. **29**, 992-1001.

Alam Q, Alam MZ, Mushtaq G, Damanhouri GA, Rasool M, Kamal MA, Haque A (2016). Inflammatory Process in Alzheimer's and Parkinson's Diseases: Central Role of Cytokines. *Curr Pharm Des*. **22**, 541-548.

An J, Muoio DM, Shiota M, Fujimoto Y, Cline GW, Shulman GI, Koves TR, Stevens R, Millington D, Newgard CB (2004). Hepatic expression of malonyl-CoA decarboxylase reverses muscle, liver and whole-animal insulin resistance. *Nature Medicine*. **10**, 268-274.

Ascherio A, Schwarzschild MA (2016). The epidemiology of Parkinson's disease: risk factors and prevention. *Lancet Neurol*. **15**, 1257-1272.

Baffy G, Derdak Z, Robson SC (2011). Mitochondrial recoupling: a novel therapeutic strategy for cancer? *Br J Cancer*. **105**, 469-474.

Barreto GE, Iarkov A, Moran VE (2014). Beneficial effects of nicotine, cotinine and its metabolites as potential agents for Parkinson's disease. *Front Aging Neurosci*. **6**, 340.

Bauer I, Grozio A, Lasiglie D, Basile G, Sturla L, Magnone M, Sociali G, Soncini D, Caffa I, Poggi A, Zoppoli G, Cea M, Feldmann G, Mostoslavsky R, Ballestrero A, Patrone F, Bruzzone S, Nencioni A (2012). The NAD+-dependent histone deacetylase SIRT6 promotes cytokine production and migration in pancreatic cancer cells by regulating Ca2+ responses. *J Biol Chem*. **287**, 40924-40937.

Beauharnois JM, Bolivar BE, Welch JT (2013). Sirtuin 6: a review of biological effects and potential therapeutic properties. *Mol Biosyst*. **9**, 1789-1806.

Bencherif M (2009). Neuronal nicotinic receptors as novel targets for inflammation and neuroprotection: mechanistic considerations and clinical relevance. *Acta Pharmacologica Sinica*. **30**, 702-714.

Bennett DA, Schneider JA, Arvanitakis Z, Wilson RS (2012). Overview and findings from the religious orders study. *Current Alzheimer Research*. **9**, 628-645.

Benowitz NL, Bernert JT, Caraballo RS, Holiday DB, Wang JT (2009). Optimal Serum Cotinine Levels for Distinguishing Cigarette Smokers and Nonsmokers Within Different Racial/Ethnic Groups in the United States Between 1999 and 2004. *American Journal of Epidemiology*. **169**, 236-248.

Berdyyeva TK, Woodworth CD, Sokolov I (2005). Human epithelial cells increase their rigidity with ageing in vitro: direct measurements. *Phys Med Biol*. **50**, 81-92.

Botigue LR, Song S, Scheu A, Gopalan S, Pendleton AL, Oetjens M, Taravella AM, Seregely T, Zeeb-Lanz A, Arbogast RM, Bobo D, Daly K, Unterlander M, Burger J, Kidd JM, Veeramah KR (2017). Ancient European dog genomes reveal continuity since the Early Neolithic. *Nat Commun*. **8**, 16082.

Brand MD (2000). Uncoupling to survive? The role of mitochondrial inefficiency in ageing. *Exp Gerontol*. **35**, 811-820.

Brand MD, Affourtit C, Esteves TC, Green K, Lambert AJ, Miwa S, Pakay JL, Parker N (2004). Mitochondrial superoxide: production, biological effects, and activation of uncoupling proteins. *Free Radic Biol Med*. **37**, 755-767.

Brewer GJ, Torricelli JR (2007). Isolation and culture of adult neurons and neurospheres. *Nat Protoc*. **2**, 1490-1498.

Cadieu E, Neff MW, Quignon P, Walsh K, Chase K, Parker HG, Vonholdt BM, Rhue A, Boyko A, Byers A, Wong A, Mosher DS, Elkahloun AG, Spady TC, Andre C, Lark KG, Cargill M, Bustamante CD, Wayne RK, Ostrander EA (2009). Coat variation in the domestic dog is governed by variants in three genes. *Science*. **326**, 150-153.

Caldeira da Silva CC, Cerqueira FM, Barbosa LF, Medeiros MH, Kowaltowski AJ (2008). Mild mitochondrial uncoupling in mice affects energy metabolism, redox balance and longevity. *Aging Cell*. **7**, 552-560.

Cardinale A, de Stefano MC, Mollinari C, Racaniello M, Garaci E, Merlo D (2015). Biochemical characterization of sirtuin 6 in the brain and its involvement in oxidative stress response. *Neurochem Res*. **40**, 59-69.

Chen H, Ding D, Wang J, Zhao Q, Meng H, Li H, Gao YT, Shu XO, Tanner CM, Hong Z, Yang G (2015). Parkinson's disease research in a prospective cohort in China. *Parkinsonism Relat Disord*. **21**, 1200-1204.

Chen H, Huang X, Guo X, Mailman RB, Park Y, Kamel F, Umbach DM, Xu Q, Hollenbeck A, Schatzkin A, Blair A (2010). Smoking duration, intensity, and risk of Parkinson disease. *Neurology*. **74**, 878-884.

Chen J, Guan Z, Wang L, Song G, Ma B, Wang Y (2014). Meta-analysis: overweight, obesity, and Parkinson's disease. *Int J Endocrinol*. **2014**, 203930.

Cho SY, Seo DB, Kim WG, Lee SJ (2014). Mild mitochondrial uncoupling prevents premature senescence in human dermal fibroblasts. *J Invest Dermatol*. **134**,

540-543.

Dawson TM (2000). New animal models for Parkinson's disease. *Cell*. **101**, 115-118.

Dietrich MO, Antunes C, Geliang G, Liu ZW, Borok E, Nie Y, Xu AW, Souza DO, Gao Q, Diano S, Gao XB, Horvath TL (2010). Agrp neurons mediate Sirt1's action on the melanocortin system and energy balance: roles for Sirt1 in neuronal firing and synaptic plasticity. *J Neurosci*. **30**, 11815-11825.

Dokukin ME, Guz NV, Sokolov I (2013). Quantitative study of the elastic modulus of loosely attached cells in AFM indentation experiments. *Biophys J*. **104**, 2123-2131.

Domanskyi S, Nicholatos JW, Schilling JE, Privman V, Libert S (2017). SIRT6 knockout cells resist apoptosis initiation but not progression: a computational method to evaluate the progression of apoptosis. *Apoptosis*. **22**, 1336-1343.

Dorn HF (1959). Tobacco consumption and mortality from cancer and other diseases. *Public Health Rep*. **74**, 581-593.

Driver JA, Logroscino G, Gaziano JM, Kurth T (2009). Incidence and remaining lifetime risk of Parkinson disease in advanced age. *Neurology*. **72**, 432-438.

Dudek H, Datta SR, Franke TF, Birnbaum MJ, Yao RJ, Cooper GM, Segal RA, Kaplan DR, Greenberg ME (1997). Regulation of neuronal survival by the serine-threonine protein kinase Akt. *Science*. **275**, 661-665.

Feldman JL, Baeza J, Denu JM (2013). Activation of the protein deacetylase SIRT6 by long-chain fatty acids and widespread deacylation by mammalian sirtuins. *J Biol Chem*. **288**, 31350-31356.

Ferrara CT, Wang P, Neto EC, Stevens RD, Bain JR, Wenner BR, Ilkayeva OR,

Keller MP, Blasiole DA, Kendziorski C, Yandell BS, Newgard CB, Attie AD (2008). Genetic networks of liver metabolism revealed by integration of metabolic and transcriptional profiling. *PLoS Genet*. **4**, e1000034.

Fick LJ, Fick GH, Li Z, Cao E, Bao B, Heffelfinger D, Parker HG, Ostrander EA, Riabowol K (2012). Telomere length correlates with life span of dog breeds. *Cell Rep*. **2**, 1530-1536.

Fleming JM, Creevy KE, Promislow DE (2011). Mortality in north american dogs from 1984 to 2004: an investigation into age-, size-, and breed-related causes of death. *J Vet Intern Med*. **25**, 187-198.

Ghosh S, Liu B, Wang Y, Hao Q, Zhou Z (2015). Lamin A Is an Endogenous SIRT6 Activator and Promotes SIRT6-Mediated DNA Repair. *Cell Rep*. **13**, 1396-1406.

Giasson BI, Duda JE, Quinn SM, Zhang B, Trojanowski JQ, Lee VM (2002). Neuronal alpha-synucleinopathy with severe movement disorder in mice expressing A53T human alpha-synuclein. *Neuron*. **34**, 521-533.

Gong B, Pan Y, Vempati P, Zhao W, Knable L, Ho L, Wang J, Sastre M, Ono K, Sauve AA, Pasinetti GM (2013). Nicotinamide riboside restores cognition through an upregulation of proliferator-activated receptor-gamma coactivator 1alpha regulated beta-secretase 1 degradation and mitochondrial gene expression in Alzheimer's mouse models. *Neurobiol Aging*. **34**, 1581-1588.

Grattendick KJ, Nakashima JM, Feng L, Giri SN, Margolin SB (2008). Effects of three anti-TNF-alpha drugs: etanercept, infliximab and pirfenidone on release of TNF-alpha in medium and TNF-alpha associated with the cell in vitro. *Int*

Immunopharmacol. **8**, 679-687.

Greene LA, Levy O, Malagelada C (2011). Akt as a Victim, Villain and Potential Hero in Parkinson's Disease Pathophysiology and Treatment. *Cell Mol Neurobiol*. **31**, 969-978.

Greer KA, Canterberry SC, Murphy KE (2007). Statistical analysis regarding the effects of height and weight on life span of the domestic dog. *Res Vet Sci*. **82**, 208-214.

Greer KA, Hughes LM, Masternak MM (2011). Connecting serum IGF-1, body size, and age in the domestic dog. *Age (Dordr)*. **33**, 475-483.

Harman D (1956). Aging: a theory based on free radical and radiation chemistry. *J Gerontol*. **11**, 298-300.

Harper JM, Wang M, Galecki AT, Ro J, Williams JB, Miller RA (2011). Fibroblasts from long-lived bird species are resistant to multiple forms of stress. *J Exp Biol*. **214**, 1902-1910.

Hayward JJ, Castelhano MG, Oliveira KC, Corey E, Balkman C, Baxter TL, Casal ML, Center SA, Fang M, Garrison SJ, Kalla SE, Korniliev P, Kotlikoff MI, Moise NS, Shannon LM, Simpson KW, Sutter NB, Todhunter RJ, Boyko AR (2016). Complex disease and phenotype mapping in the domestic dog. *Nat Commun*. **7**, 10460.

He B, Hu J, Zhang X, Lin H (2014). Thiomyristoyl peptides as cell-permeable Sirt6 inhibitors. *Org Biomol Chem*. **12**, 7498-7502.

Hedbacker K, Birsoy K, Wysocki RW, Asilmaz E, Ahima RS, Farooqi IS, Friedman JM (2010). Antidiabetic effects of IGFBP2, a leptin-regulated gene. *Cell*

Metab. **11**, 11-22.

Henley BM, Williams BA, Srinivasan R, Cohen BN, Xiao C, Mackey ED, Wold BJ, Lester HA (2013). Transcriptional regulation by nicotine in dopaminergic neurons. *Biochem Pharmacol*. **86**, 1074-1083.

Herskovits AZ, Guarente L (2013). Sirtuin deacetylases in neurodegenerative diseases of aging. *Cell Res*. **23**, 746-758.

Hoeflich A, Reyer A, Ohde D, Schindler N, Brenmoehl J, Spitschak M, Langhammer M, Tuchscherer A, Wirthgen E, Renner-Muller I, Wanke R, Metzger F, Bielohuby M, Wolf E (2016). Dissociation of somatic growth, time of sexual maturity, and life expectancy by overexpression of an RGD-deficient IGFBP-2 variant in female transgenic mice. *Aging Cell*. **15**, 111-117.

Hoffman JM, Creevy KE, Franks A, O'Neill DG, Promislow DEL (2018). The companion dog as a model for human aging and mortality. *Aging Cell*.

Holloszy JO, Smith EK (1986). Longevity of cold-exposed rats: a reevaluation of the "rate-of-living theory". *J Appl Physiol (1985)*. **61**, 1656-1660.

Housley DJE, Venta PJ (2006). The long and the short of it: evidence that FGF5 is a major determinant of canine 'hair'-itability. *Anim Genet*. **37**, 309-315.

Hughes KC, Gao X, Kim IY, Wang M, Weisskopf MG, Schwarzschild MA, Ascherio A (2017). Intake of dairy foods and risk of Parkinson disease. *Neurology*. **89**, 46-52.

Ioris RM, Galie M, Ramadori G, Anderson JG, Charollais A, Konstantinidou G, Brenachot X, Aras E, Goga A, Ceglia N, Sebastian C, Martinvalet D, Mostoslavsky R, Baldi P, Coppari R (2017). SIRT6 Suppresses Cancer Stem-

like Capacity in Tumors with PI3K Activation Independently of Its Deacetylase Activity. *Cell Rep*. **18**, 1858-1868.

Jensen MV, Joseph JW, Ilkayeva O, Burgess S, Lu D, Ronnebaum SM, Odegaard M, Becker TC, Sherry AD, Newgard CB (2006). Compensatory responses to pyruvate carboxylase suppression in islet beta-cells. Preservation of glucose-stimulated insulin secretion. *J Biol Chem*. **281**, 22342-22351.

Jiang H, Khan S, Wang Y, Charron G, He B, Sebastian C, Du J, Kim R, Ge E, Mostoslavsky R, Hang HC, Hao Q, Lin H (2013). SIRT6 regulates TNF-alpha secretion through hydrolysis of long-chain fatty acyl lysine. *Nature*. **496**, 110-113.

Jiang H, Zhang X, Lin H (2016). Lysine fatty acylation promotes lysosomal targeting of TNF-alpha. *Sci Rep*. **6**, 24371.

Jimenez AG, Winward J, Beattie U, Cipolli W (2018). Cellular metabolism and oxidative stress as a possible determinant for longevity in small breed and large breed dogs. *PLoS One*. **13**.

Johnson SJ, Diener MD, Kaltenboeck A, Birnbaum HG, Siderowf AD (2013). An economic model of Parkinson's disease: implications for slowing progression in the United States. *Mov Disord*. **28**, 319-326.

Jung ES, Choi H, Song H, Hwang YJ, Kim A, Ryu H, Mook-Jung I (2016). p53-dependent SIRT6 expression protects Abeta42-induced DNA damage. *Sci Rep*. **6**, 25628.

Kabat GC, Anderson ML, Heo M, Hosgood HD, 3rd, Kamensky V, Bea JW, Hou L, Lane DS, Wactawski-Wende J, Manson JE, Rohan TE (2013). Adult stature

and risk of cancer at different anatomic sites in a cohort of postmenopausal women. *Cancer Epidemiol Biomarkers Prev*. **22**, 1353-1363.

Kabil H, Kabil O, Banerjee R, Harshman LG, Pletcher SD (2011). Increased transsulfuration mediates longevity and dietary restriction in Drosophila. *Proc Natl Acad Sci U S A*. **108**, 16831-16836.

Kaeberlein M, Creevy KE, Promislow DE (2016). The dog aging project: translational geroscience in companion animals. *Mamm Genome*. **27**, 279-288.

Kaluski S, Portillo M, Besnard A, Stein D, Einav M, Zhong L, Ueberham U, Arendt T, Mostoslavsky R, Sahay A, Toiber D (2017). Neuroprotective Functions for the Histone Deacetylase SIRT6. *Cell Rep*. **18**, 3052-3062.

Kanfi Y, Naiman S, Amir G, Peshti V, Zinman G, Nahum L, Bar-Joseph Z, Cohen HY (2012). The sirtuin SIRT6 regulates lifespan in male mice. *Nature*. **483**, 218-221.

Kanfi Y, Shalman R, Peshti V, Pilosof SN, Gozlan YM, Pearson KJ, Lerrer B, Moazed D, Marine JC, de Cabo R, Cohen HY (2008). Regulation of SIRT6 protein levels by nutrient availability. *FEBS Lett*. **582**, 543-548.

Kelton MC, Kahn HJ, Conrath CL, Newhouse PA (2000). The effects of nicotine on Parkinson's disease. *Brain Cogn*. **43**, 274-282.

Kenborg L, Lassen CF, Ritz B, Andersen KK, Christensen J, Schernhammer ES, Hansen J, Wermuth L, Rod NH, Olsen JH (2015). Lifestyle, family history, and risk of idiopathic Parkinson disease: a large Danish case-control study. *Am J Epidemiol*. **181**, 808-816.

Koch IJ, Clark MM, Thompson MJ, Deere-Machemer KA, Wang J, Duarte L,

Gnanadesikan GE, McCoy EL, Rubbi L, Stahler DR, Pellegrini M, Ostrander EA, Wayne RK, Sinsheimer JS, Vonholdt BM (2016). The concerted impact of domestication and transposon insertions on methylation patterns between dogs and grey wolves. *Mol Ecol*. **25**, 1838-1855.

Kokkonen P, Rahnasto-Rilla M, Mellini P, Jarho E, Lahtela-Kakkonen M, Kokkola T (2014). Studying SIRT6 regulation using H3K56 based substrate and small molecules. *Eur J Pharm Sci*. **63**, 71-76.

Kowal SL, Dall TM, Chakrabarti R, Storm MV, Jain A (2013). The current and projected economic burden of Parkinson's disease in the United States. *Movement Disord*. **28**, 311-318.

Kraus C, Pavard S, Promislow DE (2013). The size-life span trade-off decomposed: why large dogs die young. *Am Nat*. **181**, 492-505.

Kugel S, Feldman JL, Klein MA, Silberman DM, Sebastian C, Mermel C, Dobersch S, Clark AR, Getz G, Denu JM, Mostoslavsky R (2015). Identification of and Molecular Basis for SIRT6 Loss-of-Function Point Mutations in Cancer. *Cell Rep*. **13**, 479-488.

Kwak GH, Lim DH, Han JY, Lee YS, Kim HY (2012). Methionine sulfoxide reductase B3 protects from endoplasmic reticulum stress in Drosophila and in mammalian cells. *Biochem Biophys Res Commun*. **420**, 130-135.

Lee MK, Stirling W, Xu Y, Xu X, Qui D, Mandir AS, Dawson TM, Copeland NG, Jenkins NA, Price DL (2002). Human alpha-synuclein-harboring familial Parkinson's disease-linked Ala-53 --> Thr mutation causes neurodegenerative disease with alpha-synuclein aggregation in transgenic mice. *Proc Natl Acad*

Sci U S A. **99**, 8968-8973.

Lee VM, Trojanowski JQ (2006). Mechanisms of Parkinson's disease linked to pathological alpha-synuclein: new targets for drug discovery. *Neuron*. **52**, 33-38.

Lesage S, Brice A (2009). Parkinson's disease: from monogenic forms to genetic susceptibility factors. *Human Molecular Genetics*. **18**, R48-59.

Li L, Nadanaciva S, Berger Z, Shen W, Paumier K, Schwartz J, Mou K, Loos P, Milici AJ, Dunlop J, Hirst WD (2013). Human A53T alpha-synuclein causes reversible deficits in mitochondrial function and dynamics in primary mouse cortical neurons. *PLoS One*. **8**, e85815.

Li X, Li WH, Liu GX, Shen X, Tang Y (2015). Association between cigarette smoking and Parkinson's disease: A meta-analysis. *Arch Gerontol Geriat*. **61**, 510-516.

Libert S, Guarente L (2013). Metabolic and Neuropsychiatric Effects of Calorie Restriction and Sirtuins. *Annu Rev Physiol*. **75**, 669-684.

Lim DH, Han JY, Kim JR, Lee YS, Kim HY (2012). Methionine sulfoxide reductase B in the endoplasmic reticulum is critical for stress resistance and aging in Drosophila. *Biochem Biophys Res Commun*. **419**, 20-26.

Liu Q, Zhao B (2004). Nicotine attenuates beta-amyloid peptide-induced neurotoxicity, free radical and calcium accumulation in hippocampal neuronal cultures. *Br J Pharmacol*. **141**, 746-754.

Lloyd AJ, Beckmann M, Wilson T, Tailliart K, Allaway D, Draper J (2017). Ultra high performance liquid chromatography-high resolution mass spectrometry

plasma lipidomics can distinguish between canine breeds despite uncontrolled environmental variability and non-standardized diets. *Metabolomics*. **13**.

Manning BD, Cantley LC (2007). AKT/PKB signaling: navigating downstream. *Cell*. **129**, 1261-1274.

Mao Z, Hine C, Tian X, Van Meter M, Au M, Vaidya A, Seluanov A, Gorbunova V (2011). SIRT6 promotes DNA repair under stress by activating PARP1. *Science*. **332**, 1443-1446.

McCoin CS, Knotts TA, Ono-Moore KD, Oort PJ, Adams SH (2015). Long-chain acylcarnitines activate cell stress and myokine release in C2C12 myotubes: calcium-dependent and -independent effects. *Am J Physiol Endocrinol Metab*. **308**, E990-E1000.

Meredith GE, Rademacher DJ (2011). MPTP mouse models of Parkinson's disease: an update. *J Parkinsons Dis*. **1**, 19-33.

Metsalu T, Vilo J (2015). ClustVis: a web tool for visualizing clustering of multivariate data using Principal Component Analysis and heatmap. *Nucleic Acids Res*. **43**, W566-570.

Micheau O, Tschopp J (2003). Induction of TNF receptor I-mediated apoptosis via two sequential signaling complexes. *Cell*. **114**, 181-190.

Middleton RP, Lacroix S, Scott-Boyer MP, Dordevic N, Kennedy AD, Slusky AR, Carayol J, Petzinger-Germain C, Beloshapka A, Kaput J (2017). Metabolic Differences between Dogs of Different Body Sizes. *J Nutr Metab*.

Mookerjee SA, Divakaruni AS, Jastroch M, Brand MD (2010). Mitochondrial uncoupling and lifespan. *Mech Ageing Dev*. **131**, 463-472.

Moran LB, Duke DC, Deprez M, Dexter DT, Pearce RK, Graeber MB (2006). Whole genome expression profiling of the medial and lateral substantia nigra in Parkinson's disease. *Neurogenetics*. **7**, 1-11.

Morens DM, Grandinetti A, Reed D, White LR, Ross GW (1995). Cigarette smoking and protection from Parkinson's disease: false association or etiologic clue? *Neurology*. **45**, 1041-1051.

Mostoslavsky R, Chua KF, Lombard DB, Pang WW, Fischer MR, Gellon L, Liu P, Mostoslavsky G, Franco S, Murphy MM, Mills KD, Patel P, Hsu JT, Hong AL, Ford E, Cheng HL, Kennedy C, Nunez N, Bronson R, Frendewey D, Auerbach W, Valenzuela D, Karow M, Hottiger MO, Hursting S, Barrett JC, Guarente L, Mulligan R, Demple B, Yancopoulos GD, Alt FW (2006). Genomic instability and aging-like phenotype in the absence of mammalian SIRT6. *Cell*. **124**, 315-329.

Murakami S, Salmon A, Miller RA (2003). Multiplex stress resistance in cells from long-lived dwarf mice. *FASEB J*. **17**, 1565-1566.

National Research Council (U.S.). Ad Hoc Committee on Dog and Cat Nutrition. (2006). *Nutrient requirements of dogs and cats*. Washington, D.C.: National Academies Press.

Oaks AW, Frankfurt M, Finkelstein DI, Sidhu A (2013). Age-dependent effects of A53T alpha-synuclein on behavior and dopaminergic function. *PLoS One*. **8**, e60378.

Obeso JA, Rodriguez-Oroz MC, Goetz CG, Marin C, Kordower JH, Rodriguez M, Hirsch EC, Farrer M, Schapira AH, Halliday G (2010). Missing pieces in the

Parkinson's disease puzzle. *Nat Med*. **16**, 653-661.

Olsen A, Vantipalli MC, Lithgow GJ (2006). Lifespan extension of Caenorhabditis elegans following repeated mild hormetic heat treatments. *Biogerontology*. **7**, 221-230.

Osman C, Wilmes C, Tatsuta T, Langer T (2007). Prohibitins interact genetically with Atp23, a novel processing peptidase and chaperone for the F1Fo-ATP synthase. *Mol Biol Cell*. **18**, 627-635.

Pankratz N, Beecham GW, DeStefano AL, Dawson TM, Doheny KF, Factor SA, Hamza TH, Hung AY, Hyman BT, Ivinson AJ, Krainc D, Latourelle JC, Clark LN, Marder K, Martin ER, Mayeux R, Ross OA, Scherzer CR, Simon DK, Tanner C, Vance JM, Wszolek ZK, Zabetian CP, Myers RH, Payami H, Scott WK, Foroud T (2012). Meta-analysis of Parkinson's disease: identification of a novel locus, RIT2. *Ann Neurol*. **71**, 370-384.

Parenti MD, Grozio A, Bauer I, Galeno L, Damonte P, Millo E, Sociali G, Franceschi C, Ballestrero A, Bruzzone S, Del Rio A, Nencioni A (2014). Discovery of novel and selective SIRT6 inhibitors. *J Med Chem*. **57**, 4796-4804.

Parkinson's Disease Foundation I (2016). http://www.pdf.org/en/parkinson_statisticsed^eds). New York.

Pearl R (1928). *The rate of living, being an account of some experimental studies on the biology of life duration*. New York,: A.A. Knopf.

Pfister JA, Ma C, Morrison BE, D'Mello SR (2008). Opposing effects of sirtuins on neuronal survival: SIRT1-mediated neuroprotection is independent of its deacetylase activity. *PLoS One*. **3**, e4090.

Powell CA, Kopajtich R, D'Souza AR, Rorbach J, Kremer LS, Husain RA, Dallabona C, Donnini C, Alston CL, Griffin H, Pyle A, Chinnery PF, Strom TM, Meitinger T, Rodenburg RJ, Schottmann G, Schuelke M, Romain N, Haller RG, Ferrero I, Haack TB, Taylor RW, Prokisch H, Minczuk M (2015). TRMT5 Mutations Cause a Defect in Post-transcriptional Modification of Mitochondrial tRNA Associated with Multiple Respiratory-Chain Deficiencies. *Am J Hum Genet*. **97**, 319-328.

Rahnasto-Rilla M, Kokkola T, Jarho E, Lahtela-Kakkonen M, Moaddel R (2016). N-Acylethanolamines Bind to SIRT6. *Chembiochem*. **17**, 77-81.

Ravichandran S, Singh N, Donnelly D, Migliore M, Johnson P, Fishwick C, Luke BT, Martin B, Maudsley S, Fugmann SD, Moaddel R (2014). Pharmacophore model of the quercetin binding site of the SIRT6 protein. *J Mol Graph Model*. **49**, 38-46.

Redman LM, Smith SR, Burton JH, Martin CK, Il'yasova D, Ravussin E (2018). Metabolic Slowing and Reduced Oxidative Damage with Sustained Caloric Restriction Support the Rate of Living and Oxidative Damage Theories of Aging. *Cell Metab*. **27**, 805-815 e804.

Registry V. (DS Steinberg, ed^eds).

Rezvani K, Teng Y, Shim D, De Biasi M (2007). Nicotine regulates multiple synaptic proteins by inhibiting proteasomal activity. *J Neurosci*. **27**, 10508-10519.

Ritz B, Lee PC, Lassen CF, Arah OA (2014). Parkinson disease and smoking revisited: ease of quitting is an early sign of the disease. *Neurology*. **83**, 1396-1402.

Rose G, Crocco P, De Rango F, Montesanto A, Passarino G (2011). Further Support to the Uncoupling-to-Survive Theory: The Genetic Variation of Human UCP Genes Is Associated with Longevity. *Plos One*. **6**.

Sai T, Uchida K, Nakayama H (2013). Involvement of monoamine oxidase-B in the acute neurotoxicity of MPTP in embryonic and newborn mice. *Exp Toxicol Pathol*. **65**, 365-373.

Sanderson SL, Simon AK (2017). In aged primary T cells, mitochondrial stress contributes to telomere attrition measured by a novel imaging flow cytometry assay. *Aging Cell*. **16**, 1234-1243.

Santo EE, Stroeken P, Sluis PV, Koster J, Versteeg R, Westerhout EM (2013). FOXO3a Is a Major Target of Inactivation by PI3K/AKT Signaling in Aggressive Neuroblastoma. *Cancer Res*. **73**, 2189-2198.

Sarbassov DD, Guertin DA, Ali SM, Sabatini DM (2005). Phosphorylation and regulation of Akt/PKB by the rictor-mTOR complex. *Science*. **307**, 1098-1101.

Satoh A, Brace CS, Ben-Josef G, West T, Wozniak DF, Holtzman DM, Herzog ED, Imai S (2010). SIRT1 promotes the central adaptive response to diet restriction through activation of the dorsomedial and lateral nuclei of the hypothalamus. *J Neurosci*. **30**, 10220-10232.

Schapira AH, Bezard E, Brotchie J, Calon F, Collingridge GL, Ferger B, Hengerer B, Hirsch E, Jenner P, Le Novere N, Obeso JA, Schwarzschild MA, Spampinato U, Davidai G (2006). Novel pharmacological targets for the treatment of Parkinson's disease. *Nat Rev Drug Discov*. **5**, 845-854.

Searles Nielsen S, Gallagher LG, Lundin JI, Longstreth WT, Jr., Smith-Weller T,

Franklin GM, Swanson PD, Checkoway H (2012). Environmental tobacco smoke and Parkinson's disease. *Mov Disord*. **27**, 293-296.

Sebastian C, Zwaans BM, Silberman DM, Gymrek M, Goren A, Zhong L, Ram O, Truelove J, Guimaraes AR, Toiber D, Cosentino C, Greenson JK, MacDonald AI, McGlynn L, Maxwell F, Edwards J, Giacosa S, Guccione E, Weissleder R, Bernstein BE, Regev A, Shiels PG, Lombard DB, Mostoslavsky R (2012a). The histone deacetylase SIRT6 is a tumor suppressor that controls cancer metabolism. *Cell*. **151**, 1185-1199.

Sebastian C, Zwaans BMM, Silberman DM, Gymrek M, Goren A, Zhong L, Ram O, Truelove J, Guimaraes AR, Toiber D, Cosentino C, Greenson JK, MacDonald AI, McGlynn L, Maxwell F, Edwards J, Giacosa S, Guccione E, Weissleder R, Bernstein BE, Regev A, Shiels PG, Lombard DB, Mostoslavsky R (2012b). The Histone Deacetylase SIRT6 Is a Tumor Suppressor that Controls Cancer Metabolism. *Cell*. **151**, 1185-1199.

Shannon LM, Boyko RH, Castelhano M, Corey E, Hayward JJ, McLean C, White ME, Abi Said M, Anita BA, Bondjengo NI, Calero J, Galov A, Hedimbi M, Imam B, Khalap R, Lally D, Masta A, Oliveira KC, Perez L, Randall J, Tam NM, Trujillo-Cornejo FJ, Valeriano C, Sutter NB, Todhunter RJ, Bustamante CD, Boyko AR (2015). Genetic structure in village dogs reveals a Central Asian domestication origin. *Proc Natl Acad Sci U S A*. **112**, 13639-13644.

Shao J, Yang X, Liu T, Zhang T, Xie QR, Xia W (2016). Autophagy induction by SIRT6 is involved in oxidative stress-induced neuronal damage. *Protein Cell*. **7**, 281-290.

Sokolov I, Dokukin ME, Guz NV (2013). Method for quantitative measurements of the elastic modulus of biological cells in AFM indentation experiments. *Methods*. **60**, 202-213.

Sokolov I, Iyer S, Subba-Rao V, Gaikwad RM, Woodworth CD (2007). Detection of surface brush on biological cells in vitro with atomic force microscopy. *Appl Phys Lett*. **91**.

Sokolov I, Iyer S, Woodworth CD (2006). Recovery of elasticity of aged human epithelial cells in vitro. *Nanomedicine*. **2**, 31-36.

Spataro N, Calafell F, Cervera-Carles L, Casals F, Pagonabarraga J, Pascual-Sedano B, Campolongo A, Kulisevsky J, Lleo A, Navarro A, Clarimon J, Bosch E (2015). Mendelian genes for Parkinson's disease contribute to the sporadic forms of the disease. *Hum Mol Genet*. **24**, 2023-2034.

Speakman JR, Talbot DA, Selman C, Snart S, McLaren JS, Redman P, Krol E, Jackson DM, Johnson MS, Brand MD (2004). Uncoupled and surviving: individual mice with high metabolism have greater mitochondrial uncoupling and live longer. *Aging Cell*. **3**, 87-95.

Speakman JR, van Acker A, Harper EJ (2003). Age-related changes in the metabolism and body composition of three dog breeds and their relationship to life expectancy. *Aging Cell*. **2**, 265-275.

Srinivasan R, Henley BM, Henderson BJ, Indersmitten T, Cohen BN, Kim CH, McKinney S, Deshpande P, Xiao C, Lester HA (2016). Smoking-Relevant Nicotine Concentration Attenuates the Unfolded Protein Response in Dopaminergic Neurons. *Journal of Neuroscience*. **36**, 65-79.

Sukumar M, Liu J, Mehta GU, Patel SJ, Roychoudhuri R, Crompton JG, Klebanoff CA, Ji Y, Li P, Yu Z, Whitehill GD, Clever D, Eil RL, Palmer DC, Mitra S, Rao M, Keyvanfar K, Schrump DS, Wang E, Marincola FM, Gattinoni L, Leonard WJ, Muranski P, Finkel T, Restifo NP (2016). Mitochondrial Membrane Potential Identifies Cells with Enhanced Stemness for Cellular Therapy. *Cell Metab*. **23**, 63-76.

Sundaresan NR, Vasudevan P, Zhong L, Kim G, Samant S, Parekh V, Pillai VB, Ravindra PV, Gupta M, Jeevanandam V, Cunningham JM, Deng CX, Lombard DB, Mostoslavsky R, Gupta MP (2012). The sirtuin SIRT6 blocks IGF-Akt signaling and development of cardiac hypertrophy by targeting c-Jun. *Nat Med*. **18**, 1643-+.

Sutter NB, Bustamante CD, Chase K, Gray MM, Zhao KY, Zhu L, Padhukasahasram B, Karlins E, Davis S, Jones PG, Quignon P, Johnson GS, Parker HG, Fretwell N, Mosher DS, Lawler DF, Satyaraj E, Nordborg M, Lark KG, Wayne RK, Ostrander EA (2007). A single IGF1 allele is a major determinant of small size in dogs. *Science*. **316**, 112-115.

Takasaka N, Araya J, Hara H, Ito S, Kobayashi K, Kurita Y, Wakui H, Yoshii Y, Yumino Y, Fujii S, Minagawa S, Tsurushige C, Kojima J, Numata T, Shimizu K, Kawaishi M, Kaneko Y, Kamiya N, Hirano J, Odaka M, Morikawa T, Nishimura SL, Nakayama K, Kuwano K (2014). Autophagy Induction by SIRT6 through Attenuation of Insulin-like Growth Factor Signaling Is Involved in the Regulation of Human Bronchial Epithelial Cell Senescence. *J Immunol*. **192**, 958-968.

Tanaka K, Miyake Y, Fukushima W, Sasaki S, Kiyohara C, Tsuboi Y, Yamada T, Oeda T, Miki T, Kawamura N, Sakae N, Fukuyama H, Hirota Y, Nagai M (2010). Active and passive smoking and risk of Parkinson's disease. *Acta Neurol Scand*. **122**, 377-382.

Tanner CM (1992). Occupational and environmental causes of parkinsonism. *Occup Med*. **7**, 503-513.

Thiriez C, Villafane G, Grapin F, Fenelon G, Remy P, Cesaro P (2011). Can nicotine be used medicinally in Parkinson's disease? *Expert Rev Clin Pharmacol*. **4**, 429-436.

Thirumurthi U, Shen J, Xia W, LaBaff AM, Wei Y, Li CW, Chang WC, Chen CH, Lin HK, Yu D, Hung MC (2014). MDM2-mediated degradation of SIRT6 phosphorylated by AKT1 promotes tumorigenesis and trastuzumab resistance in breast cancer. *Sci Signal*. **7**, ra71.

Timmons S, Coakley MF, Moloney AM, C ON (2009). Akt signal transduction dysfunction in Parkinson's disease. *Neuroscience Letters*. **467**, 30-35.

Tsika E, Moysidou M, Guo J, Cushman M, Gannon P, Sandaltzopoulos R, Giasson BI, Krainc D, Ischiropoulos H, Mazzulli JR (2010). Distinct region-specific alpha-synuclein oligomers in A53T transgenic mice: implications for neurodegeneration. *J Neurosci*. **30**, 3409-3418.

Tucker KR, Cavolo SL, Levitan ES (2016). Elevated mitochondria-coupled NAD(P)H in endoplasmic reticulum of dopamine neurons. *Mol Biol Cell*. **27**, 3214-3220.

Van Gool F, Galli M, Gueydan C, Kruys V, Prevot PP, Bedalov A, Mostoslavsky R, Alt FW, De Smedt T, Leo O (2009). Intracellular NAD levels regulate tumor

necrosis factor protein synthesis in a sirtuin-dependent manner. *Nat Med*. **15**, 206-210.

Van Meter M, Mao ZY, Gorbunova V, Seluanov A (2011). SIRT6 overexpression induces massive apoptosis in cancer cells but not in normal cells. *Cell Cycle*. **10**, 3153-3158.

Venderova K, Park DS (2012). Programmed cell death in Parkinson's disease. *Cold Spring Harb Perspect Med*. **2**.

Wang GD, Zhai W, Yang HC, Fan RX, Cao X, Zhong L, Wang L, Liu F, Wu H, Cheng LG, Poyarkov AD, Poyarkov NA, Jr., Tang SS, Zhao WM, Gao Y, Lv XM, Irwin DM, Savolainen P, Wu CI, Zhang YP (2013). The genomics of selection in dogs and the parallel evolution between dogs and humans. *Nat Commun*. **4**, 1860.

Wang M, Miller RA (2012). Fibroblasts from long-lived mutant mice exhibit increased autophagy and lower TOR activity after nutrient deprivation or oxidative stress. *Aging Cell*. **11**, 668-674.

Wang Q, Liu Y, Zhou J (2015). Neuroinflammation in Parkinson's disease and its potential as therapeutic target. *Transl Neurodegener*. **4**, 19.

Welser-Alves JV, Milner R (2013). Microglia are the major source of TNF-alpha and TGF-beta 1 in postnatal glial cultures; regulation by cytokines, lipopolysaccharide, and vitronectin. *Neurochemistry International*. **63**, 47-53.

Westerheide SD, Anckar J, Stevens SM, Jr., Sistonen L, Morimoto RI (2009). Stress-inducible regulation of heat shock factor 1 by the deacetylase SIRT1. *Science*. **323**, 1063-1066.

Wirdefeldt K, Adami HO, Cole P, Trichopoulos D, Mandel J (2011). Epidemiology and etiology of Parkinson's disease: a review of the evidence. *Eur J Epidemiol*. **26 Suppl 1**, S1-58.

Wlodarczyk A, Holtman IR, Krueger M, Yogev N, Bruttger J, Khorooshi R, Benmamar-Badel A, de Boer-Bergsma JJ, Martin NA, Karram K, Kramer I, Boddeke EW, Waisman A, Eggen BJ, Owens T (2017). A novel microglial subset plays a key role in myelinogenesis in developing brain. *EMBO J*. **36**, 3292-3308.

Yordy JD, Kraus C, Hayward JJ, White M, Shannon L, Creevy KE, Promislow D, Boyko AR Body size, inbreeding, and lifespan in domestic dogs. *In preparation*.

Zhang L, Du J, Justus S, Hsu CW, Bonet-Ponce L, Wu WH, Tsai YT, Wu WP, Jia Y, Duong JK, Mahajan VB, Lin CS, Wang S, Hurley JB, Tsang SH (2016a). Reprogramming metabolism by targeting sirtuin 6 attenuates retinal degeneration. *J Clin Invest*. **126**, 4659-4673.

Zhang X, Khan S, Jiang H, Antonyak MA, Chen X, Spiegelman NA, Shrimp JH, Cerione RA, Lin H (2016b). Identifying the functional contribution of the defatty-acylase activity of SIRT6. *Nat Chem Biol*. **12**, 614-620.

Zhang XM, Yin M, Zhang MH (2014). Cell-based assays for Parkinson's disease using differentiated human LUHMES cells. *Acta Pharmacol Sin*. **35**, 945-956.

Zhou M, Xue L, Chen Y, Li H, He Q, Wang B, Meng F, Wang M, Guan MX (2017). A hypertension-associated mitochondrial DNA mutation introduces an m1G37 modification into tRNA(Met), altering its structure and function. *J Biol Chem*.